Quantum protocols for few-qubit devices

ILLC Dissertation Series DS-2020-02

INSTITUTE FOR LOGIC, LANGUAGE AND COMPUTATION

For further information about ILLC publications, please contact

Institute for Logic, Language and Computation
Universiteit van Amsterdam
Science Park 107
1098 XG Amsterdam
phone: +31-20-525 6051
e-mail: illc@uva.nl
homepage: http://www.illc.uva.nl/

This research was supported by the EU SIQS project
(grant agreement ID: 600645), the Quantum Software
Consortium, and by a grant of the University of Amsterdam,
supporting the Research Priority Area Quantum Matter
& Quantum Information and QuSoft.

Cover design by Sarah Brands.
Printed and bound by NBD Biblion.

ISBN: 978–90–903–2694–8.

Quantum protocols for few-qubit devices

ACADEMISCH PROEFSCHRIFT

ter verkrijging van de graad van doctor
aan de Universiteit van Amsterdam
op gezag van de Rector Magnificus
prof. dr. ir. K.I.J. Maex
ten overstaan van een door het College voor Promoties ingestelde commissie,
in het openbaar te verdedigen in de Agnietenkapel
op vrijdag 17 januari 2020, te 10.00 uur

door

Koen Laurentius Groenland

geboren te Amsterdam

Promotiecommissie

Promotores:	prof. dr. H.M. Buhrman	Universiteit van Amsterdam
	prof. dr. C.J.M. Schoutens	Universiteit van Amsterdam
Overige leden:	prof. dr. S. Bose	University College London
	prof. dr. M. Christandl	University of Copenhagen
	prof. dr. J.-S. Caux	Universiteit van Amsterdam
	prof. dr. M.S. Golden	Universiteit van Amsterdam
	dr. V. Gritsev	Universiteit van Amsterdam
	dr. M. Walter	Universiteit van Amsterdam
	dr. J. van Wezel	Universiteit van Amsterdam

Faculteit der Natuurwetenschappen, Wiskunde en Informatica

List of publications

This dissertation is based on the following papers (in chronological order). In each work, all authors contributed equally unless stated otherwise.

[GS18] ***Many-body strategies for multiqubit gates: Quantum control through Krawtchouk-chain dynamics***
Koen Groenland, Kareljan Schoutens,
Phys. Rev. A **97**, 042321 (2018).
Chapter 5 is based on this paper.

[Gro19] ***Adiabatic state distribution using anti-ferromagnetic spin systems***
Koen Groenland,
SciPost Phys. **6**, 011 (2019).
Chapter 9 is based on this paper.

[GS19] ***Quantum gates by resonantly driving many-body eigenstates, with a focus on Polychronakos' model***
Koen Groenland, Kareljan Schoutens,
JSTAT **2019**, 7, 073103 (2019).
Chapters 4 and 6 are based on this paper.

[GGK19] ***Adiabatic transfer of amplitude using STIRAP-like protocols generalizes to many bipartite graphs***
Koen Groenland, Carla Groenland, Reinier Kramer,
Submitted to J. Math. Phys..
Chapter 8 is based on this paper.

[RGG+19] ***Single-step implementation of high fidelity n-bit Toffoli gates***
Stig E. Rasmussen, Koen Groenland, Rene Gerritsma, Kareljan Schoutens,
Nikolaj T. Zinner,
Submitted to Phys. Rev. A.
Chapter 7 is based on this work. The first two authors are the main contributors.

Abstract

Quantum protocols for few-qubit devices

With the advent of scalable quantum information technology, accurate control of quantum systems is becoming increasingly important. We study theoretical control protocols tailored for near-term experiments. The main results can be grouped in two categories. Part II deals with the construction of multiqubit logic gates through resonant driving, whereas in Part III we focus on adiabatic transfer of quantum states. The preceding chapters in Part I contain preliminaries to these subjects.

In **Part II**, we consider multiqubit gates, such as the $\texttt{Toffoli}_N$. These are essential for most quantum algorithms, but turn out to be hard to perform on current quantum computer experiments in practice. As opposed to the standard approach of compiling larger unitaries into sequences of elementary gates that act on at most two qubits, we propose a continuously evolving Hamiltonian which implements highly selective multiqubit gates in a strongly-coupled many-body quantum system. We exploit the selectiveness of resonant driving to exchange only 2 out of 2^N eigenstates of some background Hamiltonian, leading to a unitary time evolution we call $\texttt{iSWAP}_{t_1,t_2}$. The basis in which these states are exchanged is the eigenbasis of the background Hamiltonian, and to make this operation relevant to the computational basis, we introduce the concept of *eigengates*, operations that map between the two bases.

We analyze and simulate such gates in three concrete systems:

- the Krawtchouk chain, an example of an open XX chain that maps to free fermions,
- Polychronakos' model, an example of an XXX or Heisenberg chain with long-ranged interactions,
- and the Ising model, in which one special qubit must be coupled to all others.

In **Part III**, we consider adiabatic protocols that transfer a quantum state through a spatially extended system. Such protocols find widespread application in current physics and chemistry experiments, and may be necessary in future quantum information technologies. Still, most adiabatic protocols are only defined on linear chains. We extend two types of protocols to work on more general *bipartite* graphs, under certain restrictions.

The first type deals with a single quantum excitation hopping on a graph. The conventional protocols called STImulated Raman Adiabatic Passage (STIRAP) and Coherent Tunnelling by Adiabatic Passage (CTAP) allow the excitation to be transported between the ends of a linear chains, in a way that is highly resilient to decoherence. We prove that similar protocols can be applied on any (semi-)bipartite graph which allows a perfect matching both when the sender is removed and when the receiver is removed.

Secondly, we consider an anti-ferromagnetic XXX spin system laid out on a graph. We find that spin states can be transferred and entanglement between distant sites can be created, as long as the graph is bipartite and obeys a certain balance between the maximum spin on both parts.

Contents

I Preliminaries

1 A gentle introduction **3**

2 Condensed matter models **9**
2.1 Qubits . . . 9
2.2 Modeling interacting qubits . . . 10
2.3 The Ising model . . . 14
2.4 The XX model and free fermions . . . 15
2.5 The XXX model, or Heisenberg model . . . 17

3 Manipulating quantum states **25**
3.1 How to form a quantum gate . . . 25
3.2 How to transport a quantum state . . . 33

II Resonantly driven multiqubit gates

4 Introduction to resonant multiqubit gates **45**
4.1 Introduction . . . 45
4.2 Mapping the computational basis to the eigenbasis . . . 48
4.3 Resonant driving . . . 50

5 The Krawtchouk chain **57**
5.1 Analysing the model . . . 57
5.2 Mapping between eigenbases . . . 59
5.3 Resonant driving on Krawtchouk eigenstates . . . 60
5.4 Numerical results . . . 62
5.5 Experimental implementations . . . 63
5.6 Matrix elements of driving operators in free models . . . 64
5.7 Conclusion . . . 67

6 Polychronakos' model **69**
6.1 Analysing the model . . . 69
6.2 Mapping between eigenbases . . . 70
6.3 Resonant driving on Polychronakos eigenstates . . . 71
6.4 Numerical results . . . 72
6.5 Conclusion . . . 75

7 The Ising star model **77**
7.1 Analysing the model . . . 78

7.2 Resonant driving on Ising eigenstates . . . 79
7.3 Turning the driven evolution into a Toffoli . . . 80
7.4 Discussion of asymptotic scaling . . . 84
7.5 Experimental implementations . . . 85
7.6 Conclusion . . . 86

III Adiabatic transport of quantum states

8 STIRAP and CTAP on semi-bipartite graphs 89
8.1 Introduction . . . 89
8.2 Conventional STIRAP . . . 90
8.3 Generalizing STIRAP . . . 91
8.4 Applications . . . 96
8.5 Examples of viable graphs . . . 97
8.6 Numerics . . . 100
8.7 Conclusion . . . 102

9 State transfer in bipartite anti-ferromagnetic spin networks 105
9.1 Introduction . . . 105
9.2 Ground states of symmetry-protected subspaces . . . 107
9.3 Applications . . . 111
9.4 Errors and scaling . . . 114
9.5 Numerics on star graphs . . . 115
9.6 Experimental implementations . . . 118
9.7 Discussion and outlook . . . 118

IV The Closing Matters

Bibliography 123

List of symbols and notation 137

Nederlandse samenvatting 138

Acknowledgements 140

Part I

Preliminaries

CHAPTER 1

A gentle introduction

"My metaphor for a quantum computer is that it's like a coastline. [...] I can manipulate how these waves behave, [...] and the waves crashing on the beach are like the output of the algorithm."

Shelby Kimmel
The Schrödinger Sessions II, 7/29/2016
The front cover illustrates this metaphor.

This thesis is about quantum computers: devices just like our everyday PCs, except that they exploit the theory of microscopic particles to perform tasks that current computers may be unable to do. The reason to study such machines probably deserves some justification.

One way to look at quantum computers is from the perspective of Moore's Law: with transistors reaching atomic scales, we are clearly reaching a limit to shrinking structures on computer chips, calling for other alternatives. However, this is not the proper motivation for quantum computers. Contrary to what might be naively expected, quantum computers will probably not have a higher clock speed, nor allow more bits to be stored. Their advantage stems from the ability to perform certain operations that are classically impossible. Imagine traveling from Morocco to Spain. If your technology limits you to travel by land, you would have to traverse North-Africa, all the way past the Arabic peninsula, and through Europe, before you can reach your destination. This represents the classical algorithm. In the same analogy, a quantum computer endows you with the ability to traverse the water at the Strait of Gibraltar. The new set of operations allows you to travel through previously inaccessible routes, in a fundamentally different way.

Whether this extended set of operations is useful, depends on the precise *problem* that the computer is supposed to solve. Some problems are already solved in a virtually optimal way (from an algorithmic viewpoint at least) by our current computers - problems such as sorting a list, or running a simple text editor. Other problems can greatly benefit from the additional possibilities that quantum offers. A couple of famous examples are the simulation of chemical processes [Llo96], searching an item in an unstructured database [Gro96], and factoring large numbers (e.g. given the number 15, figure out $15 = 3 \times 5$) [Sho94], which turns out to break the encryption most commonly used on the internet. At the same time, a quantum internet would make some of these cryptographic applications safe again [BB84]. The online Quantum Algorithm

Zoo [Jor18] maintains a list of problems where quantum computers offer advantages. The list is impressive, but makes up just a tiny fraction of algorithms used in practice. It is expected that, within the foreseeable future, quantum computers will be special-purpose devices, used only for very specific problems that would otherwise take ages on a regular computer. An interesting twist might come from a large third class of problems, for which it is unknown whether a quantum computer can exploit useful shortcuts. Many promising examples in the fields of machine learning [BWP+17], linear algebra [Mon16], and finance [RL18; WE19] are in this category. Classifying these problems is an active branch of research, but is not the focus of this thesis.

So what are these 'extra operations' that a quantum computer can perform? To gain a glimpse of understanding, we introduce some basic concepts of quantum mechanics, and how these compare to the classical world we're used to. A regular computer uses bits, systems that have a mere two *states* that we label by `0` and `1`. As theorists, we don't care what these states actually are in the real world, but you may think of them as coins lying on a table, either heads up or down. The *state* of a computer with n bits can be completely described by a sequence of n bit values, such as `10011`. Examples of problems are 'calculate the function $f(x) = x + 3$ for a given x' (where we interpret the input x to be a number in binary encoding) or 'find the shortest route from Amsterdam to Groningen' (where it is less clear how to encode this problem in just bits, but note that classical computer science has already solved this problem for us!).

Enter quantum mechanics, where we will now be dealing with quantum mechanical bits, often abbreviated to qubits. The laws of quantum mechanics dictate that a quantum system with possible states `0` and `1` can also be in a *superposition* of the allowed states, meaning that is in both states *at the same time*. How could this help? Well, imagine we have 5 bits, each of which we bring into a superposition. The computer is now in all of its possible states, ranging from `00000`, `00001` all the way up to `11111`, at the very same time. We can now have it perform a *classical* calculation, such as $f(x)$, on its superposed bits. The outcome will then be a superposition of all the possible outcomes $f(x)$ for each of the inputs.

The good news here is that we used an immense amount of parallelism. We calculated the result for $2^5 = 32$ inputs with just a single execution of the function $f(x)$ - a classical machine would have to perform the same routine 32 times to achieve the same result. The number of states, which is 2^n for n qubits, is immense (more on this later), and the prospects of using all of these for parallel calculations is a good reason to be enthusiastic about quantum computing.

However, there is also bad news. We human beings are not quantum, and to read information out of the quantum computer, we need to perform a quantum measurement. Physics dictates that, when measuring a system in a superposition, the system suddenly changes into just one of the many states it was in, at *random*. This voids the whole advantage we had at calculating the function $f(x)$ over all inputs: instead of calculating it for 32 inputs at the same time, we just calculated it on a single, random input (and sometimes we can't even retrieve what that input was!).

The main message here is: quantum computers *can* employ a massive amount of parallelism, but this can not readily be used for practical purposes. To actually gain an advantage over a conventional computer, further quantum steps have to be taken: the superposition could be processed further, in such a way that the computer's state is no longer a large superposition. Rather, the output should encode the answer to the

problem of interest, with sufficiently large probability. The process where the various constituents of a superposition clash such that certain outcomes are enhanced or suppressed is called *interference*. This is very similar to the ocean swell depicted on the front cover, which is comprised of various waves that interfere as they approach the beach.

You may not be too overwhelmed by the factor 32 speedup I claimed earlier. The importance here is not the number 32 itself, but rather *the gain we get as the number of qubits becomes very large*. The number of unique states that a set of n qubits can be in is 2^n, which turns out to grow immensely quickly, even for a moderate number of qubits. To indicate, we'll compare the number of states to some other huge numbers: a mere 32 qubits have more states than there are people on earth, 45 qubits have more than the US national debt (in dollars), and with a mere 266 qubits, we can form more unique states than there are atoms in the universe! Again, it is not immediately clear if we can efficiently *use* all these states for practical purposes.

In fact, it seems downright impossible to create an accurate operation (or 'gate') that works correctly on such an immense number of states. How can one possibly check if a function acts correctly on each of the 2^n possible inputs? Luckily, the fact that we are using a large number of very simple qubits makes such problems tractable. A single, isolated qubit, having just two states, is not hard to deal with, and current technology allows near-perfect manipulation of small isolated systems. Even when we bring just two qubits together, we are dealing with a mere four states. Still, the fact that qubits *interact* with each other also means that interactions with other particles around may occur, introducing potential errors. The current state-of-the-art allows two-qubit gates whose errors are less than one or two per cent, often good enough for hypothetical large-scale computers (assuming error correction, which we introduce below) [BKR+08; BKM+14; HYC+19]. Surprisingly, using only operations that act on one or two qubits at a time, it is possible to form *any* operation on the immense set of 2^n states. This reduces the problem of building a quantum computer to optimizing a small set of simple building blocks. A set of elementary gates that can approximate any operation that is allowed by quantum mechanics is called *universal*, and it turns out that it is not hard to find such sets [DBE95].

Over the years, various small-scale quantum computers were developed, based on widely varying ideas. As an indication of the rapid progress, IBM and quantum startup Rigetti already allow anyone to program up to 16 and 19 actual qubits over the cloud [IBM; Woo18; DMH+18]. These machines are, in principle, universal computers.

Furthermore, statements about devices with as many as 49 [Int18], 51 [BSK+17], 53 [ZPH+17], and 72 [BL18] qubits have been reported, and devices with up to 128 and 160 qubits are planned [Rig18; Ion18]. These reports can be taken with a grain of salt: the devices have either not yet been proven to actually work, or are used as *simulators* that probe the internal physics of the computer. Neither of them have proved to be capable of universal operations at this moment. Similarly, D-Wave reports the use of machines with as many as 2000 qubits [DWa18] by various clients, although these machines are not universal and will most probably not be able to run arbitrary quantum algorithms.

At the time of writing this, there are indications that Google and collaborators built a device that outperforms the best classical computer on a certain calculation [Hac19]. This achievement has been popularly named 'quantum supremacy', although many

scientists prefer the more appropriate term 'quantum advantage' [Wie17]. The calculation itself is probably not useful, but proving that quantum computers are not precluded by some unknown laws of physics is an important scientific breakthrough. Still, note that the above is merely based on rumors, and we should wait for a peer-review to confirm the validity.

The first evidence of quantum advantage opens the way to the so-called NISQ era, where Noisy Intermediate Scale Quantum devices might be employed for calculations that *are* useful [Pre18]. These devices are expected to have 50-100 qubits and will be tailor-made for very specific jobs, such as simulation of chemical processes. A practical use case would most probably involve a classical computer that takes on the main workload, with the NISQ computer executing very short subroutines on request.

When looking ahead towards the more interesting era where quantum computers can perform much longer calculations, one runs into the problem of errors. One should know that, as opposed to classical bits, qubits cannot be copied and are extremely fragile. To avoid losing the information contained in a qubit, large scale quantum computers are thought to require error correction, a technique where several tens to thousands of physical qubits are combined to represent a single *logical* qubit. Until we reach such stages, every single operation causes a minor distortion to the information contained in the qubits, and after typically some $10-200$ operations, the information is effectively lost.

Other challenges that are faced by early quantum computers, are the *connectivity* and *control limitations*. The connectivity deals with the physical location of the qubits. Physics allows only qubits that are sufficiently 'nearby' to interact, and thus, most types of qubits can only talk to a limited number of neighbors. Because a qubit cannot be copied, the qubits have to be moved around frequently - either by physically displacing the information carriers, or by 'swapping' the states of neighboring qubits. All of these steps are again prone to errors, limiting the number of possible operations. Some types of qubits, such as photons and trapped ionized atoms, do not face these connectivity problems and have an edge here.

As for the controllability, it is important to know that many species of qubits operate at extremely low temperatures. Any signal that is sent from a room temperature human towards the qubit could heat up the qubits, hence disturbing their states. Most of these qubits can change at millisecond or even nanosecond timescales, and thus require any input signal to have pristine timing. Some platforms require the use of lasers, and to get these to work at the required accuracy is extremely costly, both financially and in terms of labor. Either way, no matter how one tries to build a qubit, even the best ones are challenging to control at the aimed fidelities.

This is where the results of this thesis come in. In Part II, we aim to make useful *gates* (operations) on a large number of qubits, but without requiring a long sequence of smaller operations. Instead, we make optimal use of the native behavior of the qubits when they sit close to each other, such that connectivity is no longer a problem, and such that control requirements are as simple as possible.

In Part III, we consider a setting where qubits are pinned in place, unable to move. The limitations in their connectivity give rise to some *graph*, a network that describes how information can flow between qubits. Our goal is to start with a certain quantum state at a certain location, and to transfer it to some other location. One may compare this to flicking a network of ropes to transmit a signal: even though the individual parts

of the rope barely move, a wave traveling over the ropes can travel a significant distance. The main difference with the rope analogy is that our protocols are adiabatic, which means something like *so slow that the system can relax to its most comfortable state at all times*. In particular, this avoids the hassle of accurate timing, and the receiver does not risk missing the wave that flies by over the rope.

Further reading For the rest of this thesis, I will assume strong familiarity with quantum mechanics, and in particular, second quantization. For a good introduction of these matters, I would recommend:

- David Griffith's *Introduction to Quantum Mechanics* [Gri05], which covers all the basics of quantum states, measurements, coherent time-evolution by Hamiltonians, quantum spin, the adiabatic theorem, among others.
- Alexander Altland's and Ben Simon's *Condensed Matter Field Theory* [AS10], which covers basics of quantum field theory and second quantization, along with many standard condensed-matter techniques such as basis transformations on field operators.

Moreover, I assume the reader knows the basics of Quantum Computing. A good introduction can be found in

- Michael Nielsen's and Isaac Chuang's *Quantum Computation and Quantum Information* [NC10], which is the standard work of this field. It discusses quantum information, circuits and gates, and the most important algorithms, and a lot more.
- Aforementioned book can be rather extensive for a mere introduction. For a much more compact account, I would recommend Ronald de Wolf's *Quantum Computing: Lecture Notes* [Wol19], whose first two chapters contain sufficient preliminaries for this thesis.

The following two chapters aim to fix notation, remind the reader of various basics that we built upon, and to introduce some of the more advanced techniques used throughout this thesis.

CHAPTER 2

Condensed matter models

2.1 Qubits

We are used to expressing numbers in a positional numeral system, where a number is represented by a string of *digits*. In our decimal system, with *base* $b = 10$, we use the ten digits $d \in \{0, 1, \ldots 9\}$ as building blocks. The convention is that positive integers are represented as *little-endian* strings $\vec{d} = \{d_{N-1}, d_{N-2}, \ldots, d_1, d_0\}$, where the rightmost (ending) symbol represents the digit with the smallest contribution:

$$\underbrace{d_{N-1}d_{N-2}\ldots d_1 d_0}_{\text{A string of digits}} = \underbrace{d_0 b^0 + d_1 b^1 + \ldots + d_{N-1} b^{N-1}}_{\text{A weighted sum of the digits}}.$$

This way, N digits of base b can represent b^N different numbers. For historical and engineering reasons [Gla81], we conventionally use 'binary' ($b = 2$) numbers in information technology, such that digits are represented by **bits**.

In quantum computers, we would like to similarly represent numbers as quantum states $|d_0, d_1, \ldots, d_{N-1}\rangle$, using N quantum systems that can express two different states. To this end, we introduce the *quantum bit*, or **qubit**,

$$|\Psi\rangle = \alpha|0\rangle + \beta|1\rangle, \quad \alpha, \beta \in \mathbb{C}, \quad |\alpha|^2 + |\beta|^2 = 1, \tag{2.1}$$

which is a vector in the two-dimensional complex Hilbert space $\mathbb{C}^2$, spanned by unit vectors $|0\rangle = (1,0)^T$ and $|1\rangle = (0,1)^T$. We may sometimes use 'spin up' and 'spin down' to refer to these respective states. Throughout this thesis, we will use that a global phase change of a qubit is not physically relevant.

We denote with $\vec{\sigma} = \{X, Y, Z\}$ the three Pauli matrices,

$$X = \begin{pmatrix} 0 & 1 \\ 1 & 0 \end{pmatrix}, \quad Y = \begin{pmatrix} 0 & -i \\ i & 0 \end{pmatrix}, \quad Z = \begin{pmatrix} 1 & 0 \\ 0 & -1 \end{pmatrix}, \tag{2.2}$$

which together with $\mathbb{1}_2$ form a basis for the 2×2 Hermitian matrices. The Paulis satisfy

$$[\vec{\sigma}^j, \vec{\sigma}^k] = \sum_{l=1}^{3} 2i\varepsilon^{jkl}\vec{\sigma}^l \tag{2.3}$$

where ε is the fully anti-symmetric Levi-Civita tensor. As we typically do not care about addition by identity, we may describe traceless Hermitian operators as $\hat{O} = \vec{n} \cdot \vec{\sigma}$, for

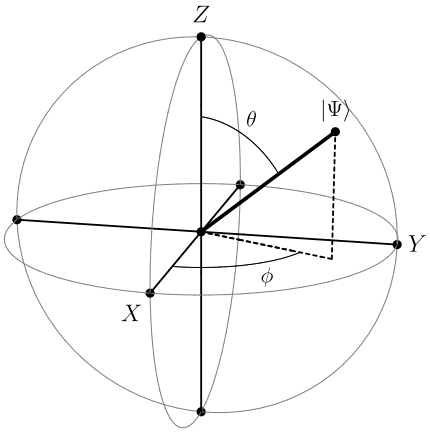

Figure 2.1: The Bloch sphere. The axes correspond to the three Pauli matrices X, Y and Z, in the sense that rotation around a vector $\vec{n}$ corresponds to the action $U = \exp(-i\vec{n}\cdot\vec{\sigma}/2)$. Moreover, any point corresponding to a unit vector $\hat{n}$ represents the unique quantum state (up to a global phase) which is the $+1$ eigenstate of $\hat{n}\cdot\vec{\sigma}$.

some three-vector $\vec{n}$. We sometimes use the spin operators $\vec{S} = \{\hat{S}^x, \hat{S}^y, \hat{S}^z\}$, such that for a spin-$\frac{1}{2}$ particle, $\vec{S} = \frac{1}{2}\vec{\sigma}$. We also introduce the raising and lowering operators

$$\sigma^+ = \frac{X + iY}{2} = \begin{pmatrix} 0 & 1 \\ 0 & 0 \end{pmatrix}, \quad \sigma^- = \frac{X - iY}{2} = \begin{pmatrix} 0 & 0 \\ 1 & 0 \end{pmatrix}. \tag{2.4}$$

Note that we interchanged these compared to frequently used notation, such that in our case, the raising operator σ^+ increases the energy of the qubit with respect to the Z-operator: $\sigma^+|1\rangle = |0\rangle$.

We often like to visualize the complex, two-dimensional qubit state on a real two-dimensional sphere, called the Bloch Sphere, as depicted in figure Fig. 2.1. We represent our qubit states as

$$|\Psi\rangle = \cos(\theta/2)|0\rangle + e^{i\phi}\sin(\theta/2)|1\rangle. \tag{2.5}$$

We interpret (θ, ϕ) as coordinates on a sphere: $\phi \in (0, 2\pi)$ is the *longitude* (the angle along the equator of the sphere, with respect to some definition of $\phi = 0$), and $\theta \in (0, \pi)$ as the *colatitude* (the angle going downwards with respect to the upwards-pointing Z-axis). The sphere allows us to graphically represent *actions* on quantum states: a rotation of α radians around a three-dimensional unit vector $\hat{n}$ over the Bloch sphere is equivalent to acting on a qubit state $|\Psi\rangle$ with $U = \exp(-i\alpha\frac{\hat{n}\cdot\vec{\sigma}}{2})$. A quantum state can also be uniquely defined as an *eigenstate* of these rotations: either as a normalized vector $\hat{n}$ (defining a position on the Bloch sphere), or as the eigenstate with eigenvalue $+1$ of some Hermitian operator $\hat{O} = \hat{n}\cdot\vec{\sigma}$.

2.2 Modeling interacting qubits

Condensed matter physics deals with the collective behavior of a very large (think 10^{20}) number of particles. In particular, we will consider spin models, which consist of N

particles which are all unable to move, but have certain internal (spin) degrees of freedom. We describe such systems by a vector in the Hilbert space $\mathscr{H} = \bigotimes_{j=1}^{N} \mathscr{H}_j$ with $\mathscr{H}_j = \mathbb{C}^{d_j}$, where d_j is the internal dimension of particle j. We use subscripts to indicate on which particle an operator acts.

In the following and in most of this thesis, we restrict to qubits, where $d_j = 2$ for all j. For example, the k'th Pauli matrix acting on the j'th qubit is denoted as

$$\vec{\sigma}_j^k = \mathbb{1}_2 \otimes \ldots \otimes \mathbb{1}_2 \otimes \vec{\sigma}^k \otimes \mathbb{1}_2 \otimes \ldots \otimes \mathbb{1}_2. \tag{2.6}$$

Exceptions are Section 2.5 and Chapter 9, where particles of arbitrary spin are allowed.

Whenever external forces act on our system's qubits, we call these (local) **fields**. We describe these by a Hamiltonian term of the form

$$H = \sum_{j=1}^{N} \vec{B}_j \cdot \vec{\sigma}_j, \tag{2.7}$$

where $\vec{B}_j \in \mathbb{R}^3$ for all j.

Moreover, the particles may **interact**, causing their internal states to change as a function of the states of other particles. The set of possible interactions is huge, and most of them may never occur in nature. To keep our focus on the most relevant types of systems, we make two assumptions:

- The only allowed interactions between particles are **2-local**. This means that the Hamiltonian is a sum of terms, $H = \sum_j h_j$, where each term h_j is Hermitian and acts non-trivially on at most two particles.
- The interactions between the particles are **symmetric**, which means that the interaction is similar even if the two particles acted on are exchanged.

The most general form of a *2-local* Hermitian operators on qubits is

$$H = \sum_{j<k} \sum_{p,q \in \{1,2,3\}} \beta_{jk}^{pq} \vec{\sigma}_j^p \vec{\sigma}_k^q \; + \; \text{(local fields)}. \tag{2.8}$$

The most frequently encountered two-body terms are of the form X_jX_k, Y_jY_k and Z_jZ_k, and we will shortly discuss the properties of models in which these are the only relevant terms. However, note that many more interactions satisfy the symmetry assumptions, such as $Z_jX_k + X_jZ_k$ or $X_jY_k - Y_jX_k$. In fact, we will encounter the latter in Chapter 6.

The naming conventions of models with a certain choice of β^{pq} appear to be somewhat confusing and sometimes contradicting. Therefore, we will always explicitly state the Hamiltonian that we consider. Below, we tease the three models that are addressed later in this chapter:

- The Ising-type interaction, of the form $H = \sum_{j<k} w_{jk} Z_j Z_k$ (also sometimes called ZZ interaction), is discussed in Section 2.3.
- The XY model, of the form $H = \sum_{j<k} w_{jk} \left(aX_jX_k + bY_jY_k \right)$. We will focus on the case $a = b$ in Section 2.4, which is often referred to as the XX or spin hopping model.

- The Heisenberg or XYZ type interaction, which is of the form $H = \sum_{j<k} w_{jk}\left(aX_jX_k + bY_jY_k + cZ_jZ_k\right)$. If a, b, c are independent, the model is often referred to as XYZ model, but to indicate that some of the three parameters are not independent, one may reflect this by making certain symbols in the model name equal. For example, in Section 2.5, we consider the 'isotropic' case $a = b = c$, which is often referred to as XXX model.

The goal: diagonalizing the Hamiltonian Important questions in theoretical physics typically deal with the *ground state* (the vector corresponding to the lowest eigenvalue of H), and thermodynamical properties of quantum systems, which can often be derived if one knows the partition function $Z = \mathrm{tr}(e^{-\beta H})$. On the other hand, for quantum computers we typically assume coherent evolution of pure states, effectively requiring zero temperature. We are then particularly interested in the dynamical properties of the system, which follow from Schrödinger's equation. Each of these questions is closely related to finding the eigensystem of the model's Hamiltonian. In this sense, one might generally describe theoretical condensed matter physics, to zeroeth order, as *the science of diagonalizing k-local Hermitian matrices*. This is, in general, a difficult task, as the Hilbert space is of dimension $\prod_j d_j$, which grows exponentially with the number of particles[1].

2.2.1 Spin models from graphs

Most well-known theoretical spin models have the same *type* of interactions throughout the system, i.e. $\beta^{pq}_{jk} = w_{jk}\beta^{pq}$, such that the system is completely described by the set w_{jk}, indicating the strength of the interaction between two particles, and a global set of β^{pq} that determine the interaction type. In such cases, it is intuitive to describe the couplings in the language of graphs, intuitively a drawing of the various spin particles as structureless dots, two of which are connected by a line if and only if they interact.

Mathematically, we describe a (simple) **graph** $G = (V, E)$ by its set of vertices $V = \{j\}_{j=1}^{N}$, corresponding to the set of particles, and the set of edges $E = \{(j,k) |\ j,k \in V,\ w_{jk} \neq 0\} \subseteq V \times V$, denoting nonzero couplings between spins. More common in this thesis are **weighted graphs**, $G = (V, E, w)$, which are described by the aforementioned set of vertices V and edges E, complemented with a set of **weights** $w : E \to \mathbb{R}$. For either type of graph, we may define the **adjacency matrix** A_G: for unweighted graphs, it is a 0/1-matrix where the entry $(A_G)_{jk}$ is 1 if and only if $(j,k) \in E$, while for weighted graphs it is the matrix formed by the set of weights $(A_G)_{jk} = w_{jk}$, with $w_{jk} := 0$ if $(j,k) \notin E$. We will sometimes abuse our conventions by assuming that an edge disappears whenever a weight w_{jk} is set to 0 on purpose, but this should be clear from the context. In general, we allow self-loops, which are edges of the form (j, j).

Thanks to the mapping to graphs, we can use various notions from graph theory. We denote with $G - j$ the graph G in which the vertex j and all the edges incident to

[1] In physics, the jargon *solving a model* is often used, which vaguely means that the eigensystem of a certain family of Hamiltonians is obtained analytically. Still, with the huge (or possibly infinite) dimensionality of space, an explicit description is often not realistic. Depending on the situation, 'solving' could mean as much as finding the ground state and its corresponding energy, finding the free energy, finding the partition function, or expressing the eigenstates in the form of correlation functions or recursive procedures.

j are removed. The **degree** of a vertex is the number of edges incident to that vertex, and likewise, the (maximum) degree of a graph is the largest degree found on any of its vertices. A **bipartite graph** has a vertex set V which can be separated into two disjoint subsets V_1, V_2 such that each edge $(j,k) \in E$ must run *between* V_1 and V_2 (that is, $j \in V_1$ and $k \in V_2$ or vice-versa). Two sites j and k are **connected** if there exists a path of edges between the two sites with nonzero weights, i.e. there exists a sequence $(w_{j,a_1}, w_{a_1,a_2}, \dots w_{a_n,k})$ of nonzero elements. A graph or subsystem is connected if all pairs of vertices within that graph or subsystem are connected. If a system is not connected, it may consist of non-connected islands. We then use **connected components** to refer to these islands, i.e. the largest possible subsystems in which all vertices are connected.

This way, we can define a spin Hamiltonian using a given graph $G = (V, E, w)$ and a type of interaction $\{\beta^{pq}\}_{p,q=1}^{3}$:

$$H = \sum_{(j,k)\in E} w_{jk} h_{jk}, \tag{2.9}$$
$$h_{jk} = \sum_{p,q\in\{1,2,3\}} \beta^{pq}\, \vec{\sigma}_j^{\,p}\, \vec{\sigma}_k^{\,q}.$$

Likewise, given a model in which the type of interaction is constant, we can deduce some interaction graph G. The weight values w_{jk} arise under various different names in literature, such as **couplings** or **interaction strengths**.

In order to represent a Hamiltonian, which has to be Hermitian, the graphs G are required to be *undirected*, meaning that edges always appear in both 'directions' ($(j,k) \in E \iff (k,j) \in E$), with opposite weights respecting $w_{jk} = w_{kj}{}^*$. The language of graphs will turn out to be useful at various points throughout this thesis, especially in Part III, where we extend the possible graphs on which certain protocols are known to work.

2.2.2 Diagonalization using symmetries

Assume our Hamiltonian H admits some symmetry, in the sense that there is a unitary operation A that does not cause the system's energy to change:

$$AHA^\dagger = H \iff [H, A] = 0. \tag{2.10}$$

Then, knowing the eigensystem of A (which is often easier to obtain) could help us diagonalize H. For each *non-degenerate* eigenvalue of A, the corresponding eigenvector must also be an eigenvector of H. Eigenvalues of A with higher multiplicities are slightly more involved. Assume we know the eigenbasis of A, and we collect all eigenspaces with the same eigenvalue. Then, A is of the form

$$A = \mu_1 \mathbb{1}_{d_1} \oplus \mu_2 \mathbb{1}_{d_2} \oplus \dots \oplus \mu_J \mathbb{1}_{d_J},$$

where $\{\mu_j\}_{j=1}^{J}$ are the distinct eigenvalues of A, each corresponding to an eigenspace of dimension d_j. Then H, in the same basis, must be of the form

$$H = H_1^{(d_1\times d_1)} \oplus H_2^{(d_2\times d_2)} \oplus \dots \oplus H_J^{(d_J\times d_J)}, \tag{2.11}$$

where we denote the shape of the matrices H_j in superscripts. The proof, with a little quantum sauce, is as follows. Let $|\phi\rangle$ be an eigenvector of A such that $A|\phi\rangle = \mu_j|\phi\rangle$.

But $|\phi\rangle$ needs not necessarily be an eigenvector of H, so perhaps $H|\phi\rangle = \sum_k \alpha_k |k\rangle$ with $\alpha_k = \langle k|H|\phi\rangle$. What we do know is that $AH|\phi\rangle = \mu_j H|\phi\rangle$, hence whatever states $|k\rangle$ appear in the superposition $\sum_k \alpha_k |k\rangle$, surely they cannot have an A-eigenvalue other than μ_j. Thus $\langle k|H|\phi\rangle = 0$ whenever $|k\rangle$ and $|\phi\rangle$ have a different A-eigenvalue, allowing us to derive Eq. 2.11. We can summarize the whole argument as *H preserves A, so it can never map a quantum number μ_j to some other quantum number.*

When H is written in the form of Eq. 2.11, we say that H **block-diagonalizes** into J blocks, with sizes d_j, and the subspace corresponding to some eigenvalue μ_j of A will be called a **sector** or **conserved subspace**.

In fact, any symmetry operator A allows us to give some structure to the eigenstates of H, by **labeling** them as $|\mu_j, \ldots\rangle$, where we leave some space in the ket for other labels that may be needed to uniquely identify a state. This is a well-known convention in the theory of angular momentum, where $|s, m\rangle$ labels a state with $\hat{S}^2_{\text{tot}}$-eigenvalue $s(s+1)$, and simultaneously $\hat{S}^z_{\text{tot}}$-eigenvalue m. Moreover, the computational basis states $|0\rangle$ and $|1\rangle$ can be interpreted as being the $+1$ and -1 eigenvectors of the operator Z. As theorists, we do not necessarily have a clue what these states actually are, especially if we do not care what Z actually 'means' in the real world. In a sense, all we care about is that the states are well-defined with respect to some labeling operator, and that all other operators involved satisfy the correct commutation relations with the labeling operator and with each other. Of course, whenever the Hamiltonian does not have enough symmetries to label all states uniquely, we may resort to the 'ugly' approach where a state is defined as the k'th eigenvector of H within a conserved subspace.

2.3 The Ising model

Let us now turn to some frequently encountered models. The **Ising model** on a weighted graph $G = (V, E, w)$ is described by

$$H_{\text{Ising}} = \sum_{(j,k)\in E} w_{jk} Z_j Z_k \tag{2.12}$$

which equivalently describes models with interactions of the form $X_j X_k$ or $Y_k Y_k$, up to a local basis transformation. We choose to analyze the model as given in Eq. 2.12 such that the Hamiltonian is diagonal, and the computational basis states are eigenstates. Note that H is invariant whenever all qubits are flipped, $H_{\text{Ising}} = X^{\otimes N} H_{\text{Ising}} X^{\otimes N}$, such that each eigenspace is (at least) two-dimensional.

Whenever $w_{jk} \leq 0$, clearly the ground state is of the form $\alpha|0^{\otimes n}\rangle + \beta|1^{\otimes n}\rangle$, because whenever all qubits are in the same state, the energy of each individual term of H is minimized. The choice of weights is often called **ferromagnetic** (FM), as the spins tend to align, just as in the material iron.

Whenever $w_{jk} \geq 0$, the bits prefer to anti-align to minimize each term. This may not always be possible: whenever G has a *cycle* of odd length, not all neighboring spins can anti-align. In such cases, the system is called **frustrated**, and finding the ground state of such systems is typically a lot harder. On the other hand, whenever the interactions form a bipartite graph with parts V_1 and V_2, then there is a clear ground subspace, spanned by the two Néel states

$$|\text{Néel}^{\pm}\rangle = |0^{\otimes|V_1|}\rangle_{V_1} |1^{\otimes|V_2|}\rangle_{V_2} \pm |1^{\otimes|V_1|}\rangle_{V_1} |0^{\otimes|V_2|}\rangle_{V_2}.$$

We call such systems **anti-ferromagnetic** (AFM) for the tendency of the spins to anti-align.

Despite its simplicity, even this fairly classical model is notoriously hard to completely solve. The 1D chain is 'easy', in the sense that it is efficiently solvable by a Jordan-Wigner mapping to free fermions (see below). On the other hand, finding the ground state or partition function of the 3D grid with local fields is equivalent to solving NP-complete problems [Ist00], so it is unlikely that a closed-form solution exists. Between these two extremes, there are many intermediate cases, many of which are unsolved open problems [MM12].

2.4 The XX model and free fermions

The **XX model**, or spin hopping model, on a weighted graph $G = (V, E, w)$, is described by

$$\begin{aligned} H_{\mathrm{XX}} &= \frac{1}{2} \sum_{(j,k)\in E} w_{jk} \left(X_j X_k + Y_j Y_k \right) \\ &= \sum_{(j,k)\in E} w_{jk} \left(\sigma_j^+ \sigma_k^- + \sigma_j^- \sigma_k^+ \right) \end{aligned} \tag{2.13}$$

The model's name XX refers to the two different interaction terms, $X_j X_k$ and $Y_j Y_k$ having equal amplitude - a model with different scalars in front of the X and Y parts would be called XY model. For some extra confusion, some literature refers to Eq. 2.13 as XY model [CDE+04; OEO+07].

First of all, notice that the total z-magnetization $Z_{\mathrm{tot}} = \sum_j Z_j$ is conserved,

$$[H_{\mathrm{XX}}, Z_{\mathrm{tot}}] = 0$$

hence the Hamiltonian decomposes into blocks of constant number of 'spin ups'. We use the term **Hamming weight** to denote the number of qubits that are in the state $|1\rangle$. All H_{XX} really does is making spin up excitations 'hop' towards empty (spin down) neighboring sites. The form of H_{XX} is reminiscent of free fermion hopping, except that the spin operators $\sigma_j^{\pm}$ at different sites commute rather than anti-commute.

As first described by Lieb, Schultz and Mattis [LSM61], if we restrict ourselves to working on an open chain ($G = P_N$), the model can be solved analytically by using the Jordan-Wigner transformation [JW28]. We define

$$f_j^\dagger = [\prod_{k<j} Z_k]\sigma_j^-, \quad f_j = [\prod_{k<j} Z_k]\sigma_j^+, \tag{2.14}$$

where f_j now obey precisely the canonical anti-commutation relations that are normally associated to fermionic particles:

$$\{f_j, f_k^\dagger\} = \delta_{jk}, \quad \{f_j, f_k\} = 0, \quad \{f_j^\dagger, f_k^\dagger\} = 0. \tag{2.15}$$

The product $\prod_{k<j} Z_k$ makes the operators highly non-local, forming the so-called *string operator* that trails the raising and lowering operators over the graph. Intuitively, the string counts the number of fermions one has to 'jump over' in order to create or annihilate a fermion at position j, which in turn leads to proper anti-commutative properties. On a general graph, this would lead to a rather involved Hamiltonian, but it

happens that on the open chain, the string operators of σ_j^+ and σ_{j+1}^- precisely cancel. Eq. 2.13 then becomes

$$H_{\text{ff chain}} = \sum_{j=1}^{N} w_{j,j+1} \left(f_j^\dagger f_{j+1} + \text{h.c.} \right). \tag{2.16}$$

The latter is an example of a **free fermion** model, in which individual particles jump around over the lattice, without explicitly affecting one another. Clearly, the particles are *non-interacting*, and we may just as well treat the system as if just a single particle is present in it. This reduces the dimensionality of our problem from 2^N down to just N, making it efficient to solve. In fact, our treatment below works for general models of free fermions hopping on any weighted graph G (with, of course, $w_{jk} = w_{kj}^*$):

$$H_{\text{ff}} = \sum_{j,k=1}^{N} w_{jk} f_j^\dagger f_k \tag{2.17}$$

Mathematically, our goal is to massage Eq. 2.16 into the form

$$H_{\text{ff diag}} = \sum_{k=1}^{N} \lambda_k c_k^\dagger c_k \tag{2.18}$$

through a canonical basis transformation

$$c_k^\dagger = \sum_{j=1}^{N} U_{j,k} f_j^\dagger, \quad c_k = \sum_{j=1}^{N} (U^\dagger)_{k,j} f_j, \tag{2.19}$$

$$f_j^\dagger = \sum_{k=1}^{N} (U^\dagger)_{k,j} c_k^\dagger, \quad f_j = \sum_{k=1}^{N} U_{j,k} c_k. \tag{2.20}$$

where U is a unitary matrix we get to pick ourselves, and the operators $c^\dagger$ are often said to create (fermionic) **modes** or **quasi-particles**. The effect of plugging this transformation into Eq. 2.17 is

$$\begin{aligned} H_{\text{ff}} &= \sum_{j,k=1}^{N} \sum_{k_1,k_2=1}^{N} w_{jk} U_{k_1,j}^\dagger U_{k,k_2} c_{k_1}^\dagger c_{k_2} \\ &= \sum_{k_1,k_2=1}^{N} \left(U^\dagger w U \right)_{k_1,k_2} c_{k_1}^\dagger c_{k_2}. \end{aligned}$$

To retrieve the form of Eq. 2.18, we require $(U^\dagger w U)_{jk} = \delta_{jk} \lambda_k$. In other words, the basis transformation amplitudes U_{jk} are precisely the entries of the matrix U that *diagonalizes* w. In fact, we could have seen this in a more handwaving way too: the Hamiltonian H_{ff} block-diagonalizes into sectors with fixed particle number. Restricting to just a single fermion, the Hamiltonian is precisely the matrix w. Clearly, the single-particle energies are the eigenvalues of w, and the eigenstates correspond to the eigenvectors of w.

Having obtained Eq. 2.18, we may now read off the full eigensystem of H_{XX}. The eigenstates are of the form

$$|\vec{s}\rangle_c = (c_1^\dagger)^{s_1} (c_2^\dagger)^{s_2} \dots (c_N^\dagger)^{s_N} |0\rangle \tag{2.21}$$

where $s \in \{0,1\}^N$ is a binary string of length N that denotes *which fermionic modes are absent/present*, and $|0\rangle$ is the fermionic vacuum. The subscript of a ket, such as the c in $|\vec{s}\rangle_c$, denotes the *basis* in which the state is given – we will use this convention throughout this thesis. The energies of the eigenstates are *sums of single-particle energies*:

$$H_{\text{ff}}|\vec{s}\rangle_c = \left(\sum_{k=1}^{N} s_k \lambda_k\right)|\vec{s}\rangle_c. \tag{2.22}$$

One might wonder what a state like $|\vec{s}\rangle_c$ looks like in our 'natural' basis, consisting of local fermionic operators f or even going back to spins $\sigma^{\pm}$. The product of $c^\dagger$ operators in Eq. 2.21 leads to a huge number of terms, each with the same number of f operators applied to $|0\rangle$. Many of these terms will drop out, because any two fermions at the same location are not allowed ($f_j^\dagger f_j^\dagger = 0$). In fact, the result is a weighted sum over *all combinations of unique f operators*, weighted by some function F:

$$|\vec{s}\rangle_c = \sum_{z\in\{0,1\}^N} F(\vec{s},\vec{z})|\vec{z}\rangle_f.$$

The function $F(\vec{s},\vec{z})$ is a large sum, in which each term is a product of weights $U_{j,k}$. These are precisely the matrix elements obtained when converting a certain c_k operators (given by $\vec{s}$) into one of the possible f_j operators (described by $\vec{z}$), except for the minus signs that appear when re-ordering the f operators. This happens to correspond precisely to taking the determinant! Hence, we claim that

$$F(\vec{s},\vec{z}) = |U_{\vec{s},\vec{z}}|,$$

where $|\cdot|$ denotes the determinant of a matrix. With $U_{\vec{s},\vec{z}}$ we denote the matrix U with only the rows k kept corresponding to $s_k = 1$, and likewise, where columns j are kept only if $z_j = 1$. We define the determinant of a non-square matrix to be zero, such that any strings $\vec{z}$ that do not have the same Hamming weight (i.e., number of particles) as $\vec{s}$ drop out. The function F is closely related to the **Slater determinant**, which is used to represent that second quantized Fock states in first quantized notation [AS10].

In Chapter 5, we will put the techniques discussed here to creative use: we try to make JW string operators that cover precisely half of the system, such that highly non-local terms appear in the Hamiltonian. The time-evolution of such Hamiltonians would allow one to make fast multiqubit logic gates that would otherwise take a large circuit. To quantify precisely how long the gate takes, we need to calculate the matrix element of the JW string sandwiched between different eigenstates. By representing these eigenstates as Slater determinants, we obtain analytical expressions for the matrix elements, again in the form of determinants of sub-matrices of U.

2.5 The XXX model, or Heisenberg model

For this model, we consider not only qubits (which are spin-$\frac{1}{2}$ particles), but also more general particles of arbitrary spin. Recall that for a *single* spin particle, the three spin operators, $\vec{S} = \{\hat{S}^x, \hat{S}^y, \hat{S}^z\}$, are Hermitian operators acting on the spin vector space $(s) = \mathbb{C}^d$, of dimension $d = 2s+1$. The spin operators have unique eigenvalues $\{-s, -s+1, \ldots s-1, s\}$, and as usual, we choose to work in the basis in which $\hat{S}^z$ is diagonal. The basis vectors are thus uniquely identified by the eigenvalue m of $\hat{S}^z$. Moreover, the

operator $\hat{S}^2 = (\vec{S})^2 = \vec{S}\cdot\vec{S}$ commutes with each of the three spin operators and has a single eigenvalue, $s(s+1)$. In fact, one may use this operator to define the value s of a spin representation (s). Note the subtle difference between the many appearances of the letter S. For clarity, we adhere to the convention that spin-related scalars (often eigenvalues) get lowercase symbols. Spin operators are capitalized and wear a hat, and spin vectors are overlined with an arrow.

The (isotropic) Heisenberg model, or XXX model, can be defined on a set of n spin particles, each with a possibly different spin. The term isotropic refers to the weights β^{pq} being equal in each of the three spin directions x, y and z, which is not to be confused with *homogeneous*, typically used to indicate that there is no spatial variation in the couplings w_{jk}. We let subscripts denote the particle (or set of particles) on which an operator acts. For example, particle j has a total spin s_j. Given a weighted graph $G = (V, E, w)$, the Heisenberg model is described by

$$\begin{aligned} H_{\mathrm{H}} &= \sum_{(j,k)\in E} w_{jk}\vec{S}_j\cdot\vec{S}_k \\ &= \sum_{(j,k)\in E} w_{jk}\left(\hat{S}_j^x\hat{S}_k^x + \hat{S}_j^y\hat{S}_k^y + \hat{S}_j^z\hat{S}_k^z\right) \\ &= \sum_{(j,k)\in E} w_{jk}\left(\frac{1}{2}\left[\hat{S}_j^+\hat{S}_k^- + \hat{S}_j^-\hat{S}_k^+\right] + \hat{S}_j^z\hat{S}_k^z\right). \end{aligned} \tag{2.23}$$

Here, the spin raising and lowering operators are defined as $\hat{S}^\pm = \hat{S}^x \mp i\hat{S}^y$. Also note that, specifically for spin-$\frac{1}{2}$ particles, the interaction can be written as a SWAP-operation, up to addition by $\mathbb{1}$:

$$\frac{1}{2}\left(X_jX_k + Y_jY_k + Z_jZ_k + \mathbb{1}_4\right) = \begin{pmatrix} 1 & 0 & 0 & 0 \\ 0 & 0 & 1 & 0 \\ 0 & 1 & 0 & 0 \\ 0 & 0 & 0 & 1 \end{pmatrix}. \tag{2.24}$$

Owing to the inner product between the vectors of spin operators $\vec{S}$ in the top line of Eq. 2.23, H_{H} depends only on the *relative* orientation of the spin particles, but does not reference any absolute direction. Hence, we expect the system to be invariant under arbitrary global rotations around the x, y and z-axis, where all spin particles rotate in the same way. We make this precise as follows. We define total spin operators

$$\hat{S}_{\mathrm{tot}}^x = \sum_{j=1}^n \hat{S}_j^x, \quad \hat{S}_{\mathrm{tot}}^y = \sum_{j=1}^n \hat{S}_j^y, \quad \hat{S}_{\mathrm{tot}}^z = \sum_{j=1}^n \hat{S}_j^z, \tag{2.25}$$

which we sometimes like to take together as $\vec{S}_{\mathrm{tot}} = (\hat{S}_{\mathrm{tot}}^x, \hat{S}_{\mathrm{tot}}^y, \hat{S}_{\mathrm{tot}}^z)$ (note the difference with $\vec{S}_j$ of a *single* spin!). These are generators of global rotations of the form $U(\vec{\theta})^{\otimes n}$, with $U(\vec{\theta}) = \exp(-i\vec{S}\cdot\vec{\theta})$. The Hamiltonian is actually invariant under these rotations, because

$$[H_{\mathrm{H}}, \hat{S}_{\mathrm{tot}}^\alpha] = 0, \quad \alpha \in \{x, y, z\}. \tag{2.26}$$

In proving the above, we save ourselves some work by noting that H_{H} is symmetric under any permutation of the labels x, y, z, hence we choose to only show commutativity for the z-component. This, in turn, can be seen from the bottom line of Eq. 2.23.

The terms $\hat{S}_j^+ \hat{S}_k^- + h.c.$ are reminiscent of hopping in the XX model (Section 2.4) and conserve the total z-magnetization. Also the terms $\hat{S}_j^z \hat{S}_k^z$ clearly commute with $\hat{S}_{\text{tot}}^z$. Altogether, we find that indeed the number of spin excitations in *any* direction is conserved, and equivalently, that the Hamiltonian is symmetric under rotations generated by any $\hat{S}_{\text{tot}}^\alpha$.

Using the previous result, we also find that

$$[H_{\text{H}}, (\hat{S}_{\text{tot}})^2] = 0, \tag{2.27}$$

where $\hat{S}_{\text{tot}}^2 = \vec{S}_{\text{tot}} \cdot \vec{S}_{\text{tot}}$. Having found two operators that commute with the Hamiltonian, we know that we can label our eigenstates as $|s, m\rangle$, where s is some eigenvalue related to $\hat{S}_{\text{tot}}^2$ (which we will come back to in a bit), and m is the z-magnetization eigenvalue of $\hat{S}_{\text{tot}}^z$. Note that we can not do better at this point, because $\hat{S}_{\text{tot}}^x$ and $\hat{S}_{\text{tot}}^y$ do not commute with $\hat{S}_{\text{tot}}^z$.

Now, what precisely are these subspaces, labeled by s and m, which are invariant under the actions of $\hat{S}_{\text{tot}}^z$ and $\hat{S}_{\text{tot}}^2$? We saw that the rotations $U(\vec{\theta})$ generated by $\vec{S}_{\text{tot}}$ commute with H. Intuitively, these operators rotate the system as a whole, leaving relative angles unchanged, hence preserving the system's energy. The system behaves *almost* as if it collectively forms a single spin particle, with a potentially huge total spin. This total spin is precisely the variable s of the collective system.

In the following, we resort to the representation theory of spin particles to make this statement more precise. We will find that the total space spanned by n 'real' spin particles decomposes into various 'virtual' spin particles. The decomposition is such that the operators $\hat{S}_{\text{tot}}^\alpha$ rotate these virtual spins as if these are elementary spin particles, and in particular, do not mix the states of different virtual particles. The particles each have a well-defined spin s, which can be retrieved by acting on the spin states with the operator $\hat{S}_{\text{tot}}^2$.

Exploiting that (s) is an irreducible representation of the algebra $\mathbf{su}(d)$, we can combine multiple spin particles, taking the tensor products of spin spaces $(s_1), (s_2)$ to form the new space $(s_1) \otimes (s_2)$. Within the new space, new irreducible representations of $\mathbf{su}(d')$ can be found, which look precisely as the single-particle spaces (s) that we are used to. The precise formulation is given by the **Clebsch-Gordan rule**:

$$(s_1) \otimes (s_2) = \bigoplus_{s=|s_1-s_2|}^{s_1+s_2} (s). \tag{2.28}$$

This rule can be applied iteratively to obtain the decomposition of the space of n spin particles, each having spin $s_1, s_2, \ldots, s_j, \ldots, s_n$:

$$\bigotimes_{j=1}^{n} (s_j) = \bigoplus_s N^s_{s_1,s_2,\ldots s_n} (s). \tag{2.29}$$

Here, $N^s_{s_1,s_2,\ldots s_n}$ denotes the multiplicity with which the spin representation (s) appears. In other words, upon combining *real* spin particles, we retrieve a huge number of *virtual* spin particles. This structure of the total Hilbert space is depicted in Fig. 2.2. In each of these spaces (s), the spin operators $\vec{S}_{\text{tot}}$ act just like how $\vec{S}$ would act on a normal, isolated particle of total spin s. The operator $\hat{S}_{\text{tot}}^2$ now plays a more interesting role: it probes spin of the virtual particle, returning the eigenvalue $s(s+1)$.

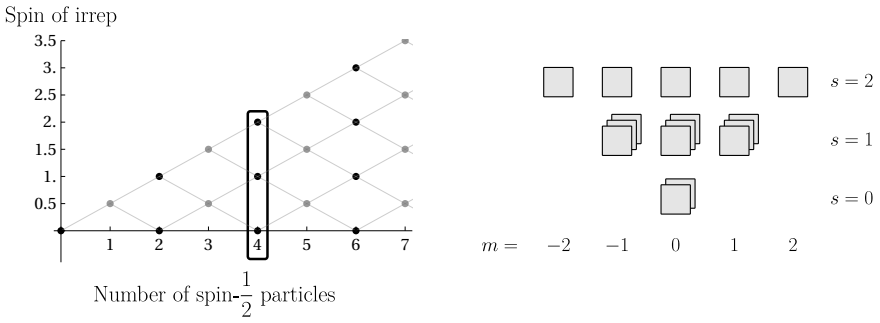

Figure 2.2: The irreducible (spin) subspaces for a system of n spin-$\frac{1}{2}$ particles. Left: The space $(s)^{\otimes n}$ (n labeled horizontally) decomposes into spaces of spin s' (vertically) by iterative application of Eq. 2.28. The multiplicities $N^{s'}_{\frac{1}{2},\ldots,\frac{1}{2}}$ are given by the number of paths leading to a point (n,s) starting at $(0,0)$. Right: For $n = 4$, eigenstates of H_{H} have a fixed total spin $s = 0, 1$ or 2 (vertical), whose $2s+1$ basis states can be labeled by their z-magnetization m (horizontal). In this case, the multiplicities of the spin spaces are 2, 3 and 1, respectively, which we depict as copies closely behind one another. This way, each square corresponds to a single state.

Let us now turn back to the Heisenberg Hamiltonian of Eq. 2.23, with the aim of diagonalizing it. We know that it commutes with $\hat{S}^2_{\mathrm{tot}}$, which takes the form

$$\hat{S}^2_{\mathrm{tot}} = \bigoplus_s s(s+1)\, \mathbb{1}_{(2s+1)\times N^s_{s_1,\ldots,s_n}} .$$

Moreover, H_{H} commutes with $\hat{S}^z_{\mathrm{tot}}$, which depends only on the Hamming weight of a state. This way, we can see that H_{H} decomposes into blocks, each acting on a subspace of fixed eigenvalues s, m. Note that the energy of two states with the same values of s, m *can* actually differ, because there may be multiple irreps with the same s. On the other hand, within each irrep (s), due to rotational invariance, the energies are equal for each m.

Ferromagnetic case Just as with the Ising model, we can easily guess *some* of the ground states when couplings are *ferromagnetic*, $w_{jk} \leq 0$. We already noted that neighboring states that have their spin aligned are energetically favorable. Indeed, we find that each two-body interaction in Eq. 2.23 is minimized whenever all spins j have either maximum z magnetization $|m = s_j\rangle$ or minimum z magnetization $|m = -s_j\rangle$. These states have the minimum and maximum possible total z-magnetization, $m = \pm\sum_j s_j$, and hence must correspond to the unique spin representation with the highest possible spin, $(s = \sum_j s_j)$. By rotational symmetry, all other values of m share the same energy under H_{H}, hence the ground space is spanned by *at least* the states $|s = \sum_j s_j, m\rangle$. We have not shown that these are the *only* ground states - there could in principle be states with different s with the same ground energy.

Anti-ferromagnetic case Equivalently, we may consider the *anti-ferromagnetic* setting of couplings, where $w_{jk} \geq 0$. On a frustration-free graph, one might naively think that the Néel state is again a lowest energy state, but one can check that the bottom line in Eq. 2.23 does not allow this state as an eigenstate (due to the hopping terms

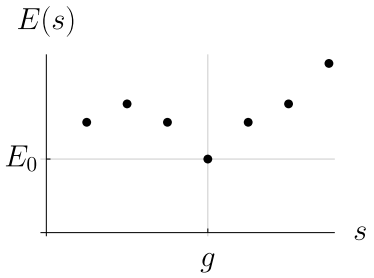

Figure 2.3: A plot of a mock function $E(s)$ that would be in line with the Lieb-Mattis theorem. As long as $s > g$, then the function is strictly increasing. If $s < g$, then we cannot say anything about the ordering of energies, but at least we know all energies are higher than the ground state occurring at $s = g$.

$\hat{S}_j^+ \hat{S}_k^-$). Lieb and Mattis [LM62] found a more concrete description of the ground state as long as the system's graph is a *bipartite* graph. On these graphs, we define the spin imbalance g as the difference between the maximum allowed spin of each part:

$$g = \sum_{j \in V_1} s_j - \sum_{j \in V_2} s_j = \max s_{V_1} - \max s_{V_2}. \tag{2.30}$$

Note that spin imbalances can be simply added when combining spin systems: if subsystems have spin imbalances $g_1, g_2, \ldots$, then the combined system has a spin imbalance $g = \sum g_j$. The result by Lieb and Mattis can then be stated as follows:

Theorem (Lieb-Mattis)**.** *Let G be a weighted, connected, bipartite graph, whose weights are anti-ferromagnetic ($w_{jk} \geq 0$). Then, the ground state of H_H has total spin $s = g$. Moreover, if $E(s)$ denotes the* lowest *energy of the subspace with fixed total spin s, then*

$$E(s+1) > E(s) \text{ for all } s \geq g,$$
$$E(g) < E(s) \text{ for all } s < g.$$

A cartoon of this result is shown in Fig. 2.3. The result shows that, in particular, if the maximum allowed spins on V_1 and V_2 are equal, then the ground state has $s = 0$, i.e. it is a singlet and non-degenerate. If $s_{V_1} = s_{V_2} + \frac{1}{2}$, then the ground state has $s = \frac{1}{2}$ and the ground state is 2-dimensional (allowing one to encode a qubit), and so forth.

Proof. The proof of the theorem uses the following argument. I recommend keeping the RHS of Fig. 2.2 in mind for a better understanding.

1. **Within the subspace of fixed $(\hat{S}_{\mathbf{tot}})^z = m$, there is a unique ground state $|\psi_{\mathbf{gs}}^m\rangle$ with all-positive coefficients (in a specific basis).**

   Consider the rotation $U = \prod_{j \in V_1} \hat{S}_j^z$. Then, $U H_{\mathrm{H}} U^\dagger$ looks as follows in the computational basis: all diagonal elements (from terms $\hat{S}_j^z \hat{S}_k^z$) are *positive* and all off-diagonal elements (from $\hat{S}_j^- \hat{S}_k^+ + \text{h.c.}$) are *negative*. Hence, within each block of fixed m, the *unique* lowest energy state is a superposition of basis states with only *positive* coefficients (by the Perron–Frobenius theorem). We denote this state by

$|\psi_{\text{gs}}^m\rangle$. The state has nonzero overlap with *all* computational basis states with $(\hat{S}_{\text{tot}})^z = m$, because the hopping terms map to all states with the same m, unless some sites are disconnected. Because it is impossible to make two orthogonal states with positive amplitude on every single basis element, this ground state must be unique (per value of m).

2. **If $|\psi_{\text{gs}}^m\rangle$ has $s = m$, then $E(s+1) > E(s)$.**

   Note that the subspace with total spin s includes all m up to and including s. This means that the lowest-energy state with fixed m, $|\psi_{\text{gs}}^m\rangle$, could possibly lie in all subspaces with total spin $s \geq m$. If $|\psi_{\text{gs}}^m\rangle$ lies in the space $s = m$, then $s+1$ must contain only states with a strictly higher energy.

   Graphically, on the LHS of Fig. 2.2, if $|\psi_{\text{gs}}^m\rangle$ has $s = m$, then the ground state of an m-column occurs in the lowermost row. All higher rows also contain states with the same m, but they happened to not hold the ground state, hence these rows must have strictly higher energies. Thus, $E(s+1)$ must be larger than $E(s)$.

3. **For a special Hamiltonian $\tilde{H}$, for all $s \geq g$, the state $|\psi_{\text{gs}}^m\rangle$ has $s = m$.** Let $\tilde{H}$ be the Hamiltonian of the isotropic Heisenberg where all allowed edges have weight $w_{jk} = 1$ (recall that the graph was assumed to be bipartite):

$$\tilde{H} = \sum_{j \in V_1,\, k \in V_2} \vec{S}_j \cdot \vec{S}_k = \vec{S}_{V_1} \cdot \vec{S}_{V_2}.$$

   Here, we defined $\vec{S}_{V_x} = \sum_{j \in V_x} \vec{S}_j$. Note that $\vec{S}_{\text{tot}} = \vec{S}_{V_1} + \vec{S}_{V_2}$ and hence $\vec{S}_{\text{tot}} \cdot \vec{S}_{\text{tot}} = (\vec{S}_{V_1})^2 + (\vec{S}_{V_2})^2 + 2\vec{S}_{V_1} \cdot \vec{S}_{V_2}$. Therefore, we can write $\tilde{H}$ in a form in which all operators mutually commute:

$$\tilde{H} = \frac{1}{2}\left(\hat{S}_{\text{tot}}^2 - (\vec{S}_{V_1})^2 - (\vec{S}_{V_2})^2\right) \tag{2.31}$$

   Then, using s_{V_1} and s_{V_2} to denote the spin eigenvalues related to $(\vec{S}_{V_1})^2$ and $(\vec{S}_{V_2})^2$, the energies $\tilde{\varepsilon}$ of $\tilde{H}$ depend only on the spin values as follows:

$$\tilde{\varepsilon} = \frac{1}{2}\left(s(s+1) - s_{V_1}(s_{V_1}+1) - s_{V_2}(s_{V_2}+1)\right).$$

   To find the ground state, one has to compromise between minimizing s and maximizing $s_{V_{1,2}}$. Due to the form of the Clebsch Gordan rule, Eq. 2.28, we can distinguish two cases. Firstly, if $s \geq g$, then for any choice of $s_{V_{1,2}}$, the minimum possible total spin is $s = |s_{V_1} - s_{V_2}|$. We will now argue that the lowest energy always occurs when $s_{V_{1,2}}$ are maximal. Without loss of generality, assume $s_{V_1} > s_{V_2}$. Then, the energy simplifies to $\tilde{\varepsilon} = -s_{V_1} s_{V_2} - s_{V_2}$. Clearly, the spins on each part should be maximized, and $s = g = |\max s_{V_1} - \max s_{V_2}|$. The state $|\psi_{\text{gs}}^m\rangle$ lives in the sector with the lowest possible energy for the given m, which is, in this case, $s = m$.

   A second case occurs when $s < g$. In this case, the rule $s > |s_1 - s_2|$ tells us that $s_{V_{1,2}}$ cannot be optimized, and it is unclear in what spin sector the state $|\psi_{\text{gs}}^m\rangle$ would live. All we know is that surely $s < g$ is suboptimal - the ground state will not be in this sector.

4. **The state $|\psi^m_{\mathbf{gs}}\rangle$ of a general $H_{\mathbf{H}}$ has the same total spin s as $|\psi^m_{\mathbf{gs}}\rangle$ of $\tilde{H}$.**

   We found that for any choice of weights w that satisfy the assumptions, the state $|\psi^m_{\mathrm{gs}}\rangle$ has only positive entries (in some basis). This holds for $|\psi^m_{\mathrm{gs}}\rangle$ of H_{H} as well as for $\tilde{H}$, meaning that both states have nonzero overlap. Therefore, the value of s of *any* $|\psi^m_{\mathrm{gs}}\rangle$ must be the same as whichever holds for $\tilde{H}$.

Putting it all together, we have to distinguish the two cases again. If we are interested in the sector $s \geq g$, then **3.** and **4.** state that $|\psi^m_{\mathrm{gs}}\rangle$ has $s = m$, and by **2.** the energy as a function of total spin $E(s)$ must be strictly increasing. On the other hand, when $s < g$, we are unable to say anything about $E(s)$. All we know is that the global ground state is not in these sectors. □

In Chapter 9, we will elaborate on these (fairly old) results in the more modern context of adiabatic state transfer, where the uniqueness of each $|\psi^m_{\mathrm{gs}}\rangle$ guarantees an adiabatic protocol to work without encountering degeneracies.

CHAPTER 3

Manipulating quantum states

3.1 How to form a quantum gate

We start by sketching the most elementary methods to change a quantum state. The changes occurring to a quantum state $|\psi\rangle \in \mathscr{H}$ in a closed system (i.e. there is no interaction with the environment) are captured by the Hamiltonian H. This operator plays a dual role in quantum mechanics. Firstly, H is the Hermitian observable whose eigenvalues determine the **energy** λ_j of an eigenstate $|\psi_j\rangle$,

$$H|\psi_j\rangle = \lambda_j|\psi_j\rangle.$$

Secondly, the Hamiltonian uniquely defines a trajectory of a state through the Hilbert space as a function of time, through **Schrödinger's equation**[1] (SE)

$$\partial_t|\Psi(t)\rangle = -iH(t)|\Psi(t)\rangle. \tag{3.1}$$

Note the different notation between $|\psi_j\rangle$ for eigenstates and $|\Psi(t)\rangle$ for time-evolving states, which are generally *not* eigenstates. SE guarantees that $|\Psi(t)\rangle$ evolves in a *unitary* way, making sure that the state is normalized at all times, and that initially orthogonal states remain orthogonal at any time t. We can thus describe the time-evolution of a state as

$$|\psi(t)\rangle = U_t|\psi(0)\rangle$$

where U_t is called the (unitary) **time evolution operator**. Note that we always assume a time evolution to start at $t = 0$. A major part of this thesis is devoted to *solving the time-evolution*, i.e. finding U_t with $H(t)$ given, or the inverse *control problem*, where we try to construct a Hamiltonian $H(t)$ which leads to a required time evolution U_t, within realistic constraints.

Solving time evolutions Sometimes the time-evolution of H is easy to find. For one, if H is time-independent, then

$$U_t = \exp(-iHt) \qquad (H \text{ time-independent})$$

[1] We assume units such that $\hbar = 1$.

where the exponential of a matrix is defined through the Taylor series. This equation is particularly interesting whenever we know the *eigenbasis* of H, such that eigenstates merely pick up a *dynamical phase*

$$|\psi_j(t)\rangle = \exp(-iHt)|\psi_j(0)\rangle = \exp(-i\lambda_j t)|\psi_j(0)\rangle.$$

Of course, finding the eigenbasis itself may be a nontrivial problem. The time evolution is more tricky to solve whenever H is time-dependent, but in Sections 3.1.2 and 3.1.3 we present two cases in which such time evolutions can be solved approximately.

Control problems Given a unitary U_t, one can always find a Hamiltonian H that causes precisely such a unitary time evolution. The solution is $H = \frac{1}{-it}\log(U)$, such that $\exp(-iHt) = U$. With this in mind, one might wonder what is so hard about control problems? The problem is that, in general, the solved Hamiltonian H will be highly non-local, and it may be impossible to engineer such Hamiltonians in nature. To enforce properties such as 2-locality (see Section 2.2), one has to resort to time-dependent Hamiltonians, or sequences of unitary steps.

Practical control problems typically assume a restricted Hamiltonian of the form [DP10]

$$H(t) = H_{\text{bg}} + \sum_j f_j(t) H_j, \tag{3.2}$$

where H_{bg} consists of forces that are always on (and cannot be turned off), whereas various terms H_j can be modulated in amplitude through scalar **controls** $f_j(t)$. The controls themselves may also be subject to certain restrictions. It should be clear that, with these assumptions, it is much more challenging to find a set of time-dependent control functions $\{f_j(t)\}$ that precisely lead to the desired unitary evolution U_t.

Especially in the context of quantum information technology, these control problems have applications in the construction of tiny computational steps on qubits, which are then called **quantum gates**. To develop some intuition for quantum control, let us consider the toy problem constructing a very simple gate: flipping the state of a single quantum bit, as described by the Pauli operator X. The problem is formalized as:

$$\begin{array}{ll} \text{Find controls} & \vec{f}(t) = \{f_x(t), f_y(t), f_z(t)\} \\ \text{such that the system} & H(t) = H_{\text{bg}} + f_x(t)X + f_y(t)Y + f_z(t)Z \\ \text{causes the evolution} & U_t = X. \end{array} \tag{3.3}$$

3.1.1 Quenches

A **quench** is a sudden (often instantaneous) change to a Hamiltonian. In particular, a system that was initially in an eigenstate, may not be after the quench, leading to a non-trivial time evolution. Quenches typically assume that the Hamiltonian, as a function of time, is piecewise time-independent (i.e. constant), but this is no hard rule. We will often use the word 'quench' to mean that a Hamiltonian is turned 'on' at $t = 0$, and is then turned 'off' at some later time T, leading to a well-defined time evolution $U_T = \exp(-iHT)$.

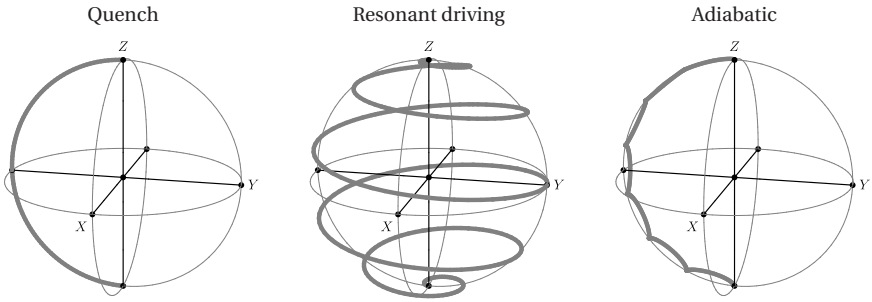

Figure 3.1: The evolution of an initial state $|0\rangle$ by each of the three protocols we discuss, depicted on the Bloch sphere. From left to right: a quench by $H = \Omega X$, a resonant driving protocol (in the lab frame), and an adiabatic protocol executed sufficiently fast, so that some diabatic error is visible ($\Omega T = 7\pi$).

To form a bit-flip, we observe that the Hamiltonian $H = \Omega X$ is precisely the field which *generates* the unitary $U = X$ after a time $t = \frac{\pi}{2\Omega}$,

$$U_t = \exp(-i\Omega X t) = \cos(\Omega t)\mathbb{1} + \sin(\Omega t)X,$$

where the factor of 2 comes from the eigenvalue gap of X. The evolution of an initial state $|\Psi(0)\rangle = |0\rangle$ is depicted on the Bloch sphere in Fig. 3.1.

In general, any time-independent quench on a two-level system can be described as a rotation of the form

$$U_{\hat{n}}(t) = e^{-it\vec{n}\cdot\vec{\sigma}} = \cos(nt)\mathbb{1} - i\sin(nt)\left(\frac{\vec{n}}{n}\right)\cdot\vec{\sigma} \tag{3.4}$$

$$\text{with } \vec{n} = \begin{pmatrix} n_x \\ n_y \\ n_z \end{pmatrix}, \quad n = |\vec{n}| = \sqrt{n_x^2 + n_y^2 + n_z^2}.$$

Such a rotation around the Bloch sphere by an angle $\theta = \frac{nt}{2}$ is sometimes referred to as a θ-pulse. For example, the X-gate we discussed before is a π-pulse around the vector $\vec{n} = (1,0,0)^T$.

We conclude that the problem in Eq. 3.3 with $H_{\text{bg}} = 0$ can be straightforwardly solved by choosing $\vec{f}(t) = \{\Omega, 0, 0\}$, with $\Omega = \frac{1}{2}$. Even if $H_{\text{bg}} \neq 0$, we may use $\vec{f}$ to cancel this field.

3.1.2 Resonant driving, and the rotating frame

Now, let us make the control problem slightly harder, by assuming that the qubit is placed in a magnetic field in the z-direction, which we cannot get rid of. We thus supplement the previous problem with the assumptions

$$H_{\text{bg}} = \frac{\Delta}{2}Z \quad \text{and} \quad f_z(t) = 0.$$

In this case, the previous strategy of turning on the field ΩX causes a rotation around $\vec{n} = (\Omega, 0, \frac{\Delta}{2})^T$, which is not what we want. Intuitively, the Z term causes a state to rotate

around the equator of the Bloch sphere, whereas the X field pulls the state north at one side of the sphere, and south on the other. If the Z-rotations are sufficiently fast, then the movement to the north and south effectively cancel, such that the X-gate is never achieved.

In general, to bridge an eigenvalue gap of size Δ (note the factor 2 due to the eigenvalue gap of Z), one needs to create a driving field with precisely this amount of energy. We claim that the following Hamiltonian does a better job:

$$\begin{aligned} H(t) &= \frac{\Delta}{2} Z + \Omega \Big[\cos(\omega_{\text{drive}} t + \phi) X + \sin(\omega_{\text{drive}} t + \phi) Y \Big] \\ &= \begin{pmatrix} \frac{\Delta}{2} & \Omega e^{-i(\omega_{\text{drive}} t + \phi)} \\ \Omega e^{+i(\omega_{\text{drive}} t + \phi)} & -\frac{\Delta}{2} \end{pmatrix}, \end{aligned} \tag{3.5}$$

with $\omega_{\text{drive}} = \Delta$. Now, when the state oscillates around the equator, the rotation axis $\cos(\omega_{\text{drive}} t) X + \sin(\omega_{\text{drive}} t) Y$ rotates at the same angular velocity, causing it to stay orthogonal to it. This way, it pushes the state north (or south) at all times, without any cancellation effects.

We make this precise using a smarter perspective, the **rotating frame** or **interaction picture**. Effectively, we perceive the system through a camera that looks at the Block sphere, facing downwards from the positive z-axis. By rotating the camera at the same angular velocity ω_{drive}, it seems as if both the rotating state and the rotation axis $\cos(\omega_{\text{drive}} t) X + \sin(\omega_{\text{drive}} t) Y$ stand still, such that we retrieve the quench of Section 3.1.1.

The rotating frame In general, for any Hamiltonian H, we can remove some part H_0 from the Hamiltonian, at the cost of making the remaining parts more complicated. We define the time-dependent basis transformation

$$U_{\text{rf}}(t) = \exp(+i H_0 t). \tag{3.6}$$

We use dots over symbols to denote time derivatives, and let tildes denote quantities in the rotating frame, such that $|\tilde{k}\rangle = U_{\text{rf}} |k\rangle$. Importantly, the rotating frame evolves under a different Hamiltonian $\tilde{H}$, which is not quite simply $U_{\text{rf}} H U_{\text{rf}}^\dagger$. We derive it by starting from the state $|\tilde{k}\rangle$ and rewriting it using all known rules from the normal frame:

$$\begin{aligned} i\partial_t |\tilde{k}\rangle &= i\dot{U}_{\text{rf}} |k\rangle + i U_{\text{rf}} |\dot{k}\rangle && \text{Chain rule} \\ &= -H_0 U_{\text{rf}}(t) |k\rangle + U_{\text{rf}}(t) H |k\rangle && \text{Applied Schödinger in standard picture} \\ &= -H_0 |\tilde{k}\rangle + U_{\text{rf}} H U_{\text{rf}}^\dagger |\tilde{k}\rangle && \text{Convert } |j\rangle \text{ back to rotating frame} \end{aligned}$$

We conclude that the Hamiltonian that governs the rotating frame is given by

$$\tilde{H} = U_{\text{rf}} H U_{\text{rf}}^\dagger - H_0. \tag{3.7}$$

The time-evolution in the rotating frame may be easier to solve. For example, one might obtain the time evolution $\tilde{U}_t$ between times 0 and t. The corresponding unitary in the lab frame is then given by

$$U_t = U_{\text{rf}}^\dagger(t) \tilde{U}_t. \tag{3.8}$$

To gain some more intuition for the effect of the rotating frame: on a Hamiltonian H with matrix elements H_{jk}, the basis transformation $U = e^{i\delta|\ell\rangle\langle\ell|t}$ causes the ℓ'th row and column obtain a rotating phase:

$$\tilde{H} = \begin{pmatrix} H_{11} & \dots & H_{1\ell}e^{-i\delta t} & \dots & H_{1n} \\ \vdots & \ddots & \vdots & & \vdots \\ H^*_{1\ell}e^{i\delta t} & \dots & H_{\ell\ell} - \delta & \dots & H_{\ell n}e^{i\delta t} \\ \vdots & & \vdots & \ddots & \vdots \\ H^*_{1n} & \dots & H^*_{\ell n}e^{-i\delta t} & \dots & H_{nn} \end{pmatrix}$$

Rabi cycles Turning back to our rotation on the Bloch sphere, we can remove the compulsory magnetic field H_{bg} through the basis transformation $U_{\text{rf}} = \exp(+i\frac{\omega_{\text{rf}}}{2}Z)$. The rotating version of the Hamiltonian in Eq. 3.5 then becomes

$$\begin{aligned} \tilde{H} &= \left(\frac{\Delta - \omega_{\text{rf}}}{2}\right) Z + \Omega U_{\text{rf}}\left[e^{-i(\omega_{\text{drive}}t+\phi)}\sigma^+ + e^{+i(\omega_{\text{drive}}t+\phi)}\sigma^-\right]U^\dagger_{\text{rf}} \\ &= \left(\frac{\Delta - \omega_{\text{rf}}}{2}\right) Z + \Omega\left[e^{-i(\omega_{\text{drive}}-\omega_{\text{rf}})t-i\phi}\sigma^+ + e^{+i(\omega_{\text{drive}}-\omega_{\text{rf}})t+i\phi}\sigma^-\right]. \end{aligned} \tag{3.9}$$

In the first step, we used that $\sigma^\pm = \frac{X \mp iY}{2}$, and in the last step, we used $U_{\text{rf}}\sigma^\pm U^\dagger_{\text{rf}} = e^{\pm i\omega_{\text{rf}}t}\sigma^\pm$. Note the difference between the omega's: ω_{drive} is a physical thing, describing the oscillation frequency of the X and Y fields in the lab frame, whereas ω_{rf} is just a parameter invented by us: it describes how fast our camera is rotating. In particular, we like to choose $\omega_{\text{rf}} = \omega_{\text{drive}}$, so the camera follows the driving axis, making the Hamiltonian time-independent:

$$\begin{aligned} \tilde{H} &= \left(\frac{\Delta - \omega_{\text{drive}}}{2}\right) Z + \Omega\left[e^{-i\phi}\sigma^+ + e^{+i\phi}\sigma^-\right] \\ &= \begin{pmatrix} \delta/2 & \Omega e^{-i\phi} \\ \Omega e^{+i\phi} & -\delta/2 \end{pmatrix}. \end{aligned} \tag{3.10}$$

In the last step, we defined the **detuning** or **off-resonance** $\delta = \Delta - \omega_{\text{drive}}$. Evolution by $\tilde{H}$ dictates *Rabi flopping*:

$$\begin{aligned} \tilde{U}_t = e^{-i\tilde{H}t} &= \cos(nt)\mathbb{1} - i\sin(nt)\left(\frac{\vec{n}}{n}\right)\cdot\vec{\sigma} \\ \text{with } \vec{n} = \begin{pmatrix} \cos(\phi)\Omega \\ \sin(\phi)\Omega \\ \delta/2 \end{pmatrix}, &\quad n = \sqrt{\Omega^2 + \frac{\delta^2}{4}}. \end{aligned} \tag{3.11}$$

From this, we conclude that a perfect rotation around the axis $\cos(\phi)X + \sin(\phi)Y$ can be performed if $\delta = 0$ and $t = \frac{\pi}{2\Omega}$, meaning that each computational basis state is inverted into the other. Specifically, at $\phi = 0$, we retrieve the X-gate, and at $\phi = \pi/2$ the gate Y. Remember that all of this is in the rotating frame - we should not forget to move back to the lab frame using Eq. 3.8, which re-inserts the accumulated phase due to H_{bg}. We will use the term **resonant driving** to indicate the choice $\delta = 0$ with the aim to implement such transitions between computational basis states.

We also consider what happens whenever the driving is **off-resonant**, in the limit where $|\delta| \gg |\Omega|$. Here, $\vec{n}$ points mainly in the Z-direction, causing hardly any mixing of the computational basis states, but rather giving the states a hard-to-predict relative phase. This effect is otherwise known as the Autler-Townes or AC Stark effect.

The rotating wave approximation Sometimes, it may be impossible to have both the X and Y fields on at the same time in Eq. 3.5. In that case, we may still work with a Hamiltonian of the form

$$H(t) = \frac{\Delta}{2} Z + 2\Omega \cos(\omega_{\text{drive}} t + \phi) X \tag{3.12}$$
$$= \begin{pmatrix} \frac{\Delta}{2} & \Omega\left(e^{-i(\omega_{\text{drive}} t+\phi)} + e^{+i(\omega_{\text{drive}} t+\phi)}\right) \\ \Omega\left(e^{-i(\omega_{\text{drive}} t+\phi)} + e^{+i(\omega_{\text{drive}} t+\phi)}\right) & -\frac{\Delta}{2} \end{pmatrix},$$

(note that we changed $\Omega \to 2\Omega$ here), which looks slightly more daunting in the same rotating frame we used before:

$$\begin{aligned} \tilde{H} = &\left(\frac{\Delta - \omega_{\text{rf}}}{2}\right) Z \\ &+ \Omega\Big[\sigma^+\left(e^{-i(\omega_{\text{drive}}-\omega_{\text{rf}})t - i\phi} + e^{+i(\omega_{\text{drive}}+\omega_{\text{rf}})t + i\phi}\right) \\ &\quad + \sigma^-\left(e^{-i(\omega_{\text{drive}}+\omega_{\text{rf}})t - i\phi} + e^{+i(\omega_{\text{drive}}-\omega_{\text{rf}})t + i\phi}\right)\Big] \end{aligned}$$

An important clean-up step that is canonically taken at this point is the **rotating wave approximation** (RWA). It tells us that $\omega_{\text{rf}} - \omega_{\text{drive}}$ is a fairly small number, whereas $\omega_{\text{rf}} + \omega_{\text{drive}}$ is huge compared to typical time-scales in our problem. Therefore, the terms $e^{\pm i(\omega_{\text{rf}}+\omega_{\text{drive}})}$ keep causing *off-resonant* rotations back and forth, so fast and so tiny that they merely cause a state to wiggle in phase space, without changing the qualitative behavior of the system. The RWA tells us that we can remove these terms from the Hamiltonian. This approximation is only valid whenever [IGM+05]

$$\begin{aligned} |\omega_{\text{drive}} - \omega_{\text{rf}}| \ll \omega_{\text{rf}}, \omega_{\text{drive}} \quad & \text{such that the other exponentials do rotate slowly, and} \\ \Omega \ll \omega_{\text{rf}}, \omega_{\text{drive}} \quad & \text{such that the wiggles are small.} \end{aligned}$$

One can check that discarding these quickly oscillating terms leaves us with the same Hamiltonian we found in Eq. 3.9, and all the previous conclusions about (off-)resonance apply again.

The resonant X-gate Turning back to our X-gate: the gate can be obtained using the Hamiltonians in Eq. 3.5 or Eq. 3.12. In Fig. 3.1, we sketch the trajectory that an initial state $|0\rangle$ follows on the Bloch sphere in the *lab frame*, in which it quickly oscillates while descending down the sphere. For the case in which driving only occurs along the X-axis (Eq. 3.12), we sketch the same time evolution in the *rotating frame* in Fig. 3.2, such that the error due to the quickly rotating waves is visible.

In Section 4.3, we will come back to the toy model presented here, as it turns out to also be relevant when constructing a quantum gate that acts on multiple qubits.

3.1.3 Adiabatic passage

Assume you are asked to transport a tray filled with fancy-looking yet somewhat wobbly cocktails. Clearly, you want the tray to arrive at its destination in the same *state* that it is now. Your best approach is to accelerate the tray rather slowly, or else you may spill the drinks!

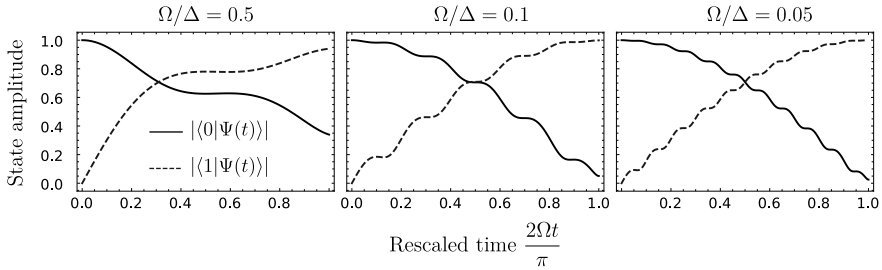

Figure 3.2: The evolution of the initial state $|\Psi(0)\rangle = |0\rangle$ due to the Hamiltonian in Eq. 3.12, in the rotating frame. We assume resonance ($\omega_{\text{rf}} = \omega_{\text{drive}} = \Delta$). When Ω/Δ is *small*, as on the right-hand side, then the RWA is justified, and the evolution is very similar to the quench $H = \Omega X$. When $\Omega/\Delta = 0.1$, the approximation errors are much more visible, and when $\Omega/\Delta = 0.5$, the evolution is far from the aimed trajectory.

The same line of thought turns out to hold in quantum mechanics. If at $t = 0$ a system is in the jth eigenstate of $H(t)$, then it will still be approximately in the jth eigenstate at later times, provided that j is non-degenerate and $H(t)$ changes sufficiently slowly. Note that the *eigenstates* themselves have probably changed in time, providing us with an intuitive method to change a quantum state to our liking. We will study the precise mechanics behind the **adiabatic theorem**, following David Griffiths [Gri05].

As $H(t)$ is now time-dependent, we define that **instantaneous eigensystem** of H as the eigenvalues $\lambda_j(t)$ and eigenvectors $|\psi_j(t)\rangle$ at time t:[2]

$$H(t)|\psi_j(t)\rangle = \lambda_j(t)|\psi_j(t)\rangle. \tag{3.13}$$

We can express any solution to Schrödinger's equation $|\Psi(t)\rangle$ in the basis of instantaneous eigenstates,

$$|\Psi(t)\rangle = \sum_j c_j(t) e^{-i\theta_j(t)} |\psi_j(t)\rangle, \tag{3.14}$$
$$\theta_j(t) = \int_{s=0}^{t} \lambda_j(s) ds',$$

where $\theta_j(t)$ is a dynamical phase that we take out of $c_j(t)$ for later convenience. Plugging this into SE, and omitting explicit time-dependence for readability, we obtain

$$\begin{aligned}
\sum_j \left(\dot{c}_j|\psi_j\rangle + c_j\partial_t|\psi_j\rangle - ic_j\dot{\theta}_j|\psi_j\rangle\right) e^{-i\theta_j} &= \sum_j c_j\lambda_j e^{-i\theta_j}|\psi_j\rangle \\
\sum_j \left(\dot{c}_j e^{-i\theta_j}|\psi_j\rangle + c_j e^{-i\theta_j}\partial_t|\psi_j\rangle\right) &= 0 \\
\dot{c}_k e^{-i\theta_k} + \sum_j c_j e^{-i\theta_j}\langle\psi_k|\partial_t|\psi_j\rangle &= 0 \\
\dot{c}_k(t) &= -\sum_j c_j\langle\psi_k|\partial_t|\psi_j\rangle e^{-i(\theta_j-\theta_k)}.
\end{aligned} \tag{3.15}$$

[2] Note that there is an ambiguity in the *phase* of the eigenvectors, which can be adjusted at each time t. We do not define these phases as these turn out to be unimportant for our purposes, but a rigorous approach can be found in Ref. [BF28].

In the first step, we canceled the last two terms, and in the second, we took the projection to the k'th eigenvector. The quantity $\langle\psi_k|\partial_t|\psi_j\rangle$ already gives some insight in what we mean with the adiabatic theorem: if the instantaneous eigenvector $|\psi_j(t)\rangle$ rotates in the direction of *other* eigenvectors very slowly, then the amplitudes $c_k(t)$ of other eigenvectors do not change too much. To better quantify how much this 'leakage' to other states actually is, we need to replace $\langle\psi_k|\partial_t|\psi_j\rangle$ by something that we obtain as follows, by differentiating the eigenvalue equation, Eq. 3.13:

$$\begin{aligned}\dot{H}|\psi_j\rangle + H\partial_t|\psi_j\rangle &= \dot{\lambda}_j|\psi_j\rangle + \lambda_j\partial_t|\psi_j\rangle \\ \langle\psi_k|\dot{H}|\psi_j\rangle + \langle\psi_k|H\partial_t|\psi_j\rangle &= \dot{\lambda}_j\langle\psi_k|\psi_j\rangle + \lambda_j\langle\psi_k|\partial_t|\psi_j\rangle.\end{aligned}$$

Hence for the 'leaky' states $k \neq j$,

$$\begin{aligned}\langle\psi_k|\dot{H}|\psi_j\rangle + \lambda_k\langle\psi_k|\partial_t|\psi_j\rangle &= \lambda_j\langle\psi_k|\partial_t|\psi_j\rangle \\ \langle\psi_k|\partial_t|\psi_j\rangle &= \frac{\langle\psi_k|\dot{H}|\psi_j\rangle}{\lambda_j - \lambda_k}.\end{aligned}$$

Note that in this step, we had to assume that λ_j is *non-degenerate*. Plugging this back in to Eq. 3.15,

$$\dot{c}_k(t) = -c_k\langle\psi_k|\partial_t|\psi_k\rangle - \sum_{j\neq k}\frac{\langle\psi_k|\dot{H}|\psi_j\rangle}{\lambda_j - \lambda_k}e^{-i(\theta_j-\theta_k)}. \tag{3.16}$$

Now, this expression is *exact*. The adiabatic approximation asserts that the oscillations $e^{-i(\theta_j-\theta_k)}$ are so fast compared to other timescales in our system that on average the second term does not influence $\dot{c}_k(t)$. The rigorous proof was first given by Born and Fock [BF28], but we follow the more accessible notation of Ref. [Kat11].

Firstly, we should define what we mean with 'slow'. Let $\tilde{H}(s)$ be a Hamiltonian on the rescaled time interval $s \in [0,1]$. Then, we can compare the same quantum protocol at different time scales: for each value of total time T, we define the time-dependent Hamiltonian $H_T(t) = \tilde{H}(t/T)$.

Now, assume the system is, at $t = 0$, initialized in the ℓth eigenstate $|\Psi(0)\rangle = |\psi_\ell(0)\rangle$. In other words, we start with state amplitudes $c_k(t=0) = \delta_{k\ell}$. Moreover, we assume that for all t and for all $k \neq \ell$, the energy gap $|\lambda_j(t) - \lambda_k(t)|$ is bounded from below by Δ. Then, under evolution by $H_T(t)$ [Kat11],

$$1 - |\langle\Psi(T)|\psi_\ell(T)\rangle|^2 = O\left(\frac{1}{\Delta^2 T^2}\right). \tag{3.17}$$

In other words, the system's state $|\Psi(t)\rangle$ remains close to the instantaneous eigenstate $|\psi_\ell(t)\rangle$, as long as the total time T of the evolution is sufficiently large, implying slow changes to $H(t)$. Likewise, by conservation of probability, all other states must be minimally populated: $c_k = O\left(\frac{1}{\Delta^2 T^2}\right)$ for all $k \neq \ell$.

Ref. [Kat11] technically assumes a finite-dimensional system, and that the degeneracies of eigenvalues stay constant (i.e. no crossings of energy levels are allowed), even for states other than our initial state $|\psi_\ell(0)\rangle$. The scaling itself is tight, in the sense that examples with the scaling stated in Eq. 3.17 exist, so the bound cannot be improved.

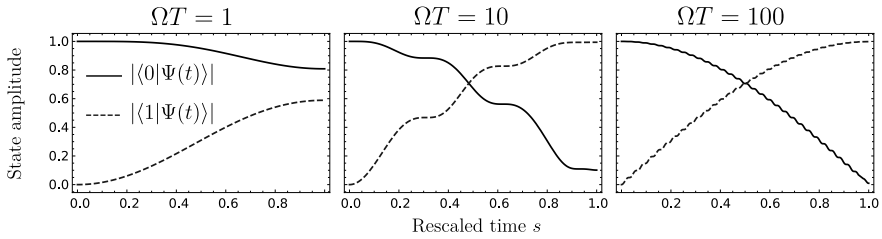

Figure 3.3: The state amplitudes $|c_k(t)|$ during the adiabatic protocol in Eq. 3.18, for different total times T. The initial state is always $|\Psi(0)\rangle = |0\rangle$. When $\Omega T \gg 1$, the system closely follows the corresponding instantaneous eigenstate, up to tiny oscillations. When $\Omega T = 10$, the errors are much more visible, and at $\Omega T = 1$, the system's state cannot keep up with the quickly changing Hamiltonian anymore. The evolution is then very different from the aimed X-gate.

The adiabatic X-gate Let us turn back to the control task of performing the gate $U_t = X$, as defined in Eq. 3.3. Remember the quench of $H = \Omega X$ in Section 3.1.1, which rotates an initial state $|0\rangle$ first towards the negative Y-axis, and then further down towards $|1\rangle$ at the negative Z-axis. Similarly, the state $|1\rangle$ is rotated towards $+Y$ and then towards $+Z$. We can simulate that evolution in the adiabatic limit, using

$$H_T(t) = \Omega\left[\cos\left(\frac{\pi t}{2T}\right)Z - \sin\left(\frac{\pi t}{2T}\right)Y\right]. \tag{3.18}$$

One can check that there are no eigenvalue crossings, and in fact, the energies remain constant at $\pm\Omega$ for each t. Thus, $\Delta = 2\Omega$ in this case. By choosing ΩT sufficiently large, can make sure that an initial state $|0\rangle$ or $|1\rangle$ follows the trajectory defined by the quench to arbitrary accuracy. To obtain a proper X-gate, one also has to care about the accumulated dynamical phases, which equal $e^{\pm i\Omega T}$ in each case. These phases become equal[3] again whenever $\Omega T \in \mathbb{Z}$. The evolution due to Eq. 3.18 is plotted on the right in Fig. 3.1. We chose $\Omega T = 7\pi$, which is sufficiently small that typical *diabatic* errors are visible. The influence of errors at various time scales is compared in Fig. 3.3.

In Part III, we will consider precisely the waiter's task to transport a tray of cocktails, where now the cocktails happen to be quantum states that we aim to transport over a graph. Again, we will find that, for sufficiently slow changes to H, the state can be transported with arbitrary accuracy, provided that there is a *gap* Δ at all times.

3.2 How to transport a quantum state

In the world of *classical* computers, we can hardly imagine living without extensive communication between our devices - whether it is over the internet, a USB cable or bluetooth. Similarly, a future *quantum* computer is expected to require communication with other quantum devices, as is also stated as one of DiVincenzo's criteria [DiV00]. Here, one should not only think of some quantum internet that connects individual users, but also of short-distance communication between nearby quantum

[3] Note that whenever ΩT is odd, a dynamical phase of -1 is given to each of the basis states. In our setting, this is an irrelevant global phase, but note that there exist settings in which a more careful treatment of phases is required.

processors: these may be limited in physical size, but can be entangled to collectively perform a larger calculations [VBC+17; BKM16]. This section reviews the most important known results from the art of moving a quantum state from one place to another.

The no-cloning theorem complicates communication of quantum states: it is impossible to make several copies and perform various attempts of lossy communication. Luckily, there are various tricks to boost fidelities, such as transferring error-correcting codes, or using quantum repeaters. A network of repeaters could work as follows. The noisy communication channel allows a set of parties to distribute entangled Bell pairs among each other, which can be turned into high-fidelity Bell states using entanglement distillation [BBP+96a; BBP+96b; KRH+17]. Next, using entanglement swapping and teleportation, arbitrary qubits can be sent with high fidelity [WEH18]. Transporting states and establishing entanglement appear to be closely related, and we will encounter many physical systems where both go hand in hand.

When it comes to communication over larger distances, photons are a clear winner. They can encode quantum states in various ways (e.g. polarization, Fock number, spatial modes, time-bins), and can travel at high speeds through vacuum or optical fibers. Moreover, high-quality optical fiber networks are already widely implemented for classical communication applications. There is ongoing research on conversion between photonic states and various other qubit platforms, such as trapped ions [MRR+14], superconducting qubits [SZR+17], cold atoms [BBR+18; TSS+19], NV centers [DTM+18], or general qubits locked in a cavity [VVN+17].

For shorter distances, the conversion to light may be omitted in favor of other techniques, which is the focus of the remainder of this chapter and, in particular, of Part III of this thesis. Some types of qubits are mobile by nature, and can be physically displaced. Examples are electrons or atoms that are held in some artificial potential field, such that they can tunnel between nearby minima of the potential. Other information carriers are immobile, such as atoms in a crystal or in a molecule, and one can picture information 'flowing' through the system while the qubits themselves sit still. The latter form of communication can intuitively be compared to flicking a rope that is spanned between two users: the resulting wave travels a long distance between the ends of the rope, while the rope's constituents merely move within their locally confined space. In this sense, classical communication of electrical signals over a copper wire is not that much different. In the following, we focus on both mobile and immobile qubits, as long as the locations of the qubits can be modeled as a finite and discrete graph-like structure.

Having set our domain of interest, we may now ask the question *for which models can we transfer quantum information between Alice and Bob, using which controls?* This brings together the topics of condensed matter models and quantum control: we assume a system defined by an interaction type and a graph, such as discussed in Section 2.2, where two vertices of the graph are marked as Alice (a) and Bob (b). Then, similar to Section 3.1, we tweak the system parameters in such a way that the unitary time evolution U_T after some time T is such that Bob can infer what the initial state at Alice was.

As a warning to the reader, many transfer protocols will look very similar. To distinguish the subtle differences between various theoretical proposals of state transfer, it is important to consider the precise *model* (including the type of particles and type of

	Single excitation	**Half filling**
	$H = \sum W_{jk} jk$	$H = \sum w_{jk} h_{jk}$
	$\|\Psi(0)\rangle = \|a\rangle$	$\|\Psi(0)\rangle = \|\phi\rangle_a \otimes \|\text{rest}\rangle$
	$\dim(\mathscr{H}) \sim N$	$\dim(\mathscr{H}) \sim \exp(N)$
Quench • Fast • Passive couplings • Accurate controls required	(near-)perfect state transfer	XXX with straddling, mirror inverting chains
Adiabatic • Slow • Time-dependent couplings • Resilient to control errors	STIRAP, CTAP, and dark passage (Chapter 8)	XXX model (Chapter 9)

Table 3.1: An overview the state transfer protocols we consider.

interaction), the *graphs* on which the transfer works, the *controls* (typically a quench or adiabatic passage), and the assumed *initial state* of the system. Important figures of merit used for comparison are mainly the (theoretical) transfer speed and fidelity, but also include the feasibility of the *control requirements*, such as the number of controllable parameters in the Hamiltonian.

An overview of the protocols we discuss here is given in Table 3.1, and more elaborate overviews can be found in Refs. [Bos07; NJ14; MBA+16]. We choose to categorize the transfer protocols based on the *initial state*, namely whether they start with a *single* (or a small number of) excitation, or with a number that is *very large* (i.e. growing with the system size N). Within these groups, we distinguish whether the protocol is based on a quench or adiabatic evolution.

One important transfer approach that does not fit within our categorization is the use of sequential `SWAP`-like gates, which are less interesting from a condensed matter viewpoint. Also not discussed are topological variants, such as Thouless pumps [Tho83; VS19], which are typically concerned with effective charge transfer or displacement of a particle's center of mass, rather than communicating quantum information [Cit16]. Note that the repeated nature of topological pumps, which displace a quantum amplitude by a certain number of sites per iteration, is somewhat similar to sequence of swaps from a quantum control perspective.

3.2.1 Single excitation hopping

As far as the models are concerned, it turns out that some physical systems lead to the same mathematics. The ferromagnetic XX and XXX models, with as local entities qubits, are typically taken to be in a magnetic field of the form $H = -B\sum_j Z_j$, such that $|0^N\rangle$ is the ground state. From that state, Alice can locally initialize

$$|\Psi(0)\rangle = \alpha|0\rangle_a \otimes |0^{N-1}\rangle_{\text{rest}} + \beta|1\rangle_a \otimes |0^{N-1}\rangle_{\text{rest}}.$$

The initial term is an eigenstate that will not evolve, whereas the second term will follow some evolution through the N-dimensional space of states with Hamming weight 1. We may use the notation $|\{j\}\rangle = X_j|0^N\rangle$ to denote the state with all qubits in the state 0, except for qubit j which is in state 1. If there is no ambiguity, we sometimes omit the curly brackets. The Hamiltonian in the sector of a single excitation then reads

$$H = \sum_{j,k\in V} W_{jk}|\{j\}\rangle\langle\{k\}| \tag{3.19}$$

This is also precisely the Hamiltonian that describes a single quantum particle (such as a fermion or boson) that hops over a graph: these are described by the interaction $\sum w_{jk} f_j^\dagger f_k$ (plus potential two-body terms that are now irrelevant), together with the translation $|\{j\rangle\} = f_j^\dagger|0\rangle$. Hence, any protocol that assumes Eq. 3.19 may represent either of the three models, and we collectively describe them as *single excitation hopping*. The main differences between the models are:

- for both the free particle hopping and the XX model, with hopping amplitudes or coupling strengths w_{jk}, the matrix W is precisely the adjacency matrix of the graph: $W = w = A_G$
- for the XXX model, with couplings w_{jk}, the matrix W is the Laplacian L_G of the graph: $W = L_G = D_G - A_G$, where D_G is the diagonal matrix with entries corresponding to the degree of each vertex.

Quenches When considering quenches, one quickly arrives at the field of **perfect state transfer** (PST) which attempts to find times t and weight matrices W precisely such that

$$\langle\{b\}|e^{-iWt}|\{a\}\rangle = 1,$$

where a and b denote the locations of Alice and Bob, respectively. This setting is equivalent to setting of **continuous time quantum walks** [MB11] where W denotes the adjacency matrix of a graph. In 2004, two independent works reported on perfect transfer between the endpoints of an open chain, using the weights

$$W_{j,j+1} \propto \sqrt{j(N-j)}, \quad W_{jj} = 0.$$

The results were found for very different physical models, namely the XX model [CDE+04], and an electron hopping between quantum dots [NPL04]. The configuration is now often called the **Krawtchouk chain**, and we will encounter it again in Chapter 5. The couplings W are precisely such that the dispersion (the energy, as a function of wave

number) becomes linear. Here and in the following, we often consider the **mirror symmetry** of a chain, such that even eigenstates have an eigenvalue +1 under the relabeling operation $j \to N - j + 1$, and odd eigenstates have an eigenvalue −1. In this case, the energies of the odd eigenstates *interlace* the energies of the even states. Then, for some energy scale of the coupling W, the even eigenstates all have *even* eigenvalues, and the odd eigenstates have *odd* eigenvalues. Hence, there is some evolution time, for which

$$|\Psi_{\text{even}}\rangle \to e^{-i(2k)\pi}|\Psi_{\text{even}}\rangle,$$
$$|\Psi_{\text{odd}}\rangle \to e^{-i(2k+1)\pi}|\Psi_{\text{odd}}\rangle.$$

By giving the odd components of *any* state a minus sign, one exactly performs a mirror operation on the state: one does not only obtain PST, but a mirror operation on any single-excitation state. For non-interacting theories, such as free fermions and the XX model, this remains true for sectors with any number of excitations.

Ever since these early results, many more graphs and weight configurations were found to perfectly transfer a state [Kay10; God12], sometimes even well after they were originally introduced, such as the Polychronakos chain H_P that we address in Chapter 6.

The ferromagnetic XXX model, with a single excitation, is very similar to the case of the XX model, except that the Hamiltonian now has diagonal entries. Bose kickstarted the field of state transfer in 2003 [Bos03] by observing that, on a uniformly coupled linear chain, an excitation initially at site 1 would appear at site N with high probability after a sufficiently large time. Such cases are sometimes called **near-perfect state transfer**, and various other examples exist [GKS+12; VZ12; BCG+17].

Adiabatic In adiabatic protocols, we typically assume time-dependent control over the couplings $W_{jk}(t)$ in Eq. 3.19. At $t = 0$ and $t = T$, the adiabatic eigenstate of the system must be located on Alice's or Bob's subsystem, which generally means that these subsystems are isolated: the couplings W_{jk} connected to Alice or Bob are then 0. In between, the couplings W_{jk} are engineered to connect aforementioned eigenstates, without causing a degeneracy. A protocol that follows this framework necessarily requires a *counter-intuitive* pulse sequence: the couplings to the *receiver* are initially strongest and are lowered over time, whereas the couplings to the *sender* start at 0 and grow stronger towards the end of the protocol. A sketch of such a protocol is given in Fig. 3.4.

Although these protocols are inherently slower than quenches, adiabatic protocols are often easier to implement experimentally because no precise timings are required, and because they are relatively resilient to decoherence and random or systematic errors in the control fields [CFP01; FBM+15].

One of the most studied adiabatic transfer techniques is STImulated Raman Adiabatic Passage (STIRAP), which considers three internal states of an atom, of which the only possible couplings are $1 \leftrightarrow 2$ and $2 \leftrightarrow 3$ [GRS+90]. For our purposes, this is essentially a chain of length 3, and indeed, the protocol was later extended allow transfer between the ends of a chain of any (odd) length N [MT97]. The protocol follows precisely the counter-intuitive sequence described above, and we will study it in more depth in Chapter 8. The atomic levels may not quite count towards *spatial* transfer, but the model takes precisely the form of Eq. 3.19 where W is the adjacency matrix of a chain, and the same mathematics have indeed been applied in spatially extended

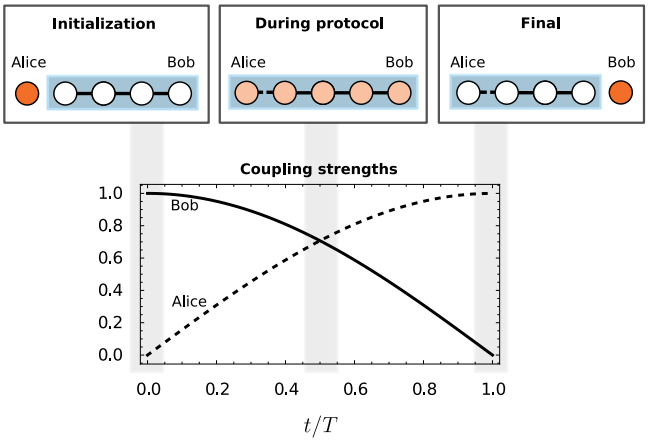

Figure 3.4: A sketch of a typical adiabatic transfer protocol, with the counter-intuitive pulse sequence. The top row indicates the initial, midway and final step of the protocol on a 5-site chain, with black lines representing the coupling strengths $W_{j,j+1}$. The blue contour indicates which sites are coupled. The bottom graph shows a possible trajectory for Alice's couplings W_{aj} and Bob's couplings W_{bj}.

systems. These include an electron hopping over quantum dots [GCH+04] (where it is called Coherent Tunneling by Adiabatic Passage (CTAP)), cold atoms hopping through optical traps [ELC+04], or a single (higher) spin excitation in the XXX [BJG15] and XX model [OEO+07; GK14] (where it is called Dark Passage).

Apart from STIRAP-based protocols, there are various variations of adiabatic transfer, most notably transfer in slightly different particle hopping chains [CSF+12; GNL18].

3.2.2 Half filling

Having considered ferromagnetic spin models, we treat the anti-ferromagnetic variants in a similar fashion. In this case, Alice may initialize the system's state as

$$|\Psi(0)\rangle = \big(\alpha|0\rangle + \beta|1\rangle\big)_a \otimes |\text{rest}\rangle, \tag{3.20}$$

where $|\text{rest}\rangle$ is generally taken to be the ground state of the Hamiltonian restricted to the graph $G - a$. We typically assume conservation of number of excitations, and that the AFM ground state can be found in the sector with roughly $N/2$ excitations, hence the name *half filling*. To be precise, if we assume N odd, then $|\text{rest}\rangle$ is a state on $N-1$ qubits with $\frac{N-1}{2}$ spin excitations. Then, the evolution of $|\psi(t)\rangle$ takes place in two excitation sectors, namely those with $\lceil \frac{N}{2} \rceil$ and $\lfloor \frac{N}{2} \rfloor$ excitations. In the case of particle-hole symmetry, i.e. $[H, X^{\otimes N}] = 0$, these sectors will evolve similarly. At any stopping time T, the mixed state ρ_B that Bob receives is found by tracing over all sites V except for Bob's:

$$\rho_B = \text{tr}_{V-B}\big(|\Psi(T)\rangle\langle\Psi(T)|\big)$$

Note that in this setting, compared to the single-excitation case, the dimensions of the relevant subspaces increases from N to $\binom{N}{\lceil N/2 \rceil}$, which is a dramatic increase in size.

This makes the task of state transfer more difficult in this setting, and various techniques in many-body physics may be required.

Quench Quenches on half-filled systems are very common in condensed matter literature, but quenches in the context of state transfer less so. We already saw that certain open spin chains that allow PST or mirror inversion in the single-excitation sector, also allow transfer in higher excitation sectors. In particular, for XX chains such as the Krawtchouk chain, the mapping to non-interacting fermions makes it clear that results about single particle transfer still hold in the case of half-filling, up to signs.

Campos Venuti et al. study quenched transfer in the XXX model with spin-$\frac{1}{2}$ and spin-1 particles [CDR07]. As they indicate, the dispersion of this AFM model is actually linear at low energies, which is very distinct from the FM case, where the dispersion is quadratic. The findings are that quenched transfer can take place in a chain, with reasonable fidelities, as long as the *outer* qubits are much more weakly coupled than the qubits in the bulk of the chain. We will refer to engineering such a relatively weak coupling at certain sites as **straddling**.

Entanglement The case of half-filling is endowed with many results that are technically not about state transfer, but deal with emerging long-distance entanglement. Many of these results will turn out to be useful later in this thesis.

The straddled XXX chain that allows quenched transfer happens to also feature strong entanglement between the more weakly coupled sites, when cooled to its ground state [CDR06; CDR07]. In the limit of asymptotically strong straddling, the ground state takes the form of a maximally entangled state on the straddled sites, even if particles have higher spin. In Chapter 9, we will see that this generalizes to certain other bipartite graphs [Gro19].

Similar straddling effects are found in the AFM XX chains. In fact, one may perform a second iteration of attaching *even more weakly coupled* qubits to the ends of the chain, which in turn form a strongly entangled pair. Performing multiple iterations, one may obtain a chain where the couplings decay exponentially towards the left and right, such as [VRL10; RRS18]

$$H = \sigma^+_{\frac{1}{2}}\sigma^-_{-\frac{1}{2}} + \sum_{j=\frac{1}{2}}^{\frac{N-3}{2}} e^{-hj}\left[\sigma^+_j\sigma^-_{j+1} + \sigma^+_{-j}\sigma^-_{-(j+1)}\right] + h.c.,$$

where the site indices run from $-\frac{N-1}{2}$ to $\frac{N-1}{2}$. With increasing h, the ground state becomes asymptotically close to a so-called **rainbow state**, referring to the rainbow pattern that one obtains when drawing an arc between each qubit and its entangled partner. Finding a rainbow state as a ground state of a 1D chain is somewhat surprising: it has asymptotically $N/2$-qubit entanglement between its left and right halve, even though local 1D chains are expected to adhere to some area law [ECP10]. The catch here is that the couplings are exponentially varying, which is an unrealistic assumption in the thermodynamic limit.

The rainbow state has connections to other models in this thesis. In fact, a quench by the aforementioned Krawtchouk chain does not only perform a perfect mirror inversion after time T (even when the initial state is the AFM ground state), but it also maps an initial Néel state $|0101\ldots\rangle$ to a rainbow state after a quench time $T/2$ [ABB14].

Another interesting fact, which, to my best knowledge, has never been published, is that every *mirror-symmetric* XX spin chain without local fields has a rainbow state as eigenstate in the middle of its spectrum. This can be proven by a symmetry argument, and is best explained by first mapping to the equivalent fermionic hopping model[4]. Assume that, within a certain symmetry sector F, all fermionic modes are filled, and all other modes are empty. For this special state, it does not matter in which fermionic basis (here c or d) the occupation numbers are written: either way, the state contains all modes in F anyway,

$$|\Psi\rangle = \prod_{c_j^\dagger \in F} c_j^\dagger |0\rangle \propto \prod_{d_j^\dagger \in F} d_j^\dagger |0\rangle$$

In our case, we use the left-right mirror symmetry of the chain to guarantee that the system block-diagonalizes into an even and an odd part. We can choose F to be the *odd* block, such that $\{\, c_j^\dagger|0\rangle \mid c_j^\dagger \in F \,\}$ are odd single-particle eigenstates, which have an eigenvalue -1 when acted on by the operator that sends $j \to N-j+1$[5]. Then, $|\Psi\rangle$ is the unique eigenstate that contains all odd modes (and no even modes). Moreover, we can choose $d_j^\dagger = \frac{1}{\sqrt{2}}\left(f_j^\dagger - f_{N-j+1}^\dagger\right)$ to be another basis of anti-symmetric states, where $f_j^\dagger$ are again the *local* operators, creating a fermion at site j. Adding each of these states to the system gives rise to a state identical to $|\Psi\rangle$, up to a global phase. Now, mapping back to a spin model through the JW transform, this state becomes

$$|\Psi'\rangle \propto \prod_{j=1}^{N/2} \left(\sigma_j^+ + (-1)^j \sigma_{N-j+1}^+\right)|0\rangle$$

This is precisely a rainbow state, and we showed that it is an eigenstate of the symmetric XX chain. A similar result holds for the *even* sector. Lastly, we note that this state is always in the *middle* of the spectrum of the system: in a symmetric chain without local fields, the single-particle spectrum is symmetric around zero, and increasing energies alternatingly correspond to even and odd states. Therefore, for odd N, the two Rainbow eigenstates both have precisely zero energy. For even N, energies of the 'even' and the 'odd' rainbow states are nonzero, but relatively small, and differ from each other by a sign.

Adiabatic Adiabatic transfer in anti-ferromagnetic models received quite some scientific attention, partially because coupled quantum dots, with a single electron per dot, approximately form an AFM XXX model. Various models have been studied, such as the Heisenberg model [FBM+15; AHH+17; Gro19], the $J_1 - J_2$ model [CH12], spin-1 particles with generalized bilinear–biquadratic Heisenberg interaction [ERS07], and the XXZ model [OSF+13].

As in the ferromagnetic case, a typical adiabatic protocol is supposed to start and end such that the sending/receiving site is an eigenstate of the Hamiltonian. Indeed, each of the references in the previous paragraph uses the counter-intuitive pulse sequence, or a slight variations thereof.

[4] Many thanks to Freek Witteveen for pointing this out to me.

[5] Note the subtle difference between the symmetry operation of relabeling the sites ($j \to N-j+1$) that is relevant to the *left-right symmetric* chain, as opposed to the sign related to the exchange of fermionic particles, which holds for *any* fermionic system.

As with quenches, the huge dimensionality of the half-filled case makes analysis of the models rather hard. In Chapter 9, we will discuss transfer in the XXX model, relying heavily on the theory presented in Section 2.5.

3.2.3 Transfer on graphs that are not chains

Most results quoted in this section deal with the transfer of states over linear chains. From a practical point of view, this makes much sense: a chain is the graph with the highest ratio between diameter and number of sites, connecting two endpoints with as few sites as possible. Still, various applications may require state transfer over more general graphs, such as networks where multiple parties are strongly coupled at all times. As an example, Vandersypen et al. [VBC+17] consider future challenges in scaling up quantum computers based on electron spin qubits in quantum dots. They find that individual arrays of qubits need to be placed in vicinity of classical hardware that is responsible for control tasks, such as gate pulses and measurements. They sketch a computer chip design where a large number of 'qubit islands' are connected with long range couplers, such that other electronics can be placed in between the islands. Such designs could greatly benefit from more flexible coupling methods, where all islands could be connected to the same network, rather than placing an individual coupler between every nearby island. Similar reasoning may hold for other platforms as well. Still, results on non-chain graphs seems surprisingly scarce, and we will discuss the known results throughout this subsection.

By far the most results on non-chain graphs can be found in the context of perfect state transfer (using quenches on single-excitation systems). The field of algebraic graph theory chases a main question of characterzing graphs that allow PST, leading to a plethora of results [BFF+11]. Various classes of graphs are known to exhibit state transfer [BGS08; BP09; CG11], and various graph properties can be linked to the absence or presence of state transfer [God12; BFF+11].

Some results are known in the adiabatic variant of the single-excitation transfer, particularly in the context of CTAP. Longhi generalizes the chain-based transfer of quantum particles to transfer between the opposite corners of a square grid in any dimension [Lon14]. The result uses a smart decomposition of the grid into individual 1D chains, each of which requires a standard STIRAP/CTAP protocol for the transfer. In the same work, Longhi presents a transfer scheme on a triangular lattice, cut in the shape of a triangle, where CTAP is possible using specifically engineered couplings. The scheme works thanks to an earlier results by Bradly et al. [BRG+12], who consider the transfer of N bosonic particles hopping between three coupled sites. The states of this space can be represented using two parameters n_1, n_2 as $|n_1, n_2, N - n_1 - n_2\rangle$, and Bradly et al. present a scheme that adiabatically maps a state $|N, 0, 0\rangle$ to the state $|0, N, 0\rangle$. The same states, however, can be interpreted as sites on a two-dimensional lattice $|n_1, n_2\rangle$, whose couplings are given by the bosonic hopping amplitudes. These couplings do not only give the triangular connectivity, but also form Krawtchouk chains along the main directions of the grid, the very same that we discussed earlier in this section.

Another interesting CTAP result that involves more than just a linear chain is by Greentree et al. [GDH06], who consider multiple receivers dangling along the odd sites of a linear chain, along with a sender dangling along site 1. Within this configuration, the amplitude of the sender can be transported to any one of the receivers. Other

works, such as Refs. [CFX+13; BJG15], describe a variation where the chain splits into multiple paths or branched endpoints. The extension to these graphs is not surprising because these systems can be mapped back to a linear chain by symmetries. However, interesting physics can be observed when the transferred state is sent to multiple symmetric receivers, such that the final state forms a superposition between the various endpoints.

Apart from these results, I am not aware of any documentation of state transfer on general graphs, outside of the PST setting. Two of the main results of the thesis, presented in Part III, deal with adiabatic transfer on more general graphs. One of our results deals with CTAP and STIRAP, in which we consider a class of graphs much larger than those presented in the previous paragraphs (Chapter 8). The other results deals with the AFM XXX model, which is to my best knowledge the only result of state transfer in truly non-chain graphs in the setting of half filling (Chapter 9).

Looking at Table 3.1, it seems that some models have not had a general graph treatment yet, which may be interesting directions for future research. In particular, this includes quenches on half-filled systems, but also adiabatic transfer in the *single-excitation* Ising and XXX model. I don't know how to tackle the first or second case, but there is much to say about the third.

Musings on adiabatic transport in the FM XXX model The Hamiltonian of an XXX model, restricted to a single spin up, takes the form of the Laplacian matrix of the model's graph, $H = L_G = D_G - A_G$. It is not hard to check that all eigenvalues of L_G are either 0 or positive, and the multiplicity of the zero eigenvalue is equal to the number of connected components. The good news is that, in this settings, we always find a unique ground state with energy precisely 0, regardless of the graph, as long as it is *connected*. The bad news is that, once we disconnect Alice or Bob from the graph, the ground state becomes degenerate, possibly jeopardizing the adiabatic process. If only we had a way to overcome this degeneracy, we would find that adiabatic transfer works in *any* graph of this model! One potential solution is the following: if we allow ourselves the use of inhomogeneous local fields, of the form $H' = \sum_j B_j Z_j$, the we can make sure that the disconnecting party always has a *lower* energy than the ground state of the main connected component. Simply setting $B_j < 0$ for the connecting party j and $B_k > 0$ for all other parties $j \neq k$ would be sufficient. Realizing such inhomogeneous magnetic fields at the scale of inter-spin distances is experimentally challenging, and studying the viability of this protocol would be an interesting direction of future research.

Part II

Resonantly driven multiqubit gates

CHAPTER 4

Introduction to resonant multiqubit gates

4.1 Introduction

What constitutes a true multiqubit gate? Surely a unitary operation like $U = X \otimes Z$ should not be considered as such: even though it acts on two qubits, the operation merely consists of two local single-qubit gates in parallel, and the qubits could even be spacelike separated throughout the process. Although it is not quite well-defined what we mean with a proper multiqubit gate, we can at least set two requirements:

1. The operation creates some form of N-partite entanglement, hence it can not be written in a tensor product form.

2. The operation must be 'understandable', either for a computer-based compiler (i.e. there must be an efficient description of what the gate does), or, even better, easily understandable for humans.

The prototypical example is the $\texttt{Toffoli}_N$ or $\texttt{C}^{N-1}\texttt{NOT}$ gate on N qubits, which performs a bitflip on the Nth qubit if and only if the other $N-1$ qubits are in the state $|1\rangle$. Spelled out as a matrix in the computational basis, it is written

$$\texttt{Toffoli}_3 = \begin{pmatrix} 1 & 0 & 0 & 0 & 0 & 0 & 0 & 0 \\ 0 & 1 & 0 & 0 & 0 & 0 & 0 & 0 \\ 0 & 0 & 1 & 0 & 0 & 0 & 0 & 0 \\ 0 & 0 & 0 & 1 & 0 & 0 & 0 & 0 \\ 0 & 0 & 0 & 0 & 1 & 0 & 0 & 0 \\ 0 & 0 & 0 & 0 & 0 & 1 & 0 & 0 \\ 0 & 0 & 0 & 0 & 0 & 0 & 0 & 1 \\ 0 & 0 & 0 & 0 & 0 & 0 & 1 & 0 \end{pmatrix}. \tag{4.1}$$

Note that other multiple-controlled single qubit gates, such as the (double-)controlled-Z, can easily be obtained from the $\texttt{Toffoli}$ gate through local basis transformations. The form of Eq. 4.1 is particularly convenient: the gate acts trivially on most quantum states, except for a single two-dimensional subspace in which a π-rotation takes place. This property makes the gate both easily understandable for humans, but also highly non-local. We will elaborate on this highly selective property throughout this chapter.

When implemented on actual hardware, multiqubit gates are generally decomposed into the set of available single- and two-qubit gates. As two-qubit gates are typically more prone to errors, focus is on counting the number of two-qubit gates required for a certain circuit. Moreover, the CNOT is canonically taken as the only available two-qubit gate, calling for the CNOT-count as a figure of merit. Decomposing the $\texttt{Toffoli}_N$ into the shortest possible circuit of operations taken from some set of 1- and 2-qubit gates has become a formidable scientific challenge. The rules of this game can be interpreted in various ways: Can one use any two-qubit gate, or does it have to be a CNOT? Can ancillary qubits be used? Are we counting the *depth* of the circuit, or the number of two-qubit gates, or the total number of all gates? For example, in their widely adopted textbook, Nielsen and Chuang [NC10] ask[1] how many gates from various gate sets are needed to construct a $\texttt{Toffoli}_N$. It is now known that the $\texttt{Toffoli}_3$ requires as many as 5 freely chosen two-qubit gates, or 6 CNOTs [YDY13].

For larger N, the required number of basic operations or ancilla qubits grows steeply. The $\texttt{Toffoli}_N$ can be implemented with a circuit of *depth* $O(\log(N))$, requiring $O(N)$ ancilla bits. If no ancillas may be used, the number of CNOTs is lower bounded at $2N$, although the be best known implementations require a quadratic number of CNOTs [SM09]. The size of these circuits has been prohibitive in scaling up quantum algorithms on current quantum computer prototypes: even though various systems with 5-20 qubits are available [RNT+17; OMA+17; LFS+19; Aro19], the largest multiple control gate ever performed is, to our best knowledge, the $\texttt{Toffoli}_4$ [FML+17].

Circumventing this decomposition has also attracted significant attention. Ref. [RRG07] considers a shorter circuit for the $\texttt{Toffoli}_3$ by requiring one *qutrit*, and Ref. [FSB+12] implements a similar scheme on superconducting transmon qubits. Refs. [ISM11; Shi18] propose a $\texttt{Toffoli}_N$ by exploiting the Rydberg blockade, and Ref. [GP19] proposes a drivently driven $\texttt{Toffoli}_3$ for spin qubits. In the following, we chase the same goal, by using resonant driving in a strongly coupled quantum system to create a gate similar to the $\texttt{Toffoli}_N$.

4.1.1 Resonant driving as a control technique

Resonant driving techniques are well-known in atomic physics, where they are used to populate specific orbitals [Gri05; WBB16], and in experimental quantum information processing, where they are exploited to form quantum gates on one or two qubits [CFH97; GZC03; GCS17; ZSR+18]. When a pair of eigenstates with a unique energy gap is resonantly driven for an appropriate amount of time, the unitary time-evolution operator, in the asymptotic limit of increasingly weak driving, approaches the form

$$\texttt{iSWAP}_{t_1,t_2} = \begin{pmatrix} \mathbb{1} & & & & \\ & 0 & \dots & -ie^{i\phi} & \\ & \vdots & \mathbb{1} & \vdots & \\ & -ie^{-i\phi} & \dots & 0 & \\ & & & & \mathbb{1} \end{pmatrix}. \tag{4.2}$$

Here, all diagonal entries are 1, except in the subspace spanned by the resonant states, which we denote by t_1 and t_2. The phase ϕ corresponds to the phase of the driving field. We observe that this operation is very similar to $\texttt{Toffoli}_N$, and it features the

[1] See Research Problem 4.4.

same favorable properties, namely that it is both easily understandable for humans and highly non-local.

Note that it is generally highly nontrivial to form gates of the type $\texttt{iSWAP}_{t_1,t_2}$ using a local Hamiltonian. They could in principle be generated by a time-independent Hamiltonian of the form $H = |t_1\rangle\langle t_2| + h.c.$, but such interactions, which act only on many-particle states t_1 and t_2 but not any others, are typically highly nonlocal, and hence are never encountered in nature [Pre13]. When restricting to realistic 2-local Hamiltonians, in which each term is allowed to act non-trivially on at most two qubits, time-dependent control fields are required. Our goal is to cleverly engineer 2-local Hamiltonians whose time evolution swaps just 2 out of 2^N states and leaves all other states put, without resorting to discrete gate decompositions. To do so, we employ systems of the form

$$H(t) = H_{\text{bg}} + \Omega' \cos(\omega t + \phi) H_{\text{drive}},$$

where H_{bg} is a background Hamiltonian whose eigenstates are known, and H_{drive} is some local driving field which incites a transition between two eigenstates of H_{bg}, which we will call $|t_1\rangle_{H_{\text{bg}}}$ and $|t_2\rangle_{H_{\text{bg}}}$[2]. If these eigenstates have a unique energy gap, the resulting time evolution U_{drive} can be made to look as in Eq. 4.2.

Note that the resulting U_{drive} has this special form in the *eigenbasis* of H_{bg}. For further quantum information processing, we propose an operation which maps each computational basis vector to a unique eigenstate, which we call the *eigengate* U_{eg}. The complete protocol is then described by

$$\texttt{iSWAP}_{t_1,t_2} \approx U_{\text{eg}}^{\dagger} U_{\text{drive}} U_{\text{eg}}.$$

An implementation of this protocol would require the following ingredients:

- A constantly applied background Hamiltonian H_{bg} which has a unique energy gap ω between two eigenstates $|t_1\rangle_{H_{\text{bg}}}$ and $|t_2\rangle_{H_{\text{bg}}}$.
- A driving field H_{drive} which couples the states $|t_1\rangle_{H_{\text{bg}}}$ and $|t_2\rangle_{H_{\text{bg}}}$, whose amplitude can be made oscillatory at the right frequency ω.
- An operation which maps (any) two computational basis states, call them $|t_1\rangle$ and $|t_2\rangle$, to energy eigenstates $|t_1\rangle_{H_{\text{bg}}}$ and $|t_2\rangle_{H_{\text{bg}}}$ respectively. We also need the inverse of this operation.
- An efficient method to keep track of the dynamical phases due to H_{bg}.

Throughout this part, we will elaborate on these four requirements, and treat specific examples in which the proposed protocol is shown to work.

The resulting operation could find applications in noisy intermediate-scale quantum computers [Pre18], where decoherence prohibits long gate sequences, but evolution by engineered Hamiltonians might be natively available. We find that there is a trade-off between gate time and fidelity, where the error $\mathscr{E} \propto t_d^{-2}$ scales as the inverse-square of the driving duration t_d. Moreover, as the number of involved qubits increases, the performance of our gate may decrease. Therefore, we will compare our proposals to the scaling of conventional gate decompositions.

[2] Recall that we use subscripts below kets to indicate the basis we consider.

4.1.2 Related work

In 2010, two independent groups [BMM+10; KP10] described a result that similarly exploits resonant driving in a many-body system to construct quantum gates. They considered an interacting spin chain of which only the first one or two sites can be controlled, and prove that universal operations over all states are possible. The scope of these papers, achieving single- and two-qubit gates with limited control, is very different from our goal, which is the creation of an unconventional multiqubit operation on a system with much more generous controllability. Moreover, both earlier papers focus mostly on proof of existence, and do not mention concrete examples of systems which would allow their protocol. In this part, we present experimentally feasible examples which we simulate numerically.

An experiment by Senko et al. [SSR+14] applied resonant driving on a many-body system, very similar to our proposal. The experiment involved trapped ions that collectively simulate an Ising model (see Section 2.3), acted on by an oscillatory driving field. By starting in an eigenstate and measuring the system after driving at various oscillation frequencies, the energy gaps between certain states could be inferred. The experiment was presented as a method to perform *coherent* spectroscopy, allowing the accuracy of the Ising model to be tested, which sets it apart from our approach for constructing quantum gates. Still, the techniques used are similar. The experiment was mostly a proof-of-concept, but the results are a good indication that the resonant transitions presented in this part are within the possibilities of near-term quantum computers.

The most obvious competitor of our protocol is conventional compiling of any quantum operation into a universal set of single- and two-qubit gates. Extensive research efforts have greatly optimized compiling methods, and in the asymptotics of many qubits, compiling approach becomes increasingly favorable compared to our proposal. For a recent overview, see Ref. [CFM17]. We present our results not as an alternative to compiling, but rather as a creative twist to the fields of condensed matter and quantum control, which might find applications on specialized near-term devices. We also present our methods, such as the eigengate presented in Section 4.2, as tools that may find applications elsewhere.

4.2 Mapping the computational basis to the eigenbasis

4.2.1 Eigengates from quenches

Let A and B be Hermitean operators (or Hamiltonians). We call U_{eg} an **eigengate** between A and B if it maps every eigenstate of A to an eigenstate of B. Such eigengates can be implemented by *quenching* (suddenly applying) a third Hamiltonian H which satisfies

$$e^{-iH\frac{\pi}{2}} A e^{iH\frac{\pi}{2}} = B. \tag{4.3}$$

It is not clear which tuples (A, B, H) satisfy Eq. 4.3 in general, but we claim the following sufficient condition:

$$[H, A] = iB \quad \text{and} \quad [H, B] = -iA. \tag{4.4}$$

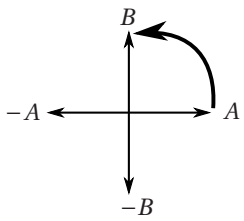

Figure 4.1: An eigengate generated by H rotates operator A between B, $-A$, $-B$ and back into A. Note that consecutive application of two eigengates inverts the spectrum of A or B.

Note that one can freely rescale A, B and H (together with the rotation angle $\pi/2$), as this does not change the eigenstates, hence pertaining the same eigengate. To prove our claim, we first recall the Hadamard Lemma,

$$e^{-iHt}Ae^{iHt} = \sum_{n=0}^{\infty} \frac{(-it)^n}{n!} (\mathrm{ad}_H)^n A \tag{4.5}$$
$$\mathrm{ad}_H A := [H, A]$$

and plug Eq. 4.4 into Eq. 4.5:

$$\begin{aligned} e^{-iHt}Ae^{iHt} &= A + (-it)(iB) + \frac{(-it)^2}{2!}A + \frac{(-it)^3}{3!}(iB) + \frac{(-it)^4}{4!}A + \ldots \\ &= \sum_{k=0}^{\infty} \frac{(-it)^{2k}}{2k!}A + \sum_{k=0}^{\infty} \frac{(-it)^{2k+1}}{(2k+1)!}iB \\ &= \cos(t)A + \sin(t)B. \end{aligned}$$

Hence, the operator A evolves to B in the Heisenberg-picture if we apply H for a time $t = \frac{\pi}{2}$. We graphically depict such rotations in Fig. 4.1. Recall that subscripts of kets denote the basis in which the vector is described. Then, for every eigenvector $|j\rangle_A$ of A, we may define

$$|j\rangle_B = U_{\mathrm{eg}}|j\rangle_A$$

where $U_{\mathrm{eg}} = \exp(-iH\frac{\pi}{2})$ is an eigengate from A to B. Unitaries are isospectral mappings, preserving the spectrum of Hermitean operators, hence for all j, if $A|j\rangle_A = \lambda_j|j\rangle_A$, then $B|j\rangle_B = \lambda_j|j\rangle_B$. Examples of valid (A, B, H) tuples include the Pauli matrices (X, Y, Z), and $(L_0^\alpha, L_1^\alpha, H_{\mathrm{P}})$ which we will discuss in Chapter 6 on Polychronakos' model.

There is some leftover symmetry $H \to H + G$ for any G such that $[G, A] = [G, B] = 0$. In other words, within each subspace spanned by eigenvectors of A with the same eigenvalue, the operator U_{eg} may cause an arbitrary unitary rotation which we cannot track using the method presented here.

4.2.2 Eigengates from adiabatic evolution

Another method to turn eigenstates of A into eigenstates of B is by adiabatic evolution. For $t \in [0, \pi/2]$, we consider the adiabatic Hamiltonian

$$H_{\mathrm{adiabatic}} = \cos(t)A + \sin(t)B. \tag{4.6}$$

Because the LHS of Eq. 4.5 shows an isospectral transformation of A, the eigenvalues of Eq. 4.6 remain the same at all times. Assuming the relevant units of energy are large compared to the units of time, the total time-evolution converges to the form

$$\begin{aligned} U_{\text{eg,adiabatic}} &= \mathcal{T}\exp\left(-i\int_0^{\frac{\pi}{2}} H_{\text{adiabatic}}(t)\,dt\right) \\ &= \underbrace{\exp\left(-iG\frac{\pi}{2}\right)}_{\text{Acts only within degenerate subspaces}} \underbrace{\exp\left(-iH\frac{\pi}{2}\right)}_{\text{Eigengate}} \underbrace{\exp\left(-iA\frac{\pi}{2}\right)}_{\text{Dynamical phase}}, \end{aligned}$$

where the form of G in the last equation is unknown, but limited to act nontrivially only within each subspace of fixed eigenvalue. On individual eigenstates of A, the adiabatic evolution operator acts as

$$U_{\text{eg,adiabatic}}|j\rangle_A = \exp\left(-iG\frac{\pi}{2}\right)\exp\left(-i\lambda_j\frac{\pi}{2}\right)|j\rangle_B.$$

4.2.3 Eigengates for resonantly driven transitions

Our goal is to arrive at a quantum gate that exchanges exactly two states in the *computational basis* by driving a unique transition in some background Hamiltonian's *eigenbasis*. This is where eigengates come in.

We require A to be *any* Hamiltonian which is diagonal in the computational basis, while B is the background Hamiltonian in which the driving takes place. In that case, the eigengate U_{eg} between A and B maps computational states to eigenstates. Using states in the eigenbasis of B, we may selectively exchange eigenstates using resonant driving. Finally, an inverse eigengate (or equivalently, a $\frac{3\pi}{2}$ rotation by H) then maps back to the computational basis, giving the desired result.

Although sufficient and highly convenient, the eigengate is not *necessary* for this protocol: any unitary map that sends two computational basis states to the transitioning states would be sufficient.

As an interesting aside, the eigengate's feature to invert the energy spectrum when employed twice, has applications in perfect state transfer. In particular, whenever A is a sum of single-qubit terms such that an excitation at qubit i has energy opposite to an excitation at qubit j, then $(U_{\text{eg}})^2$ exchanges the state of qubits i and j. This assumes conservation of the number of excitations, and the uniqueness of the relevant energies. As an example, in Chapter 5 will later see that the mirror inversion dynamics of the Krawtchouk chain correspond precisely to $(U_{\text{eg}})^2$ for that system [CDE+04; GS18].

4.3 Resonant driving

This section studies the effect of resonant driving on many-body systems. We now consider a Hamiltonian of the form

$$H(t) = H_{\text{bg}} + \Omega'\cos(\omega t + \phi)\,H_{\text{drive}} \tag{4.7}$$

where $\Omega' \ll 1$ and $\|H_{\text{bg}}\| \sim \|H_{\text{drive}}\|$, justifying a perturbative treatment of the second term. To leading order in Ω', we consider all pairs of eigenstates of H_{bg}, where each pair approximately forms an independently interacting two-level system. In particular, we

assume that we know a basis in which H_{bg} is diagonal, whereas H_{drive} has only off-diagonal terms which are all real numbers[3]. For a pair of these diagonal states $|s_1\rangle$, $|s_2\rangle$, we model the approximate time evolution using

$$H = \Delta\frac{Z}{2} + \Omega\cos(\omega t + \phi)X \tag{4.8}$$

where $\Omega = \Omega'\langle s_1|H_{\text{drive}}|s_2\rangle$, and Δ is the gap in the spectrum of H_{bg} between $|s_1\rangle$ and $|s_2\rangle$. As we found in Section 3.1.2, for sufficiently small Ω, no transitions between eigenstates of H_{bg} occur unless ω is close to some energy gap Δ. With the goal of making an operation of the form $\texttt{iSWAP}_{t_1,t_2}$, we make sure that a *single* pair of states is on resonance. All off-resonant states will be named spectator states, which merely pick up a dynamical phase.

Leaving all spectators unchanged is particularly challenging, in part because H_{bg} is responsible for a continuously growing dynamical phase on each eigenstate. There are various ways to regain control over these phases:

- One keeps track of all dynamical phases that occur throughout the whole protocol, and undoes these at the end of the resonant driving. With 2^N eigenstates, this is generically infeasible unless there is an exploitable symmetry between the eigenstates. An example of such a symmetry occurs in free particle Hamiltonians, where many-particle states have energies which are sums of single-particle energies. In such cases, an appropriate eigengate can map all accumulated phases back onto a local qubit, such that phases can be undone with a local phase shift on each of the qubits.

- One chooses the driving time t_d (and hence the corresponding amplitude Ω) precisely such that all two-level systems make an integer number of rotations during the protocol. This amounts to making sure that $\delta\, t_d = k2\pi$ ($k \in \mathbb{Z}$) for each transition. The choice of t_d becomes increasingly constrained as the systems grows and increasingly many values of δ have to be taken into account.

- One decomposes the driving procedure in two steps, which cancel each other's accumulated phase to leading order.

In the next subsection, we elaborate on the latter approach, which we dub the halfway inversion.

As an aside, note that the form of Eq. 4.8 implies that we require the rotating wave approximation (see Section 3.1.2) to ensure a clean transition between states. Throughout this part of the thesis, we assume this approximation to be valid.

4.3.1 The halfway inversion

Let us first remind the reader of the Hahn (or spin) echo. We consider a set of two-level systems which each evolve under a Hamiltonian of the form $H = \varepsilon_j Z$, where the energy ε_j is unknown for each system j. For any time t, one can enforce each of these system to return to their initial state by implementing a Hahn echo, where the system

[3]The derivation for complex-valued H_{drive} is similar to our approach below, but would introduce more notational clutter. A more clean way of dealing with complex driving terms is by simply re-defining the relative phase between eigenstates of H_{bg}.

is suddenly flipped by the X operation at times $t/2$ and t. This is easily seen to work for any choice of ε_j, by using $XZX = -Z$:

$$U_{\text{tot}} = (Xe^{-i\varepsilon_j Z\frac{t}{2}}X)e^{-i\varepsilon_j Z\frac{t}{2}} = e^{+i\varepsilon_j Z\frac{t}{2}}e^{-i\varepsilon_j Z\frac{t}{2}} = \mathbb{1}. \tag{4.9}$$

Note that during the driving step of our protocol, the term H_{bg} of Eq. 4.7 causes its eigenstates to rotate according to their energies λ_j. If H_{bg} can be obtained from some other Hermitean operator using an eigengate, then sequential application of two eigengates U_{eg}^2 precisely inverts the spectrum of H_{bg}, effectively applying X to each two-level system formed by a pair of eigenstates. Importantly, note the difference between the driving step performed by Eq. 4.8, which swaps *only* the pair of states that is on resonance but is error-prone and slow ($|\Omega|$ must be small), contrasted with U_{eg}^2 which inverts *all* states, and is exact and relatively fast.

Inspired by the Hahn echo, we propose to follow the same approach on a many-body system:

$$U_{\text{tot}} = X\, U_{t_d/2}^{\text{drive}}(\phi_2)\, X\, U_{t_d/2}^{\text{drive}}(\phi_1) \tag{4.10}$$

Here, $U_t^{\text{drive}}(\phi)$ is the time evolution due to Eq. 4.8, and $t_d = \pi/\Omega$ is the driving time needed for a full inversion of the resonant pair. In Eq. 3.11, we obtained an expression for $\tilde{U}_{t_d}^{\text{drive}}(\phi)$, which is the same operation in the *rotating frame*. The same expression in terms of the known rotating frame operators reads:

$$U_{\text{tot}} = \underbrace{X\, \exp\left(-i\omega Z\frac{t_d}{4}\right) \tilde{U}_{t_d/2}^{\text{drive}}(\phi_2)\, X\, \exp\left(-i\omega Z\frac{t_d}{4}\right)}_{I} \tilde{U}_{t_d/2}^{\text{drive}}(\phi_1).$$

The first part can be rewritten as

$$\begin{aligned}
I &= X\, \exp(-i\omega t_d Z/4)\, \exp\left[-i\,t\,\vec{\sigma}\cdot\begin{pmatrix} n_x \\ n_y \\ n_z\end{pmatrix}\right] X \exp(-i\omega t_d Z/4) \\
&= X\, \exp(-i\omega t_d Z/4)\, \exp\left[-i\,t\,\vec{\sigma}\cdot\begin{pmatrix} n_x \\ n_y \\ n_z\end{pmatrix}\right] \exp(+i\omega t_d Z/4)\, X \\
&= X\, \exp\left[-i\,t\,\vec{\sigma}\cdot\begin{pmatrix} n_x\cos(\omega t_d/2) + n_y\sin(\omega t_d/2) \\ n_y\cos(\omega t_d/2) - n_x\sin(\omega t_d/2) \\ n_z\end{pmatrix}\right] X \\
&= \exp\left[-i\,t\,\vec{\sigma}\cdot\begin{pmatrix} \Omega\cos(\phi_2+\omega t_d/2) \\ -\Omega\sin(\phi_2+\omega t_d/2) \\ -\delta/2\end{pmatrix}\right].
\end{aligned}$$

In the last step, we used that $\vec{n} = (\Omega\cos(\phi_2), \Omega\sin(\phi_2), \delta/2)^T$ and applied several trigonometric product-to-sum identities. Recall that $\delta = \Delta - \omega$. All in all, we find that

$$U_{\text{tot}} = \exp\left[-i\frac{t_d}{2}\,\vec{\sigma}\cdot\begin{pmatrix} \Omega\cos(\phi_2+\omega t_d/2) \\ -\Omega\sin(\phi_2+\omega t_d/2) \\ -\delta/2\end{pmatrix}\right] \exp\left[-i\frac{t_d}{2}\,\vec{\sigma}\cdot\begin{pmatrix} \Omega\cos(\phi_1) \\ \Omega\sin(\phi_1) \\ \delta/2\end{pmatrix}\right].$$

Let us first show that, despite the halfway inversion, it is still possible to perform a transition without any error if $\delta = 0$. Note that, in this picture, we perform two consecutive

$\pi/2$ pulses, which form an optimal π-pulse if and only if both rotation axes align. To this end, we fix

$$\phi_2 = -\phi_1 - \omega t_d/2, \tag{4.11}$$

such that the overall rotation becomes

$$U_{\text{tot}} = \exp\left[-i\frac{t_d}{2}\,\vec{\sigma}\cdot\begin{pmatrix}\Omega\cos(\phi_1)\\ \Omega\sin(\phi_1)\\ -\delta/2\end{pmatrix}\right]\exp\left[-i\frac{t_d}{2}\,\vec{\sigma}\cdot\begin{pmatrix}\Omega\cos(\phi_1)\\ \Omega\sin(\phi_1)\\ \delta/2\end{pmatrix}\right]. \tag{4.12}$$

It is now clear that, for $\delta = 0$, any rotation axis in the $X-Y$ plane can be obtained by an appropriate choice of ϕ_1. We sketch a more intuitive picture of what happens to an inverting state in this case in Fig. 4.2.

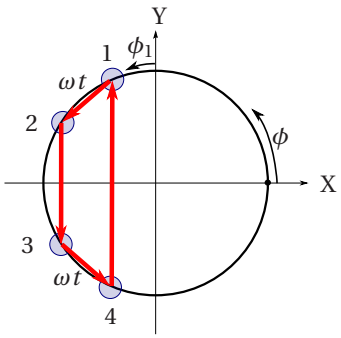

Figure 4.2: The relative phase ϕ between the two resonant states under our halfway inversion protocol, depicted on the unit circle. One could interpret this as the projection of Bloch sphere vector to the $X-Y$ plane. At $t = 0$, an initial state on the $+Z$-axis is first resonantly driven towards a point that is ϕ_1 radians away from the $+Y$-axis **(1)**, whilst rotating around the Bloch sphere at frequency ω towards **(2)**. The halfway inversion mirrors the relative phase over the X-axis **(3)**, after which the rotation at frequency ω takes the state to **(4)**. A second halfway inversion takes the state back to **(1)**, completely canceling the rotation ωt due to the background Hamiltonian.

Now, let us turn to the off-resonant case ($\delta \neq 0$). Ideally, we would like the off-resonant pairs of states to not change at all, leading to $U_{\text{tot}} = \mathbb{1}$. However, we argue that this is impossible. Note that we could have chosen a different flip X together with rotation vector $\vec{n}$ precisely such that *all* rotations would cancel, as in Eq. 4.9. Because this works for *any* δ, this prohibits us from performing the required inversion on the resonant pair of states. Below, we will find that the Z-component of the rotation vector was canceled by the halfway inversion, but the impossibility to cancel the X- and Y-components leads to our main source of errors.

Let us now quantify the accuracy of U_{tot} in the case of off-resonance, $\Omega \ll \delta$, where we aim to not cause any transitions at all. We define the error $\mathscr{E}$ of a unitary U with respect to a target unitary U_{goal} as

$$\mathscr{E}(U, U_{\text{goal}}) = 1 - \frac{1}{\dim(U)}|\text{Tr}(UU_{\text{goal}}^{\dagger})|. \tag{4.13}$$

Comparing U_{tot} to the identity operator for the case of Eq. 4.12, we find

$$\begin{aligned}\mathscr{E}(U_{\text{tot}}, \mathbb{1}) &= 1 - |\cos^2(nt_d/2) - \frac{(\Omega^2 - \frac{\delta^2}{4})}{n^2}\sin^2(nt_d/2)| \\ &= 1 - |1 - \sin^2(nt_d/2)\left(\frac{\Omega^2}{\Omega^2 + \frac{\delta^2}{4}}\right)| \\ &= \sin(nt_d/2)^2\left(\frac{8\Omega^2}{\delta^2} + O\left(\frac{\Omega^4}{\delta^4}\right)\right). \end{aligned} \tag{4.14}$$

This shows that the error can be made arbitrarily small, by choosing a smaller Ω/δ, or equivalently, a longer gate time t_d while keeping H_{bg} constant.

The factor $\sin(nt_d/2)$ could in principle cause the error to vanish if $nt_d = k\pi$ ($k \in \mathbb{Z}$) for every pair of states. Note that with many two-level systems, this is highly unlikely to happen and hard to track. Interestingly, by just considering the energy gaps δ, one can shave off another two orders of $\frac{\Omega}{\delta}$ from $\mathscr{E}$ in the specific case where $\delta t_d = k4\pi$ ($k \in \mathbb{Z}$):

$$\begin{aligned} nt_d/2 &= \sqrt{\Omega^2 + \frac{\delta^2}{4}}\, t_d/2 \\ &= \frac{\delta t_d}{4}\left[1 + 2\cdot\frac{4A^2}{\delta^2} + O\left(\frac{A^4}{\delta^4}\right)\right] \\ &= k\pi + \frac{2\pi\Omega}{\delta} + O\left(\frac{\Omega^2}{\delta^2}\right) \\ \sin(nt_d/2)^2 &= \frac{4\pi^2\Omega^2}{\delta^2} + O\left(\frac{\Omega^4}{\delta^4}\right) \qquad \text{if } k \in \mathbb{Z}. \end{aligned}$$

Hence, in the special case that all dynamic phases due to H_{bg} reset, $\mathscr{E}(U_{\text{tot}}, \mathbb{1}) = O\left(\frac{\Omega^4}{\delta^4}\right)$.

Unfortunately, in most cases, we do not find the same $O\left(\frac{\Omega^4}{\delta^4}\right)$ scaling when driving a many-body system, even when engineering the energy gaps δ. Numerically, we find the culprit to be the two-level systems consisting of one spectator state and one transitioning state: the off-resonant transition between these pairs is not accounted for by the halfway inversion, and hence still contributes an error of the order $O\left(\frac{\Omega^2}{\delta^2}\right)$. Nonetheless, the cases where $\delta t_d \approx k4\pi$ lead to a significant improvement of our protocol's fidelity, as we will see in the numerical results in Section 6.4.

4.3.2 Putting it all together: Resonantly driven multiqubit gates

We turn back to the many-body Hamiltonian proposed at the start of this chapter,

$$H = H_{\text{bg}} + \Omega' \cos(\omega t + \phi) H_{\text{drive}}$$

and its resulting unitary evolution $U_t^{\text{drive}}(\phi)$. We found that for sufficiently small Ω' and an appropriately chosen frequency ω and driving time t_d, we asymptotically approximate the operation iSWAP which selectively exchanges two basis states:

$$\texttt{iSWAP}_{t_1,t_2} := -ie^{i\phi}|t_1\rangle\langle t_2| - ie^{-i\phi}|t_2\rangle\langle t_1| + \sum_{j\notin\{t_1,t_2\}} |j\rangle\langle j|.$$

Note the difference between the phases $e^{\pm i\phi}$: we used the convention that $|t_2\rangle$ is the state with the *lower* energy (e.g. $Z|t_2\rangle = -|t_2\rangle$ in the two-level system formed by $|t_1\rangle$, $|t_2\rangle$). This gate is implemented by the sequence

$$\texttt{iSWAP}_{t_1,t_2} \approx U_{\text{eg}}^\dagger\, U_{t_d/2}^{\text{drive}}\left(-\phi - \frac{\omega t_d}{2}\right) U_{\text{eg}}^2\, U_{t_d/2}^{\text{drive}}(\phi)\, U_{\text{eg}} \qquad \text{(with halfway inversion)}$$

Alternatively, one can leave out the halfway inversion, and instead undo the dynamical phases by inverting the spectrum of H_{bg}, optionally even in the computational basis after an eigengate is performed:

$$\begin{aligned}\texttt{iSWAP}_{t_1,t_2} &\approx U_{\text{eg}}^\dagger\, e^{+iH_{\text{bg}}t_d}\, U_{t_d}^{\text{drive}}(\phi)\, U_{\text{eg}} \qquad \text{(without halfway inversion)}\\ &\approx e^{+iH_{\text{cb}}t_d}\, U_{\text{eg}}^\dagger\, U_{t_d}^{\text{drive}}(\phi)\, U_{\text{eg}}.\end{aligned}$$

Here $H_{\text{cb}} = U_{\text{eg}}^\dagger H_{\text{bg}} U_{\text{eg}}$ is the eigengate-partner of H_{bg} in the computational basis. The phases of the iSWAP operation are again $-i\exp(\pm i\phi)$, the same as with the halfway inversion.

We are left with finding systems in which such resonantly driven gates can be realistically implemented. The following three chapters each discuss a potential system. Firstly, in Chapter 5, we look at the Krawtchouk chain, an example of an XX chain with precisely chosen weights w. This system features a perfect eigengate, and the link to free fermions allows us to calculate explicit matrix elements $\langle t_1|H_{\text{drive}}|t_2\rangle$. Unfortunately, these turn out to be exceedingly small for pairs of states with a sufficiently unique energy gap Δ. In Chapter 6, we shy away from nearest neighbor couplings, focussing on an XXX chain with long-ranged interactions that was first introduced by Polychronakos. Again, we find a quench that implements a perfect eigengate, but the matrix elements are again small. Lastly, in Chapter 7, we consider a star-shaped configuration of qubits with Ising interaction. As this model is diagonal in the computational basis, no eigengates are needed. Moreover, we find that in this case the matrix elements do not decay with the system size, potentially beating the conventional decomposition into two-qubit gates.

CHAPTER 5

The Krawtchouk chain

In this chapter, we study a driven multiqubit gate on the Krawtchouk chain. This system maps to free fermions, allowing us to obtain the complete energy spectrum, and allowing us to efficiently calculate the effect of driving fields in the fermionic picture. This particular system turns out to have an elegant interpretation of the eigengates in terms of the **so**(3) algebra, linking the eigengates to rotations on the sphere. As a downside, the free-fermionic nature makes the actual resonantly driven gate scale unfavorably with larger numbers of qubits.

5.1 Analysing the model

We assume a Hamiltonian, acting on $N = n+1$ qubits,

$$H = \sum_{x=0}^{n-1} \frac{J_x(t)}{2}\left(X_x X_{x+1} + Y_x Y_{x+1}\right) + \sum_{x=0}^{n} (\alpha_x(t) X_x + \beta_x(t) Y_x + \gamma_x(t) Z_x), \tag{5.1}$$

where $\{J_x, \alpha_x, \beta_x, \gamma_x\}$ are real, time-dependent functions over which we assume arbitrary and independent control. Note that in this specific case, we start counting the qubits at $x = 0$. The specific choice of couplings

$$J_x^K = -\frac{J}{2}\sqrt{(x+1)(n-x)} \tag{5.2}$$

gives rise to the so-called Krawtchouk chain Hamiltonian

$$H^K = \sum_{x=0}^{n-1} \frac{J_x^K}{2}\left(X_x X_{x+1} + Y_x Y_{x+1}\right). \tag{5.3}$$

We already noted some of the remarkable properties of this system in Section 3.2.1. The authors of Refs. [CDE+04; NPL04] observed that applying H^K for a time $t = \pi/J$ exactly mirrors the left- and the right sides of the chain, allowing perfect state transfer (PST) between the ends of the chain. Another surprising application is that a $t = \pi/J$ pulse, acting on the product state $|+\rangle^{\otimes N}$, gives the so-called *graph state* on a complete graph,

which can be turned into a N-body GHZ state by 1-qubit rotations (see for example [CAJ05]). For N odd, $N = \pm 1 \mod 4$,

$$\begin{aligned} |\mathrm{GHZ}\rangle &= \left(\frac{|0^N\rangle + |1^N\rangle}{\sqrt{2}}\right) \\ &= e^{\pm i\frac{\pi}{4}} \exp[-i\frac{\pi}{4}X]^{\otimes N} \exp[-i\frac{\pi}{J}H^K]|+\rangle^{\otimes N}. \end{aligned} \tag{5.4}$$

The *Krawtchouk eigengates* U_K we present below employ a 'half-pulse' of duration $t = \pi/(2J)$, (Eq. 5.13), or rather a pulse combining the Hamiltonian H^K with its dual H^Z, (Eq. 5.14). The half-pulse was previously used in Ref. [ABB14] to generate the specific state $U_K|1010\ldots10\rangle$, which turns out to be a rainbow state.

The Krawtchouk chain Eq. 5.1 is an example of an XX model spin chain, and we can use the techniques discussed in Section 2.4. In particular, if $\alpha_x = \beta_x = 0$ for all x, then H conserves the total spin in the Z-direction, hence the eigenstates have a well-defined total spin. We may interpret the spin-up excitations as fermionic particles through a Jordan-Wigner (JW) transform [JW28]:

$$f_x^\dagger = [\prod_{j<x} Z_j]\sigma_x^-, \;\; f_x = [\prod_{j<x} Z_j]\sigma_x^+, \tag{5.5}$$

with $\sigma_x^+ = (X_x + iY_x)/2$, $\sigma_x^- = (X_x - iY_x)/2$. Indeed, the operators f_x, $f_{x'}^\dagger$ obey canonical *anti-commutation* relations. The quadratic terms in Eq. 5.1 turn into

$$H = \sum_{x=0}^{n-1} J_x(t)\left(f_x^\dagger f_{x+1} + \mathrm{h.c.}\right) \tag{5.6}$$

and we conclude that the fermions are non-interacting.

Following Ref. [CDE+04], we observe that action of H^K on the Fock space states $|0\ldots010\ldots0\rangle$ with Hamming weight 1 is the same as the action of the angular momentum operator L_X acting on the spin states of a particle with spin $s = \frac{n}{2}$. Denoting the 1-particle state with the '1' at position x as $|\{x\}\rangle$, and the spin state with $L_z = m$ as $|m\rangle\rangle$, the identification is

$$|\{x\}\rangle \leftrightarrow |m = x - \frac{n}{2}\rangle\rangle. \tag{5.7}$$

As a consequence, the eigenvalues λ_k of 1-particle eigenstates $|\{k\}\rangle_{H^K}$ of H^K make up a linear spectrum

$$\lambda_k = J(k - \frac{n}{2}), \quad k \in \{0, \ldots, n\}. \tag{5.8}$$

The eigenstates $|\{k\}\rangle_{H^K}$ can be expressed as [ACD+04]

$$|\{k\}\rangle_{H^K} = \sum_{x=0}^{n} \phi_{k,x}^{(n)} |\{x\}\rangle, \quad \phi_{k,x}^{(n)} = \sqrt{\frac{\binom{n}{x}}{\binom{n}{k}2^n}} K_{k,x}^{(n)}, \tag{5.9}$$

where $K_{k,x}^{(n)}$ denote Krawtchouk polynomials,

$$K_{k,x}^{(n)} = \sum_{j=0}^{k} (-1)^j \binom{x}{j}\binom{n-x}{k-j}. \tag{5.10}$$

The many-body eigenstates with q particles are created by products of q fermionic modes $c_k^\dagger = \sum_{x=0}^n \phi_{k,x}^{(n)} f_x^\dagger$,

$$|\{k_1 k_2 \dots k_q\}\rangle_{H^K} = c_{k_1}^\dagger c_{k_2}^\dagger \dots c_{k_q}^\dagger |0\rangle. \tag{5.11}$$

They satisfy

$$H^K |\{k_1 \dots k_q\}\rangle_{H^K} = \left(\sum_{j=1}^q \lambda_{k_j}\right) |\{k_1 \dots k_q\}\rangle_{H^K}. \tag{5.12}$$

Recall that the subscripts of kets denote the eigenbasis in which they are stated, which is well-defined thanks to the JW transformation. As all eigenvalues are (half-)integer multiples of J, all dynamical phases reset after time $t = 2\pi M/J$ for M (even) integer.

5.2 Mapping between eigenbases

We now turn to a construction of an *eigengate*: a quantum circuit that efficiently generates the many-body eigenstates from states in the computational basis. We find two simple circuits that do the job,

$$U_K = \exp\left(-i\frac{\pi}{2J}H^Z\right)\exp\left(-i\frac{\pi}{2J}H^K\right)\exp\left(-i\frac{\pi}{2J}H^Z\right) \tag{5.13}$$

$$= \exp\left(-i\frac{\pi}{J}\frac{(H^K + H^Z)}{\sqrt{2}}\right). \tag{5.14}$$

Here H^Z is the operator [KE05]

$$H^Z = \frac{J}{2}\sum_{x=0}^n (x - \frac{n}{2})(\mathbb{1} - Z)_x \,. \tag{5.15}$$

Its 1-body spectrum is the same, Eq. 5.8, as that of H^K, but the eigenvectors are very different: while H^Z is diagonal on states $|\{x_1 x_2 \dots x_q\}\rangle$ in the computational basis, H^K is diagonal on the Krawtchouk eigenstates $|\{k_1 k_2 \dots k_q\}\rangle_{H^K}$.

The key property is that the operator U_K exchanges the eigenstates of H^Z and H^K and thus performs the change of basis that we are after. Labeling both sets $\{x_1 x_2 \dots x_q\}$ and $\{k_1 k_2 \dots k_q\}$ by a binary index s taking values in $\{0,1\}^{n+1}$, we have

$$U_K |s\rangle = i^{qn} |s\rangle_{H^K} \quad \forall s \in \{0,1\}^{n+1}, \tag{5.16}$$

or, in a different notation,

$$H^K U_K = U_K H^Z. \tag{5.17}$$

In fact, in this special case there is a third Hamiltonian,

$$H^Y = \sum_{x=0}^{n-1} \frac{J_x^K}{2}\left(Y_x X_{x+1} - X_x Y_{x+1}\right) \tag{5.18}$$

which satisfies the **so**(3) commutation relations with H^K and H^Z:

$$[H^i, H^j] = i\epsilon_{ijk} H^k, \quad i,j,k \in \{K,Y,Z\}, \tag{5.19}$$

where ϵ_{ijk} is the totally antisymmetric tensor. The commutation relations allow us to picture the unitary U_K as a rotation on the Bloch sphere, which agrees perfectly with the Hadamard transformation for $n = 1$, $s = 10, 01$, up to a factor i.

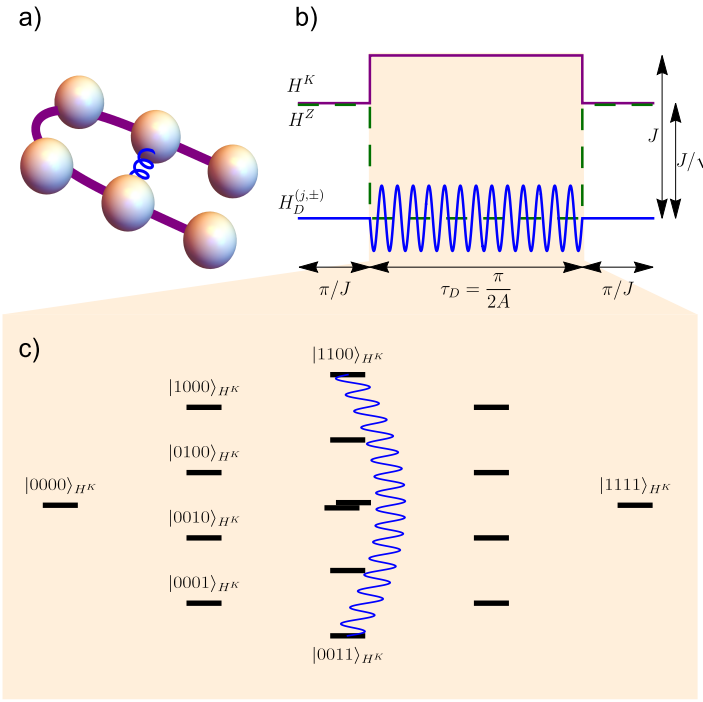

Figure 5.1: Overview of the proposed protocol for $\texttt{iSWAP}_N$ gates. a) The $N = 6$ qubit chain (spheres) evolving under the Krawtchouk Hamiltonian (solid lines). The driving Hamiltonian $H_D^{(1,-)}$ is depicted as the corkscrew line. b) Field strengths as function of time. c) The spectrum of H^K for $N = 4$, with the resonant transition depicted as the curvy line.

5.3 Resonant driving on Krawtchouk eigenstates

We first assume N odd and consider a driving term coupling $|0^{\frac{n}{2}+1}1^{\frac{n}{2}}\rangle_{H^K}$ and $|1^{\frac{n}{2}+1}0^{\frac{n}{2}}\rangle_{H^K}$. The Hamming distance between these two states is N. Nevertheless it turns out that the two states can be coupled by a 1-qubit driving term. To see this, we write the JW transform as

$$\sigma_x^- = [\prod_{j<x}(1-2\hat{n}_j)]f_x^\dagger, \quad \sigma_x^+ = [\prod_{j<x}(1-2\hat{n}_j)]f_x \tag{5.20}$$

with $\hat{n}_j = f_j^\dagger f_j$. Targeting the middle qubit, $x = \frac{n}{2}$, we observe that the operator σ_x^+ contains precisely the right number of annihilation and creation operators operators to connect the two states. However, we find that amplitude of the matrix element is exceedingly small,

$${}_{H^K}\langle 1^{\frac{n}{2}+1}0^{\frac{n}{2}}|\sigma_{\frac{n}{2}}^-|0^{\frac{n}{2}+1}1^{\frac{n}{2}}\rangle_{H^K} = (-2)^{-\frac{n^2}{4}}. \tag{5.21}$$

Due to this, a resonant driving protocol based on this transition is problematic for $N \geq 5$.

The numbers work out better for a 2-qubit term driving a transition from $|0^{\frac{N}{2}}1^{\frac{N}{2}}\rangle_{H^K}$ to $|1^{\frac{N}{2}}0^{\frac{N}{2}}\rangle_{H^K}$ for N even. We propose the driving terms

$$\begin{aligned} H_D^{(j,+)} &= J_D \cos(\omega t)[\sigma_j^+\sigma^-_{j+\frac{N}{2}} + \sigma_j^-\sigma^+_{j+\frac{N}{2}}], \\ H_D^{(j,-)} &= iJ_D \cos(\omega t)[\sigma_j^+\sigma^-_{j+\frac{N}{2}} - \sigma_j^-\sigma^+_{j+\frac{N}{2}}]. \end{aligned} \tag{5.22}$$

Note that the locations of the 1-qubit terms are precisely such that, together with the JW string, the required $\frac{N}{2}$ fermion creation ánd annihilation operators are contained in the driving fields. Making the string any longer would result in effectively less fermionic operators due to symmetry with respect to a global $\prod_x Z_x$ reflection. For $N = 6$, we use the 'central' 2-qubit driving operator that connects sites $x = 1$ and $x = 4$, which gives a coupling

$$A = \frac{1}{2}|_{H^K}\langle 1^3 0^3|H_D^{(1,-)}(t=0)|0^3 1^3\rangle_{H^K}| = \frac{5}{64}J_D \tag{5.23}$$

whereas the largest matrix element of this operator in the 3-particle sector is $\frac{9}{32}J_D$. Surprisingly, the matrix elements can be calculated explicitly even for larger N, as we show in Section 5.6.

Fig. 5.1 depicts the protocol for the resonant driving. Having performed a first Krawtchouk eigengate, taking time $t_{\text{eg}} = \pi/J$, we turn on the combination

$$H^K + H_D^{(1,-)}(t), \tag{5.24}$$

starting at $t = 0$, with the driving frequency $\omega = 9J$ adjusted to the energy difference between $|0^3 1^3\rangle_{H^K}$ and $|1^3 0^3\rangle_{H^K}$. Choosing a driving time $t_d = 2\pi M/J$ with M integer guarantees that all relative dynamical phases return to unity at time t_d. Choosing in addition $A = \frac{5}{64}J_D = \frac{\pi}{2t_d} = \frac{J}{4M}$ leads to a time-evolution that effectuates the transition

$$|0^3 1^3\rangle_{H^K} \to i|1^3 0^3\rangle_{H^K}, \;\; |1^3 0^3\rangle_{H^K} \to i|0^3 1^3\rangle_{H^K}. \tag{5.25}$$

The protocol is completed by a second Krawtchouk eigengate of time $t_{\text{eg}} = \pi/J$. Summarizing,

$$\begin{aligned} |0^3 1^3\rangle &\xrightarrow{U_K} |0^3 1^3\rangle_{H^K} \xrightarrow{U_D} i|1^3 0^3\rangle_{H^K} \xrightarrow{U_K^\dagger} i|1^3 0^3\rangle, \\ |1^3 0^3\rangle &\xrightarrow{U_K} |1^3 0^3\rangle_{H^K} \xrightarrow{U_D} i|0^3 1^3\rangle_{H^K} \xrightarrow{U_K^\dagger} i|0^3 1^3\rangle. \end{aligned} \tag{5.26}$$

A realistic implementation could apply an envelope over all control signals to guarantee smooth evolution of the fields.

The same reasoning holds for systems of any (even) size N, leading to the operation $\texttt{iSWAP}_{t_1,t_2}$ that we presented earlier in Eq. 4.2, with $\phi = \pi$. In this case, we always have $t_1 = |0^{\frac{N}{2}}1^{\frac{N}{2}}\rangle$ and $t_2 = |1^{\frac{N}{2}}0^{\frac{N}{2}}\rangle$ (or vice versa). To avoid notational clutter, we refer to this operation as $\texttt{iSWAP}_N$ in the remainder of this chapter.

The procedure can be extended with the halfway inversion discussed in Section 4.3.1. After driving for time $t_d/2$, we turn off H^K and turn on H^Z for time π/J, which is equivalent to applying a gate of the form $\text{diag}(1, \pm i)$ on each qubit. This effectively performs perfect state transfer on the energy spectrum, mapping indices $k \to n-k$, or equivalently, a π-rotation around the H^Z-axis of the $\mathbf{so}(3)$ Bloch sphere.

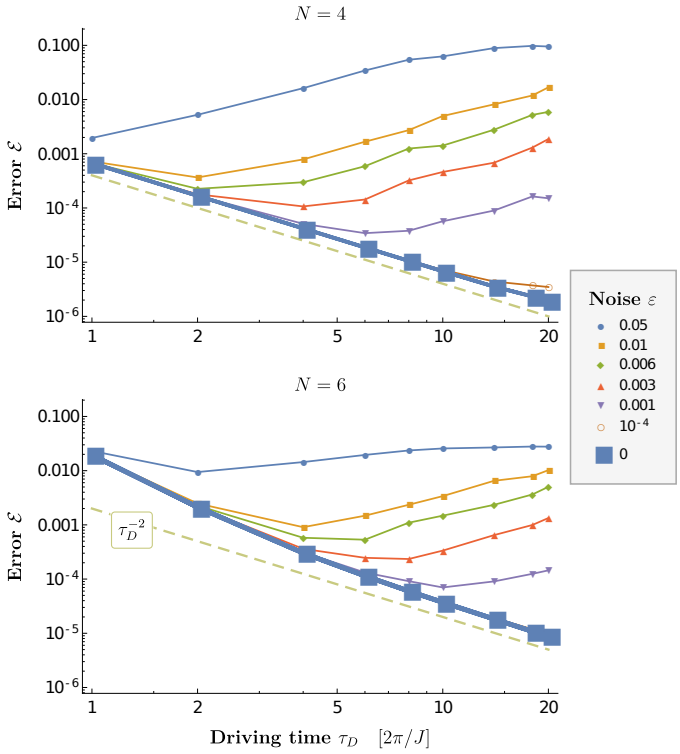

Figure 5.2: Fidelities of the resonant driving part of the $\texttt{iSWAP}_4$ and $\texttt{iSWAP}_6$ protocols, including the halfway inversion. The thick lines indicate the errors in the ideal case, thin lines under various values of noise ε. The errors fall off like t_d^{-2} (dashed), until the noise ε becomes the leading source of errors.

We complete the driving part of the protocol by driving once more for time $t_d/2$ followed by another H^Z-pulse of time π/J. This works without modification if Jt_d is an integer multiple of π, and for general t_d when the phase ϕ of the driving function is adjusted in the second driving step. The halfway inversion is included in the numerics belows.

5.4 Numerical results

Fig. 5.2 plots the gate error, defined as in Eq. 4.13, for runtimes up to $M = 20$. The $N = 4$ results have been obtained with driving operator

$$H_D^{(0,+)}(t) + H_D^{(1,+)}(t) \tag{5.27}$$

with resonant frequency $\omega = 4J$. To probe the effect of non-ideal couplings J_x^K, we performed the same simulations under multiplicative noise, such that $J_x^K \to (1+\varepsilon_x)J_x^K$ where ε_x is chosen uniformly from $[-\varepsilon, \varepsilon]$. The multiplicative noise is independent of the actual field strengths J, making it largely independent of implementation details. The results shown are the averages of at least 180 simulations.

From Fig. 5.2, we can read off the time taken by $\texttt{iSWAP}_N$ gates and make a comparison with the time taken by a fully entangling two-qubit gate. As comparison, we consider the gate formed by applying the similar $XX+YY$-type Hamiltonian on 2 qubits, leading to the operation $\texttt{iSWAP}_2$ [SS03]. The spatially varying Krawtchouk couplings, Eq. 5.2, grow up to strength $\max_x J_x^K = -\frac{J}{2}\frac{N}{2}$ (for N even), and for a fair comparison we assume the couplings J_x^K may grow no larger than $J^{\max}/2$ for any N. Therefore, we penalize time as a function of N by multiplying by a factor $\frac{N}{2}\frac{J}{J^{\max}}$. The 2-qubit $\texttt{iSWAP}_2$ gate with coupling maximized at $J^{\max}/2$ then takes time $\frac{\pi}{J^{\max}}$. Note that on top of the driving time, the protocol requires 2 eigengates taking unpenalized time $t_{\text{eg}} = \frac{\pi}{J}$, as well as a halfway inversion consisting of single-qubit gates of the form $\text{diag}(1,\pm i)$, whose duration we neglect here. We also neglect the error due to a noisy eigengate, which turn out to be an order of magnitude lower than the driving errors encountered here [GS18].

For $N = 6$, at sufficiently low noise $\varepsilon < 0.01$, we see an error $\mathscr{E}$ in the order of 10^{-3} for $M = 4$ meaning it can be achieved in time $t = 2t_{\text{eg}} + t_d = 10\pi/J$. Penalizing for the largest couplings being 3 times larger than in the $N = 2$ case, we conclude that our $\texttt{iSWAP}_6$ gate takes time equivalent to 30 2-qubit $\texttt{iSWAP}_2$ gates. For $N = 4$ an error of well below 10^{-3} is already achieved with $M = 1$ and we penalize with a factor 2, giving a runtime equivalent of 8 $\texttt{iSWAP}_2$ gates. Note that this is faster than the 10 gates required for a 3-qubit `Toffoli` as proposed in [SS03].

5.5 Experimental implementations

To our best knowledge, the only reported experiment in which non-trivial Krawtchouk couplings have been realized on spin-like qubits, is by Li et al. [LMH+18]. They use superconducting qubits with tunable couplings to mimic H^K on four qubits, showing a transfer fidelity of 99.2% in the subspace of a single spin excitation. It may be expected that simulating H^K in sectors with more excitations will be less accurate, because the transmon-type qubits used in the experiment are technically nonlinear oscillators with bosonic excitations, which are prone to excitations outside of the computation subspace (going from state $|0\rangle$ or $|1\rangle$ into state $|2\rangle$).

Other experiments, such as Refs. [PKK+13; CSH+16], report to be the first to engineer Krawtchouk couplings and test PST, but use photonic waveguides which behave different when more than 1 particle is involved. Using NMR, experimental PST was demonstrated on 3 qubits using constant couplings [ZLZ+05], and on up to 6 using iterative procedures [ÁMD+10; NJ14].

For other platforms, various theoretical proposals for approximations of Krawtchouk spin chains can be found in literature. The NMR platform could implement spatially varying couplings by using techniques presented in Ref. [AC13], and numerical tests for this platform have been performed in, for example, Ref. [ABB14]. Alternatively, cold atoms in a 1D optical lattice could be tuned to a regime where a two species Bose-Hubbard description reduces to an XX chain. The authors of Ref. [CAJ05] present a numerical study exploring the viability of this scheme to realize graph state generation using Krawtchouk couplings.

5.6 Matrix elements of driving operators in free models

In general, for driven multiqubit gates, it is essential to know the coupling strength between the two resonant states induced by the driving field. This calls for calculating quantities such as

$$M = \langle t_1 | H_{\text{drive}} | t_2 \rangle.$$

For many-body eigenstates t_1, t_2, this can be a highly nontrivial problem, and in some cases one may have to resort to measurements on the hardware itself to find these values.

However, for models that can be mapped to free fermions, we may sometimes obtain exact expressions for the driving matrix elements. As in the case of the Krawtchouk chain, we consider driving fields that are functions of raising and lowering operators σ^- or $\sigma^-\sigma^+$, acting between the states with the highest and lowest energy under some Hamiltonian H:

$$M_j^{(1)} = {}_H\langle 1^{\frac{n}{2}+1}\, 0^{\frac{n}{2}} \,|\sigma_j^-|\, 0^{\frac{n}{2}+1}\, 1^{\frac{n}{2}} \rangle_H \qquad (N \text{ odd}), \tag{5.28}$$

$$M_{j,d}^{(2)} = {}_H\langle 1^{\frac{N}{2}}\, 0^{\frac{N}{2}} \,|\sigma_j^-\sigma_{j+d}^+|\, 0^{\frac{N}{2}}\, 1^{\frac{N}{2}} \rangle_H \qquad (N \text{ even}). \tag{5.29}$$

Note that from these expressions, we can easily obtain the related values for the conjugate driving terms (see below).

Now, let us apply the Jordan-Wigner transform as defined in Eq. 5.5, and assume that H is diagonalized by the fermionic transformation

$$c_k^\dagger = \sum_{x=0}^{n} \phi_{k,x}^{(n)} f_x^\dagger, \tag{5.30}$$

where $\phi_{k,x}^{(n)}$ is a unitary matrix over indices k, x. These allow us to express Eqs. 5.28 and 5.29 into the values of $\phi_{k,x}^{(n)}$.

Odd lengths For the case of N odd, we find that the only nonzero value of $M_j^{(1)}$ correspond to cases where σ_j^- can be written in the form of $\frac{n}{2}$ annihilation operators, and $\frac{n}{2}+1$ creation operators (note that in our definition of the JW transformation, σ^- corresponds to a fermionic creation operator). The only site j on which the JW string is sufficiently long to produce this number of fermionic operators, is right in the middle, at site $j = \frac{n}{2}$. One might naively think that choosing j larger than that would make the string longer, but by left-right mirror symmetry of the problem, one may reason that also for $j > \frac{n}{2}$ the value of $M_j^{(1)}$ is zero.

For $j = \frac{n}{2}$, we may simplify the expression for $M_j^{(1)}$, through some rather tedious but otherwise straightforward algebra [GS18]. In the end, we obtain

$$M_{j=\frac{n}{2}}^{(1)} = 2^{\frac{n}{2}} \left| \phi^{(n)}_{\{0,\ldots,\frac{n}{2}\},\{0,\ldots,\frac{n}{2}\}} \right| \left| \phi^{(n)}_{\{0,\ldots,\frac{n}{2}-1\},\{\frac{n}{2}+1,\ldots,n\}} \right|, \tag{5.31}$$

where $|\phi_{\vec{x},\vec{y}}|$ denotes the minor of matrix ϕ with only rows $\vec{x}$ and columns $\vec{y}$ kept.

Now, specializing to the case of the Krawtchouk chain, using

$$\left| K^{(n)}_{\{0,\ldots,\frac{n}{2}\},\{0,\ldots,\frac{n}{2}\}} \right| = (-2)^{\frac{n(n+2)}{2}}$$
$$\left| K^{(n)}_{\{0,\ldots,\frac{n}{2}-1\},\{\frac{n}{2}+1,\ldots,n\}} \right| = (-2)^{\frac{n(n-2)}{2}}$$

we find

$$M^{(1)}_{j=\frac{n}{2}} = (-2)^{-n^2/4}.$$

The exponential decay of the matrix elements means that the driving times t_d rise quickly as the number of qubits n is increased, making the protocol unfeasible for large system sizes.

Even lengths For the case of $M^{(2)}_{j,d}$, we similarly find that the JW string must fill precisely half of the chain, such that $d = \frac{n+1}{2}$ is the only non-zero case. We find

$$M^{(2)}_{j,d=\frac{n+1}{2}} = 2^{\frac{n-1}{2}} \left|\phi^{(n)}_{\{j,\ldots,j+\frac{n-1}{2}\},\{0,\ldots,\frac{n-1}{2}\}}\right| \left|\phi^{(n)}_{\{j+1,\ldots,j+\frac{n+1}{2}\},\{\frac{n+1}{2},\ldots,n\}}\right|,$$

which, together with

$$\left|K^{(n)}_{\{j,\ldots,j+d-1\},\{0,\ldots,\frac{n-1}{2}\}}\right| = (-2)^{\frac{(n-1)(n+1)}{8}},$$
$$\left|K^{(n)}_{\{j+1,\ldots,j+d\},\{\frac{n+1}{2},\ldots,n\}}\right| = (-1)^{\frac{(j+1)(n+1)}{2}} (-2)^{\frac{(n-1)(n+1)}{8}},$$

leads to closed-form expressions for the matrix elements $M^{(2)}_{j,d=\frac{n+1}{2}}$. For $n = 5$ one finds $M^{(2)}_{j=1,d=3} = 5/64$ while for $n = 3$ we have $M^{(2)}_{0,2} = M^{(2)}_{1,2} = \sqrt{3}/8$.

Similar to the odd case, the values of $M^{(2)}$ fall off rapidly with n. For example, for $N = 2, 6, \ldots$, putting $j = \frac{n-1}{4}$, we find asymptotic behavior

$$M^{(2)}_{j=\frac{n-1}{2},d=\frac{n+1}{2}} \sim c_0\, c_1^n\, c_2^{n^2}\, n^{-1/6}$$

with $c_2 = 2^{3/4}3^{-9/16} = 0.9065\ldots$. This implies that the run-time of the resonant driving protocol (in its current form) increases rapidly with n.

Conjugate terms Lastly, we note that matrix elements of the conjugates of the discussed driving fields may have a different phase. In particular, for N even, we find

$${}_{H^K}\langle 1^{\frac{N}{2}}\, 0^{\frac{N}{2}}\, |\sigma^+_j \sigma^-_{j+\frac{N}{2}}|\, 0^{\frac{N}{2}}\, 1^{\frac{N}{2}}\rangle_{H^K} = (-1)^{\frac{N}{2}} M^{(2)}_{j,\frac{N}{2}}.$$

Hence, to achieve constructive interference, the optimal driving terms are of the form $H_D^{(j,+)}$ if $N/2$ is even, or $H_D^{(j,-)}$ if $N/2$ is odd.

5.6.1 Optimal scaling of matrix elements

One might wonder whether there exist systems for which the matrix elements in Eqs. 5.28 and 5.29 do *not* decrease as rapidly. In fact, it turns out that there exist transformations $\phi^{(n)}_{k,x}$ such that $M^{(1)}_{j=\frac{n}{2}}$ is *constant* in n. We can derive this as follows, focusing specifically on the case of N *odd*. Hadamard's inequality states that the determinant of a matrix ϕ is bounded by the product of the sizes of it's rows:

$$|\det(\phi)| \leq \prod_{i=0}^{n} |\phi_i|.$$

Here, ϕ_i denotes the vector obtained by taking the ith row (or column) of ϕ, and $|\phi_i|$ is the normal vector length (2-norm). For Eq. 5.31, we obtain

$$|M^{(1)}_{j=\frac{n}{2}}| \leq 2^{\frac{n}{2}} \left[\prod_{x=0}^{\frac{n}{2}-1} |\phi_{x,\{0,\ldots,\frac{n}{2}\}}||\phi_{x,\{\frac{n}{2}+1,\ldots,n\}}| \right] |\phi_{\frac{n}{2},\{0,\ldots,\frac{n}{2}\}}|.$$

On the other hand, by unitarity, for each value of x we require that

$$|\phi_{x,\{0,\ldots,\frac{n}{2}\}}|^2 + |\phi_{x,\{\frac{n}{2}+1,\ldots,n\}}|^2 = 1$$

The matrix element is optimized when $|\phi_{x,\{0,\ldots,\frac{n}{2}\}}| = |\phi_{x,\{\frac{n}{2}+1,\ldots,n\}}| = \frac{1}{\sqrt{2}}$ for all x, except for the case $x = \frac{n}{2}$ where $|\phi_{\frac{n}{2},\{0,\ldots,\frac{n}{2}\}}| = 1$. This intuitively means that the matrix $\phi_{k,n}$ has, on it's first $\frac{n}{2}$ *columns*, equal amplitude on the $\frac{n}{2}$ uppermost and $\frac{n}{2}$ lowermost *rows*. This gives the bound

$$|M^{(1)}_{j=\frac{n}{2}}| \leq 1. \tag{5.32}$$

This bound is actually *tight*, because Hadamard's inequality is satisfied whenever the relevant blocks consist only of orthogonal sets of vectors. These blocks are, in our conventions, precisely the upper-left and bottom-left quarters of the matrix $\phi^{(n)}_{k,x}$. In such cases, the matrix element $|M^{(1)}_{j=\frac{n}{2}}| = 1$ indicates that the two states $|1^{\frac{n}{2}+1}\, 0^{\frac{n}{2}}\rangle_H$ and $|\, 0^{\frac{n}{2}+1}\, 1^{\frac{n}{2}}\rangle_H$ are almost identical: they differ from each other only by a bitflip X on the middle qubit (and possibly an irrelevant phase).

An explicit example of a unitary matrix that satisfies our bound, is

$$\phi' = \begin{pmatrix} 1/\sqrt{2} & 0 & 0 & 0 & -1/\sqrt{2} \\ 0 & 1/\sqrt{2} & 0 & -1\sqrt{2} & 0 \\ 0 & 0 & 1 & 0 & 0 \\ 0 & 1/\sqrt{2} & 0 & 1\sqrt{2} & 0 \\ 1/\sqrt{2} & 0 & 0 & 0 & 1/\sqrt{2} \end{pmatrix}.$$

This $N = 5$ case trivially generalizes to larger sizes. In the fermionic picture, the state $|\, 0^{\frac{n}{2}+1}\, 1^{\frac{n}{2}}\rangle_H$ looks like $\frac{n}{2}$ particles, each of which is in a superposition between two sites x and $n-x$. The other state, $|1^{\frac{n}{2}+1}\, 0^{\frac{n}{2}}\rangle_H$, looks similar, but with an additional particle localized at site $x = \frac{n}{2}$. In the spin language, these correspond precisely to the *rainbow states* we discussed before in Section 3.2.2. In fact, *every left-right-symmetric XX chain* has these rainbow states as eigenstates, hence for each of these systems, the corresponding fermionic diagonalization transformation $\phi^{(n)}_{k,x}$ has a certain ordering in which $|M^{(1)}_j| = 1$. This ordering is precisely such that the states which are *symmetric* under mirroring the chain left-to-right (i.e. $x \to n-x$) occupy the bottom-most rows of $\phi^{(n)}_{k,x}$, and the *anti-symmetric* states are in the top-most rows (or the other way around).

Given that our prefered driving operator has such a large matrix element between these rainbow states, one might wonder if we can use these for a resonantly driven gate. The good news is that an eigengate is readily available: because the rainbow states are eigenstates of *any* left-right symmetric XX-chain, we may use the Krawtchouk eigengates U_K to create rainbow states from simple computational basis states. This specific eigengate was already observed in Ref. [ABB14], in the context of a quench that creates maximal entanglement between the left and right halves of the chain.

The bad news is that it is hard to create a unique energy gap between the rainbow states. On left-right symmetric chains, the states with even and odd parity are alternating in the spectrum. Therefore, the rainbow states are of the form $U_K|0101\ldots\rangle$ and $U_K|1010\ldots\rangle$, and their energies are close to 0. The sector with roughly half filling contains an exponentially large number of states (in N), and these are most dense around the energy 0. Due to the spectral crowding, we find that near-resonant states become increasingly problematic in driven protocols as N increases.

The rainbow states can be pushed towards the bottom or top of the spectrum by using couplings that decay exponentially towards the ends to the chain, as is the case for the rainbow Hamiltonian discussed in Ref. [RRS18]. In the limit of increasingly strong decay of the couplings, a rainbow state becomes the ground state of the system, but unfortunately we find that this ground state is strongly degenerate, prohibiting the unique transition we hope to find.

5.7 Conclusion

In conclusion, for the XX spin model, it is possible to find reasonably realistic eigengates and unique transitions. We study a specific example on the Krawtchouk chain. Unfortunately, we find that the matrix elements decay rapidly with N, making large multiqubit gates unfeasible. On the other hand, large matrix elements that are constant in N can be found, but we argue that these correspond to frequency-crowded parts of the spectrum.

An interesting direction of future research would be to find a best-of-both-worlds combination, where perhaps the matrix elements decay slowly, but are such that a sufficiently unique transition exists.

CHAPTER 6

Polychronakos' model

In this section, we consider resonant multiqubit gates in a tuned XXX chain model with long ranged interactions. The model was first described by Polychronakos [Pol93], but we will follow the definitions of Frahm [Fra93], who found an associated algebraic structure which we employ in our protocol. This algebraic structure is similar in spirit to the celebrated Yangian symmetry of the Haldane-Shastry model [Hal88; Sha88; HHT+92], to which the Polychronakos chain is a close relative. Both models are members of a wider class of integrable 1D systems with inverse-square two-body interactions, going back to the Calogero-Moser-Sutherland model of interacting particles on a line [Cal69b; Cal69a; Cal71; Sut71; Sut72; Sut75; Mos75].

6.1 Analysing the model

We consider a one-dimensional chain of N spin-$\frac{1}{2}$ particles, with particle j fixed at position x_j, evolving under the Hamiltonian

$$H_{\mathrm{P}} = \sum_{j<k} h_{jk} P_{jk}, \quad \text{where } h_{jk} = \frac{1}{(x_j - x_k)^2},$$

$$P_{jk} = \frac{1}{2}\left(\mathbb{1}_j \mathbb{1}_k + \vec{\sigma}_j \cdot \vec{\sigma}_k\right) = \begin{pmatrix} 1 & 0 & 0 & 0 \\ 0 & 0 & 1 & 0 \\ 0 & 1 & 0 & 0 \\ 0 & 0 & 0 & 1 \end{pmatrix}.$$

The locations x_j are given by the equilibrium positions of the classical Calogero system with potential

$$V(x_1, \ldots, x_N) = \frac{1}{2}\sum_j x_j^2 + \sum_{j<k} \frac{1}{(x_j - x_k)^2}$$

or, equivalently, by the roots of the Hermite polynomial $H_N(x)$. Frahm was able to describe the eigenbasis by finding ladder operators, and in particular, defined the following operators:

$$L_0^\alpha = \frac{1}{2}\sum_{j=1}^{N} x_j \vec{\sigma}_j^\alpha \qquad \alpha, \beta, \gamma \in \{x, y, z\}$$

$$L_1^\alpha = \frac{1}{4}\sum_{j \neq k} w_{jk} \varepsilon^{\alpha\beta\gamma} \vec{\sigma}_j^\beta \vec{\sigma}_k^\gamma \qquad w_{jk} = \frac{1}{x_j - x_k}$$

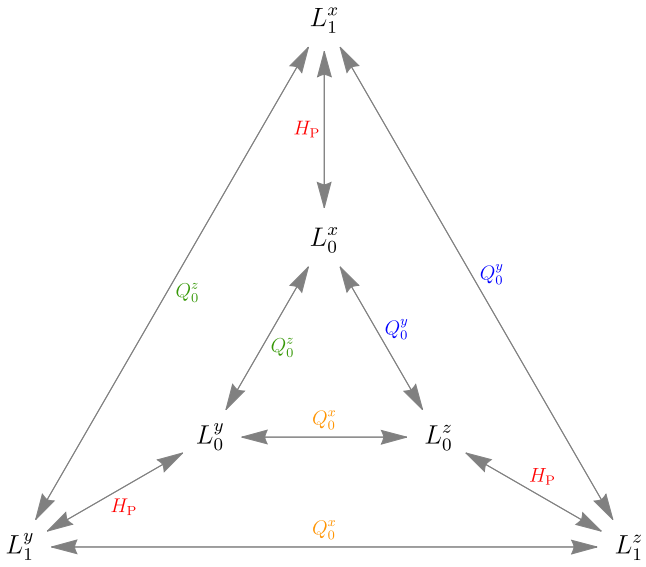

Figure 6.1: A map of various eigengates between the operators $\{L_r^\alpha\}_{r,\alpha}$ in Polychronakos' model. A quench by the operator next to an arrow implements the corresponding eigengate.

where $\varepsilon^{\alpha\beta\gamma}$ is the Levi-Civita symbol or fully anti-symmetric tensor. These operators were found to have the following relation with H_P:

$$[H_P, L_0^\alpha] = iL_1^\alpha$$
$$[H_P, L_1^\alpha] = -iL_0^\alpha.$$

6.2 Mapping between eigenbases

By noting that the eigenstates of L_0^z are the computational basis states, and the commutation relations between $(L_0^\alpha, L_1^\alpha, H_P)$ are of the form of Eq. 4.4, we readily obtain two methods to obtain an eigengate for L_1^z: either by continuous evolution

$$U_{\text{eg}}^P = \exp(-iH_P\pi/2),$$

or by adiabatically evolving $H_{\text{adiabatic}} = \cos(t)L_0^z + \sin(t)L_1^z$ for $t \in [0, \pi/2]$. Interestingly, owing to the form of L_0^z, applying the operation U_{eg}^P twice performs a spatial mirror inversion and perfect state transfer on the spin chain (see Section 3.2).

Another eigengate which interchanges the operator superscripts x, y and z can be formed by quenching with the total spin operator (see Section 2.5)

$$Q_0^\beta = \frac{1}{2}\sum_j \vec{\sigma}_j^\beta \qquad \beta \in \{x, y, z\}$$

as it satisfies

$$[Q_0^\alpha, L_r^\beta] = i\epsilon^{\alpha\beta\gamma}L_r^\gamma. \qquad r \in \{0, 1\}.$$

The different eigengates in this model are summarized in Fig. 6.1.

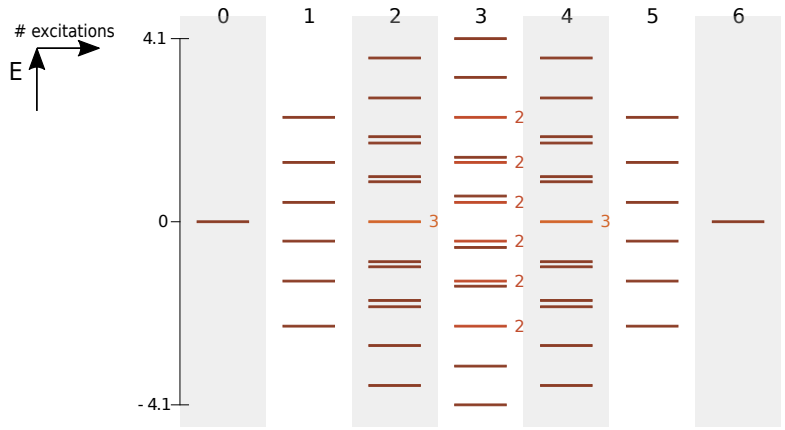

Figure 6.2: The spectrum of each of the operators $\{L_i^\alpha\}$, depicted for $N = 6$. The horizontal ordering denotes the number of α-excitations (or Hamming weight) $\frac{N}{2} - < Q_0^\alpha >$. Subspaces with multiplicity larger than 1 have their multiplicity displayed to their right.

6.3 Resonant driving on Polychronakos eigenstates

The energy spectra of all $\{L_r^\alpha\}$ are identical to that of L_0^z as these operators are linked by an isospectral transformation. Since H_P commutes with each total spin operator $\{Q_0^\alpha\}$, we conclude that the eigensystem of each L_i^α separates into non-interacting blocks of constant Q_0^α (e.g. total spin projection in the α direction). From here onwards, we will focus on $\alpha = z$, but we stress that identical results hold for the x and y superscripts, up to a local basis transformation.

The spectrum of L_0^z for $N = 6$ is depicted in Fig. 6.2 with energies represented vertically and the value of Q_0^z horizontally. Let $|\{k_1, k_2, \ldots, k_p\}\rangle$ with $k_1 < k_2 < \ldots < k_p$ represent the state with qubits k_j in state $|1\rangle$ and all other qubits in the state $|0\rangle$. The energies of states expressed in this notation are conveniently calculated as

$$L_0^z|\{k_1, k_2, \ldots, k_p\}\rangle = \sum_{j=1}^{p} x_{k_j}|\{k_1, k_2, \ldots, k_p\}\rangle.$$

In words: for each qubit in state $|1\rangle$, add energy equal to the position x_j of that qubit.

Because the positions x_j are symmetric around 0, the highest- and lowest energy states are nondegenerate for even N, and are given by:

$$|\text{high}\rangle = |t_1\rangle = |0\rangle^{\otimes \frac{N}{2}}|1\rangle^{\otimes \frac{N}{2}} = |\{\frac{N}{2}+1, \ldots, N\}\rangle \qquad (N \text{ even})$$
$$|\text{low}\rangle = |t_2\rangle = |1\rangle^{\otimes \frac{N}{2}}|0\rangle^{\otimes \frac{N}{2}} = |\{1, \ldots, \frac{N}{2}\}\rangle$$

As the energy gap between $|t_1\rangle$ and $|t_2\rangle$ is unique, we may select these two states for a resonantly driven multiqubit gate. However, these states are of product form in the eigenbasis, hence a local operator cannot have nonzero matrix element between $|t_1\rangle$ and $|t_2\rangle$. Therefore, we employ an eigengate U_{eg}^P to turn $|t_1\rangle, |t_2\rangle$ into spatially extended states $|t_1\rangle_{L_1^z}$ and $|t_2\rangle_{L_1^z}$, while preserving the spectrum and in particular the unique energy gap. We can then resort to the driving protocol proposed in Section 4.3.2 to create

an $\texttt{iSWAP}_{t_1,t_2}$ gate by choosing $H_{\text{bg}} = L_1^z$ and choosing for H_{drive} any operator that couples $|t_1\rangle_{L_1^z}$ and $|t_2\rangle_{L_1^z}$.

It is not clear in general what choices of H_{drive} lead to lower gate errors at similar driving times. One constraint is that the coupling must preserve the expectation value of Q_0^α (i.e. the number of spins in state $|1\rangle$), indicating that couplings such as σ^x or $\sigma^z \otimes \sigma^y$ cannot drive the required transition. For some common nontrivial 1- and 2-local driving operators and small system sizes N, we tabulate the matrix elements ${}_{L_1^z}\langle t_1|H_{\text{drive}}|t_2\rangle_{L_1^z}$ below.

$N=4$	
H_{drive}	${}_{L_1^z}\langle t_1\|H_{\text{drive}}\|t_2\rangle_{L_1^z}$
σ_2^z	$-0.413049i$
$\sigma_2^z\sigma_3^z$	0.829345
$\sigma_1^z\sigma_4^z$	0.829345
$\sigma_2^x\sigma_3^x$	−0.552743
$\sigma_2^y\sigma_3^y$	−0.552743
$\sigma_1^x\sigma_4^x$	0.390066
$\sigma_2^x\sigma_3^y$	0

$N=6$	
H_{drive}	${}_{L_1^z}\langle t_1\|H_{\text{drive}}\|t_2\rangle_{L_1^z}$
σ_3^z	$0.116012i$
$\sigma_3^z\sigma_4^z$	−0.327919
$\sigma_1^z\sigma_5^z$	−0.353636
$\sigma_1^z\sigma_5^z$	0.265128
$\sigma_3^x\sigma_4^x$	0.200378
$\sigma_2^x\sigma_3^x$	−0.147838
$\sigma_1^x\sigma_5^x$	−0.14341

$N=8$	
H_{drive}	${}_{L_1^z}\langle t_1\|H_{\text{drive}}\|t_2\rangle_{L_1^z}$
σ_4^z	$-0.027894i$
$\sigma_4^z\sigma_5^z$	−0.0839009
$\sigma_1^z\sigma_6^z$	0.120287
$\sigma_2^z\sigma_7^z$	0.131574
$\sigma_4^x\sigma_5^x$	0.0471167
$\sigma_1^x\sigma_6^x$	0.0502561
$\sigma_2^x\sigma_7^x$	0.0452589

6.3.1 Tracking dynamical phases

As the energies of L_1^z are sums of single-excitation energies, it is possible to keep track of dynamical phases of individual states efficiently. One could in principle perform an eigengate U_{eg}^P, drive a transition in time t_d, and map back to the computational basis using $(U_{\text{eg}}^P)^\dagger$. The accumulated dynamical phases on qubit j is then equal to $x_j t_d$, which may be undone by a single-qubit phase gate, or by following the halfway inversion protocol.

6.4 Numerical results

We test our claims by simulating the driving step of our protocol, through numerically solving Schrödinger's equation given by the Hamiltonian

$$H_P(t) = L_1^z + \Omega_P \cos(\omega t) H_{\text{drive}}.$$

We consider the cases $N = 4$ and $N = 6$, and two different driving operators H_{drive} which fit in the connectivity of the linear chain. The driving frequency ω is always chosen to be exactly the energy gap between states $|t_1\rangle_{L_1^z}$ and $|t_2\rangle_{L_1^z}$. Moreover, after fixing the driving time t_d, we choose Ω_P such that a π-rotation occurs between the transitioning states, e.g. $|{}_{L_1^z}\langle t_2|H_{\text{drive}}|t_1\rangle_{L_1^z}|\ \Omega_P\ t_d = \pi$. Apart from the halfway inversion, we apply no further optimizations to the protocol.

The results are presented in Fig. 6.3. For extremely short driving times, where $t_d \approx 1$ such that Ω_P is of the order of energy differences of the background Hamiltonian, the gate is highly inaccurate. However, for longer driving times, $t_d > 10$, the gate becomes increasingly accurate, with the error decaying roughly as t_d^{-2} as expected. We also note that the fidelity seems to not strongly depend on the choice of driving operator.

In Fig. 6.4, we depict the effect of the halfway inversion compared to leaving it out. In the latter case, we undo the accumulated dynamical phases with the operation $\exp(+iL_0^z t_d)$ after the system is mapped back to the computational basis. The graph

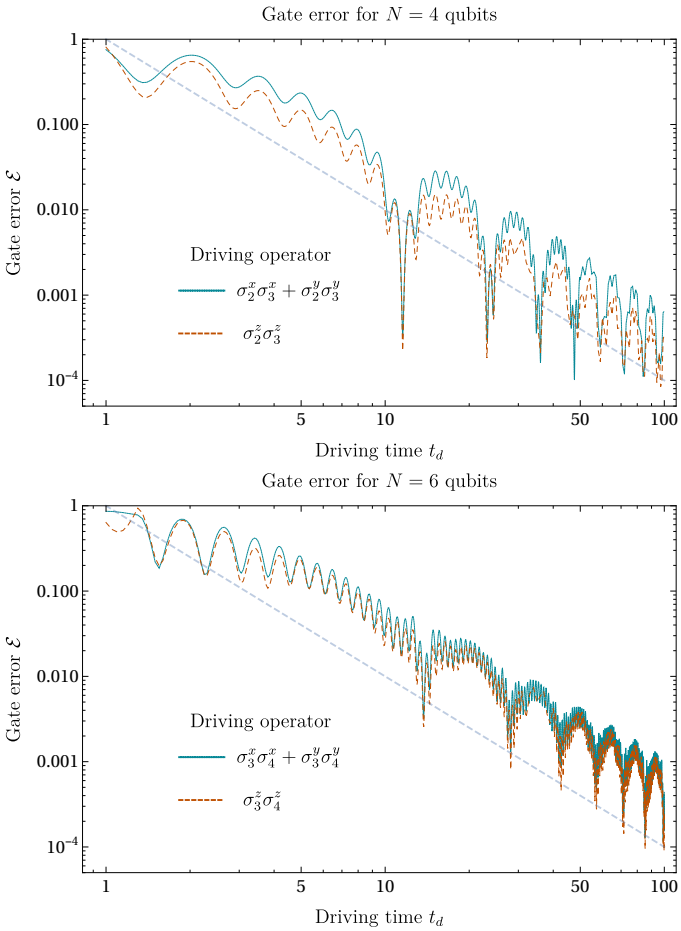

Figure 6.3: Gate error due to the resonant driving stage of our protocol, given various gate times and two different choices of H_{drive}, for a number of qubits equal to $N = 4$ (top) and $N = 6$ (bottom). In these results, we applied the halfway inversion, but no further optimizations. The dashed line follows $\mathcal{E} = t_d^{-2}$. Although the fidelity is strongly oscillatory in t_d, a global tendency towards inverse quadratic decay is clearly visible.

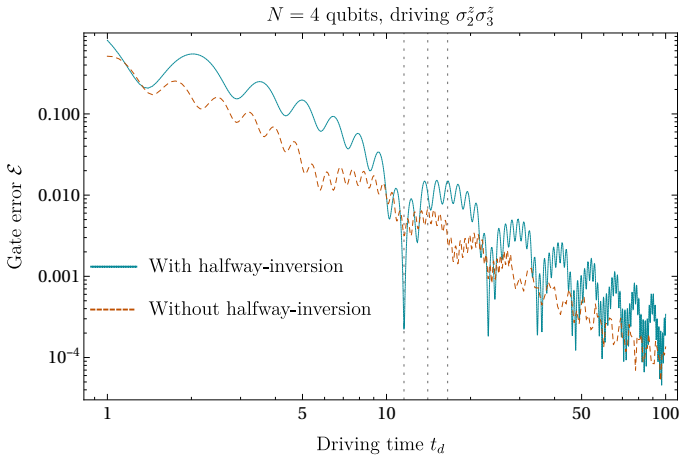

Figure 6.4: A comparison of the gate error either with or without a halfway inversion applied, for the case $N = 4$ and $H_{\text{drive}} = \sigma_2^z\sigma_3^z$. The halfway inversion shows stronger oscillatory behavior, leading to minima that improve the total protocol fidelity by more than an order of magnitude at equal driving times. The times $t_d \in \{11.55, 14.05, 16.55\}$ are highlighted with a gray, dotted line.

shows that the halfway inversion does not necessarily reduce the error at all times, but dramatically improves the error at very specific times.

We suspect that these specific times are precisely the times where, at the time of the halfway inversion, the relative phases of each two-level system are roughly 0, causing the error's leading order term $8\sin(nt)(\Omega^2/\delta^2)$ (Eq. 4.14) to be minimized. We informally check this statement in Fig. 6.5, where the phases corresponding to highly optimal time $t_d = 11.55$ and local maximum $t_d = 16.55$, as well as the point precisely in between, are compared. The circles show the accumulated phase due to H_{bg} for the indicated two-level system, with the rightmost point of the circle corresponding to zero phase. Clearly, the optimal timing is associated with near-optimal phase resets, whereas the more erroneous timing shows phases that could contribute a significant error of order Ω^2/δ^2.

6.4.1 Comparison of gate times

So how do our driving times t_d compare to other quantum gate times in the same system? A conventional two-qubit gate could be constructed if each of the individual Hamiltonian terms $h_{jk}P_{jk}$ could be turned on independently. A $\pi/4$ pulse would suffice to create maximal entanglement, so we require times t such that $h_{jk}t = \pi/4$. For $N = 4$, the corresponding times t lie between 0.86 and 1.0 for neighboring qubits, and up to 8.56 for the most distant qubits. These should be compared to the 11.55 units of time required to perform an $\texttt{iSWAP}_{1100,0011}$ at low error $\mathcal{E} < 0.001$. Hence, within the time of our four-qubit iSWAP operation, up to 13 two-qubit gates could be done.

Similarly, for $N = 6$, neighboring qubits could be entangled in times between 0.60 and 0.81, or up to 17.36 to entangle the outermost qubits. This should be compared to the driving time $t_d = 13.75$ to obtain a driven gate with error $\mathcal{E} < 0.003$. Hence, our six-qubit resonant gate takes time equivalent to up to 23 two-qubit gates.

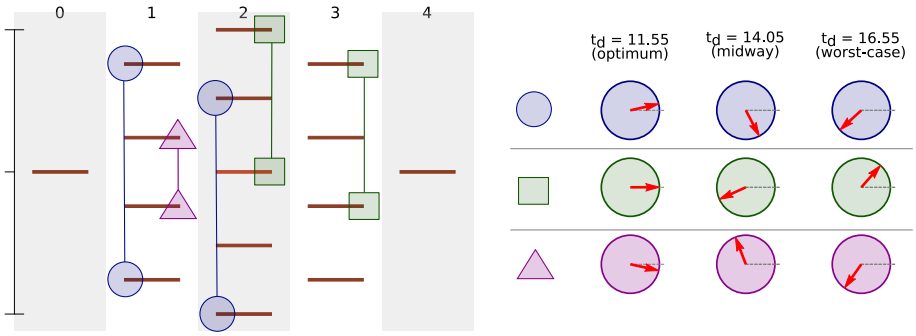

Figure 6.5: For near-resonant two-level systems, the accumulated phases at the time of the halfway-pulse ($t_d/2$) affect the fidelity of protocol. In the spectrum of L_1^z with $N = 4$ qubits, we select three different energy gaps (indicated by a pair of connected circles, squares or triangles), for which we depict the corresponding relative phases at t_d as vectors on the unit sphere. A relative phase of 0 corresponds to a vector pointing to the right (dashed lines). At $t_d = 11.55$, corresponding to a local minimum of our gate error $\mathscr{E}$, all phases are close to zero. On the other hand, at local maximum $t_d = 16.55$, the phases are all far from zero. The (non-)alignment of these phases explains the oscillatory behavior of our protocol's error as a function of time.

In general, it is unclear how to compare gate times between different gate sets, or how to optimally decompose `iSWAP` operations into smaller constituents. Turning to the well-studied `Toffoli` gate, the best bounds we could find are listed in Ref. [SM09], stating that a `Toffoli` on four qubits requires between 8 and 14 `CNOT` operations. Note that these results assume full connectivity between all qubits, and do not account for the cost of single-qubit gates. For larger numbers of qubits, the `CNOT` cost is found to scale linearly in N as long as auxiliary qubits may be used - without auxiliaries, it would be quadratic. Different physical interactions may also lead to different gate counts. For example, Ref. [SS03] finds that constructing a `CNOT` out of our interaction P_{jk} requires two $\pi/4$ pulses, and constructing a mere three-qubit `Toffoli` using the closely related XX interaction requires as much as ten fundamental entangling operations. We conclude that it is not possible to make a rigorous comparison between different gate sets, but that the duration of our resonantly driven gate is competitive with conventional decompositions, with both approaches having unique advantages and disadvantages depending on the specific implementation.

6.5 Conclusion

The operators L_0^α and L_1^α turn out to be related by fast quenches of Hamiltonians such as H_P and Q_0^α. This provides a large amount of utility when these interactions are available to a system, allowing straightforward basis transformations, such as the eigengate for L_1^z that we considered here. It would be interesting to look for further applications of these quenches.

Just as with the Krawtchouk chain, the driven multiqubit gates are limited in use due to the unfavorable scaling of the matrix elements for the driving operators that we consider. In the next chapter, we discuss a system in which these numbers do not decay with system size, but this requires a star-shaped graph where many qubits are

strongly coupled to a single ancilla. Finding a well-understood *linear chain* that allows driven multiqubit gates even in the large N limit remains an open problem.

CHAPTER 7

The Ising star model

In the previous chapters, we proposed and analyzed multiqubit gates based on resonant driving, and found that the gate times increased rapidly as the number of qubits n grew. In this chapter, we take on the ambitious task to construct resonant gates that are efficient for larger system sizes, even beating optimal circuit decompositions of such gates.

In Section 4.1, we describe that the best known decomposition of the $\texttt{Toffoli}_n$ gate requires a circuit of depth $O(\log(n))$, which involves $O(n)$ ancillary qubits. Is there any hope that a continuous evolution can implement the same gate, such that the gate time T grows *slower* than logarithmically in n? We investigate this question by coupling n qubits to a single ancilla. Straightforwardly simulating the resulting evolution using the the Trotter-Suzuki formula [Llo96] would result in a circuit of depth $O(n)$, whereas the continuous evolution takes a constant amount of time. This makes our configuration an interesting candidate for a resonant gate that outperforms the circuit decomposition.

We impose that the interaction between the ancilla and the other qubits is of the Ising type (see Section 2.3), and that the interaction strengths are equal. This allows us to efficiently calculate the eigensystem of the Hamiltonian. We then find an appropriate driving field on the ancilla, such that the system's evolution approximates a $\texttt{Toffoli}_n$ gate after a time T, where T is *constant* in n. Moreover, the approximation error does not increase with n, and can be made arbitrarily small by choosing a larger gate time T.

The constant gate time clearly beats the $\log(n)$ depth required by the best known quantum circuit. However, the assumption that a large number of qubits are coupled with constant amplitude may be unrealistic for very large n. Moreover, the frequency required to perform resonant driving *does* increase with n, which puts unrealistic constraints on control hardware. Still, our proposal could greatly enhance implementations of quantum algorithms on near-term quantum computers with a moderate (5-100) number of qubits [Pre18].

Our contribution is closely related to earlier work on gates that exploit the Rydberg blockade, a strong long-ranged interaction that is effectively of the Ising type. The blockade interaction is available to certain types of atoms that are called Rydberg atoms. As an example, Ref. [ISM11] proposes a five-step pulse sequence on ultracold Rydberg atoms that leads to the $\texttt{Toffoli}_n$ gate. Here, the number of control qubits $n-1$ is arbitrary, as long as the target qubit is sufficiently close to all control qubits to notice their Rydberg blockade interaction. Similarly, a more recent proposal

by [Shi18] involves a five-pulse sequence on three Rydberg atoms that forms the universal $\texttt{Deutsch}(\theta)$ gate, of which the $\texttt{Toffoli}_3$ is a special case.

In the following, we do not simply assume a perfect Rydberg blockade, but rather consider an all-to-all Ising model with limited interaction strengths. Due to the symmetry of our model, we are able to explicitly calculate the error introduced by resonant driving fields.

7.1 Analysing the model

We consider a set of $N = n+1$ qubits, which we label by $[n] := \{0, 1, \ldots, n\}$. We assume that each pair $\{j, k \in [n] : \ j \neq k\}$ is coupled with Ising-type interaction, of stength w_{jk}, as described by the Hamiltonian

$$H_{\text{Ising}} = \frac{J}{2} \sum_{j<k} w_{jk} Z_j Z_k. \tag{7.1}$$

Qubit 0 will be our special ancilla qubit, and the other qubits will be called work qubits. We denote our quantum states in the computational basis as $|x_0, \vec{x}\rangle$, where $x_0 \in \{0,1\}$ represents the state of the ancilla, and $\vec{x} \in \{0,1\}^n$ denotes the states of the work qubits. The states $|x_0, \vec{x}\rangle$ are the eigenstates of H_{Ising}, whose energies we denote by $E_{x_0,\vec{x}}$.

Now, consider the effect of a driving field on the ancilla, of the form

$$H_{\text{drive}} = \alpha(t) X_0 + \beta(t) Y_0. \tag{7.2}$$

This may cause the ancilla to flip, but does not directly affect the other qubits. Hence, under the combined Hamiltonian $H_{\text{Ising}} + H_{\text{drive}}$, the Hilbert space decomposes into conserved subspaces, each of which can be labeled by the state $\vec{x}$ of the work qubits:

$$\mathscr{H}_{\vec{x}} = \text{span}(|0, \vec{x}\rangle, |1, \vec{x}\rangle). \tag{7.3}$$

Within each of these subspaces, the combined Hamiltonian $H = H_{\text{Ising}} + H_{\text{drive}}$ acts as

$$\begin{aligned} H_{\vec{x}} &= \begin{pmatrix} E_{0,\vec{x}} & \alpha(t) - i\beta(t) \\ \alpha(t) + i\beta(t) & E_{1,\vec{x}} \end{pmatrix} \\ &= \begin{pmatrix} \Delta_{\vec{x}}/2 & \alpha(t) - i\beta(t) \\ \alpha(t) + i\beta(t) & -\Delta_{\vec{x}}/2 \end{pmatrix} + \bar{E}_{\vec{x}}\, \mathbb{1}, \end{aligned} \tag{7.4}$$

where we defined the energy gap $\Delta_{\vec{x}} = E_{0,\vec{x}} - E_{1,\vec{x}}$ and the mean energy $\bar{E}_{\vec{x}} = \frac{E_{0,\vec{x}} + E_{1,\vec{x}}}{2}$.

Now, consider the special configuration of couplings

$$\begin{aligned} &w_{0k} = 1 \quad \forall\ k \in \{1, \ldots, n\} \qquad \text{(Star couplings)} \\ &w_{jk} = 0 \quad \forall\ j \geq 1. \end{aligned} \tag{7.5}$$

This gives rise to a star-shaped connectivity, where all work qubits are coupled to the ancilla, but not among each other. Now, H_{Ising} has a spectrum as indicated in Fig. 7.1: the ground energy is $E = -Jn/2$ when all work qubits are *different* from the ancilla, and $+J$ energy is added for each work qubit that is the same. The complete eigensystem is

$$\begin{aligned} &\{|0, \vec{x}\rangle : |\vec{x}|_H = q\} \qquad E_{0,\vec{x}}/J = \frac{n}{2} - q \qquad \text{(Star couplings)} \\ &\{|1, \vec{x}\rangle : |\vec{x}|_H = q\} \qquad E_{1,\vec{x}}/J = -\left(\frac{n}{2} - q\right) \end{aligned}$$

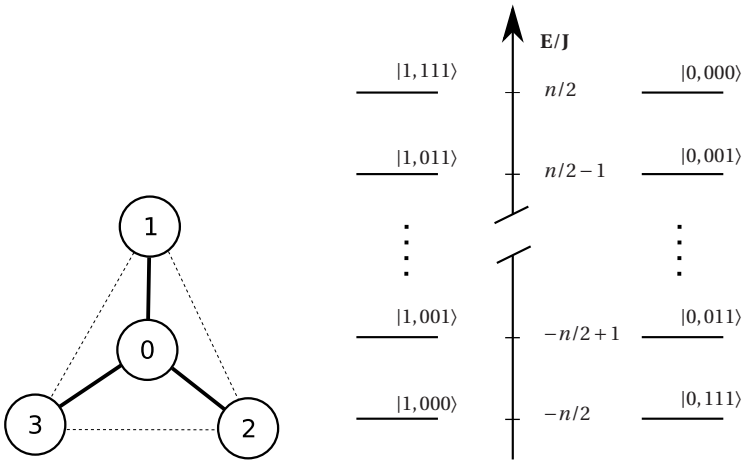

Figure 7.1: The left image sketches the connectivity of our model. The right-hand side displays the energy spectrum in units of E/J for the Star couplings when $n = 3$.

where $|\vec{x}|_H = q \in \{0,\dots,n\}$ denotes the Hamming weight (i.e. the number of ones) of the bitstring $\vec{x} \in \{0,1\}^n$. For this configuration, $H_{\vec{x}}$ takes a particularly simple form: the gap $\Delta_{\vec{x}} = J(n-2q)$ is the same for all subspaces with the same Hamming weight q, and the mean energy $\bar{E}_{\vec{x}} = 0$ vanishes for all subspaces.

Now, let us turn on the couplings w_{jk} between the work qubits, leaving the couplings connected to the ancilla fixed at $w_{0k} = 1$. The resulting changes in energy due to H_{Ising} can now only depend on the state $\vec{x}$ of the work qubits, not on the state of the ancilla. Hence, the energy gap $\Delta_{\vec{x}} = E_{0,\vec{x}} - E_{1,\vec{x}}$ will not change as a response to this. In fact, the only parameter of $H_{\vec{x}}$ that changes is $\bar{E}_{\vec{x}}$, leading to a subspace-dependent phase.

Even more generally, we may *also* allow varying couplings to the ancilla. In this case, the energy gap varies per subspace,

$$\Delta_{\vec{x}} = J \sum_{j=1}^{n} w_{0j}(-1)^{\vec{x}_j}, \tag{7.6}$$

but does not change $\bar{E}_{\vec{x}}$. In general, this changes each of the 2^n subspaces in a different way, making the time evolution even harder to track.

In the following, we will first assume the most general case, allowing us to obtain exact expressions for the time evolution of any individual subspace $H_{\vec{x}}$. Next, we will resort to certain assumptions that allow us to compute the time evolution of the *full* 2^N-dimensional system in an efficient way, i.e. requiring a time that scales polynomially with the system size n.

7.2 Resonant driving on Ising eigenstates

We consider two possible driving fields for Eq. 7.2,

$\alpha(t) = 2\Omega\cos(\Delta_{\text{res}}t + \phi), \quad \beta(t) = 0$	single quadrature
$\alpha(t) = \Omega\cos(\Delta_{\text{res}}t + \phi), \quad \beta(t) = \Omega\sin(\Delta_{\text{res}}t + \phi)$	two quadratures

where ϕ is the driving phase, and Ω is the Rabi frequency, which sets the energy scale. Due to the decomposition in Eq. 7.3, the approximation that driving excitations occur in isolated two-level systems that we dicussed in Section 4.3 becomes *exact*. For the case of two-quadrature driving, we can analytically solve the evolution of the two-dimensional subsystems, by moving to the rotating frame for each space $\mathscr{H}_{\vec{x}}$. Using the transformation

$$U_{\text{int}}(t) = \exp\left(+it\left(\frac{\Delta_{\text{res}} Z}{2} + \tilde{E}_{\vec{x}}\mathbb{1}\right)\right) \tag{7.7}$$

the Hamiltonian $H_{\vec{x}}$ becomes time-independent:

$$\begin{aligned}\tilde{H}_{\vec{x}} &= \begin{pmatrix} \frac{\Delta_{\vec{x}}-\Delta_{\text{res}}}{2} & \Omega e^{-i\phi} \\ \Omega e^{i\phi} & -(\frac{\Delta_{\vec{x}}-\Delta_{\text{res}}}{2}) \end{pmatrix} \\ &= \delta Z + \Omega\left(\cos(\phi)X + \sin(\phi)Y\right).\end{aligned}$$

We use tildes to indicate that quantities are valid in the rotating frame, and use δ as shorthand for the off-resonance, $\delta = \frac{\Delta_{\vec{x}}-\Delta_{\text{res}}}{2}$. Having removed the time-dependence, the unitary effect of $\tilde{H}_{\vec{x}}$ after time t can be calculated as

$$\begin{aligned}\tilde{U}_{\vec{x}}(t) = \exp(-i\tilde{H}_{\vec{x}}t) &= \cos(\nu t)\mathbb{1} - i\sin(\nu t)\frac{\vec{\sigma}\cdot\vec{v}}{\nu} \\ \vec{v} = \begin{pmatrix} \Omega\cos(\phi) \\ \Omega\sin(\phi) \\ \delta \end{pmatrix}, &\quad \nu = \sqrt{\Omega^2+\delta^2},\end{aligned} \tag{7.8}$$

where $\vec{\sigma} = \{X, Y, Z\}$. Note that δ is the only parameter that implicitly depends on $\vec{x}$.

As before, we find selective state inversion. When the subspace labeled $\vec{x}$ is on resonance, i.e. when $\Delta_{\text{res}} = \Delta_{\vec{x}}$, then a rotation around a vector in the $X-Y$ plane occurs, leading to a perfect inversion at stopping time $T = \frac{\pi}{2\Omega}$:

$$\tilde{U}_{\vec{x}}(T) = -i(\cos(\phi)X + \sin(\phi)Y) \qquad \text{(on resonance, } \Delta_{\text{res}} = \Delta_{\vec{x}}\text{)}.$$

For off-resonant subspaces, i.e. assuming $|\Omega| \ll |\Delta_{\text{res}} - \Delta_{\vec{x}}|$, a rotation very close to the non-driven case ($\Omega = 0$) is obtained:

$$\tilde{U}_{\vec{x}}(t) \approx \exp\left(-i\delta Z t\right) \qquad \text{(off resonance, } \Delta_{\text{res}} \neq \Delta_{\vec{x}}\text{)}. \tag{7.9}$$

We will assess the error introduced by the driving fields compared to the non-driven case shortly.

7.3 Turning the driven evolution into a `Toffoli`

Let us now assess how the resonant transition is similar to a `Toffoli` gate. If all w_{0j} are nonzero and have the same sign, then the subspace $\vec{x} = 11\ldots1$ has the largest or smallest energy gap $\Delta_{\vec{x}}$, which is unique. Choosing $\Delta_{\text{res}} = \Delta_{\vec{x}=1\ldots1}$, the resulting evolution after time T is then very similar to a `Toffoli` gate, where the ancilla is flipped if

and only if the work qubits are in a state $|1\rangle$. Moving back from the rotating frame to the lab frame using $U_{\vec{x}} = U_{\text{int}}^{\dagger}(t)\tilde{U}_{\vec{x}}$, we obtain the following operation U_{tot} at time T:

$$U_{\text{tot}} \approx \begin{array}{c} \text{basis:} \quad 0\vec{x} \quad 1\vec{x} \quad\quad\quad 01\ldots1 \quad\quad 11\ldots1 \\ \begin{pmatrix} \ddots & & & & & & \\ & \ddots & & & & & \\ & & e^{-iE_{0,\vec{x}}T} & 0 & & & \\ & & 0 & e^{-iE_{1,\vec{x}}T} & & & \\ & & & & \ddots & & \\ & & & & & \ddots & \\ & & & & & 0 & -ie^{-i\phi-iE_{0,1\ldots1}T} \\ & & & & & -ie^{i\phi-iE_{1,1\ldots1}T} & 0 \end{pmatrix} \end{array}$$

Even if one accepts the approximation in Eq. 7.9, there are two important differences from an actual $\texttt{Toffoli}_N$ gate:

1. The additional phase $-ie^{\pm i\phi}$ in the resonant subspace $\vec{x} = 1\ldots1$. Note that this is *not* a global phase.

2. The additional phases $E_{x_0,\vec{x}}T$ due to H_{Ising}.

The 2^N different energies $E_{x_0,\vec{x}}$ can in general be hard to compute for a large system. Undoing them may be even harder. However, one can conceive various specific configurations where resetting the phases is possible.

In particular, whenever the system is symmetric under permutations on the work qubits, then all subspaces with the same Hamming weight q behave the same, and only $n+1$ different subsystems have to be considered. Various techniques can then be used to undo the dynamical phases. One example is to choose a total gate time T such that all phases are $E_{x_0,\vec{x}}T$ become a multiple of 2π. For example, in the star configuration, the energy differences are all integer multiples of J, hence choosing a total driving time $T = 2k\pi/J$ ($k \in \mathbb{N}$) gets rid of unwanted phases.

Assuming we have somehow removed the phases due to H_{Ising}, we turn to removing the phases $-ie^{\pm i\phi}$, for which we propose the circuit below:

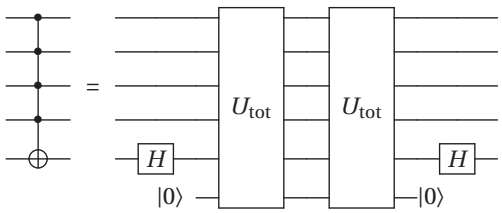

(7.10)

Note that applying the resonant operation *twice*, leads to a phase -1 in the resonant subspace. This is similar to a multiple-controlled Z gate except that the sign is applied both when the ancilla is in state $|0\rangle$ and when it is in state $|1\rangle$. Hence, we obtain a multiple-controlled Z-gate which applies a sign -1 to the work qubits if and only if all these qubits are in the state $|1\rangle$. The state of the ancilla is unimportant, and we may just as well initialize it to $|0\rangle$ before the protocol. Finally, the controlled-Z is mapped to a controlled-X by using two Hadamard gates – these can be applied to any work qubit, and that qubit then takes the role of target of the $\texttt{Toffoli}_n$.

7.3.1 Expressing the gate error

We turn back to Eq. 7.9, which we claim is a good approximation to the off-resonant evolution stated in Eq. 7.8. To assess the quality of this approximation, we consider two different measures of gate error. Firstly, the *trace error* or *matrix inner product* is defined as

$$\mathscr{E}_{\mathrm{tr}}(U, U_{\mathrm{goal}}) = 1 - \frac{1}{\dim(U)} \mathrm{tr}(U U_{\mathrm{goal}}^{\dagger})$$

which gives an averaged error. Secondly, the *operator norm* of the difference is given by

$$\mathscr{E}_{\mathrm{norm}}(U, U_{\mathrm{goal}}) = ||U - U_{\mathrm{goal}}||$$

which returns the largest eigenvalue of $U - U_{\mathrm{goal}}$ and hence captures the worst-case error of our gate.

Let us now assume a permutation symmetry among the work qubits. Then the evolution $\tilde{U}_{\vec{x}}$ depends only on the Hamming weight q of the vector $\vec{x}$, and we will use U_q to denote the evolution in subspaces with $|\vec{x}|_H = q$. We can then simplify the expressions for the gate error. For the matrix inner product,

$$\mathscr{E}_{\mathrm{tr}}(U, U_{\mathrm{goal}}) = 1 - \frac{1}{\dim(U)} \sum_{q=0}^{n} \mathrm{tr}(U_q U_{\mathrm{goal},q}^{\dagger}) \binom{n}{q}$$

where the binomial coefficient counts the number of subspaces with the corresponding Hamming weight. Likewise,

$$\mathscr{E}_{\mathrm{norm}}(U, U_{\mathrm{goal}}) = \max_q ||U_q - U_{\mathrm{goal,q}}||.$$

In the following, we choose to work in the interaction picture, as defined by Eq. 7.7. This way, the energies $E_{x_0,\vec{x}}$ due to H_{Ising} drop out, allowing us to assess purely the driving error at any gate time T. Then, the work qubits need not even be completely permutation symmetric: assuming identical couplings to the ancilla is sufficient to justify a q-dependent treatment. Still, to obtain a proper quantum gate, the dynamical phases need to be undone somehow.

To form a resonant gate, we choose the driving frequency Δ_{res} to be resonant with the subspace with weight $q_0 = 0$, i.e. $\Delta_{\mathrm{res}} = \Delta_{\vec{x}=0\ldots0}$. Note that his is equivalent to the case $q_0 = n$ of the `Toffoli` gate we considered before, but will lead to slightly cleaner notation. We stress that other configurations and other resonant frequencies Δ_{res} can be addressed analogously.

We choose to keep T as a free parameter, such that the errors will become a function of the total gate time. Setting $\Omega = \frac{\pi}{2T}$ guarantees that for any T, a perfect inversion occurs in the resonant subspace. The evolution in the resonant subspace $q = 0$ is always exact (no error), while the off-resonant evolutions $\tilde{U}_q$ for $q \neq 0$ are compared to the goal $\tilde{U}_{\mathrm{goal,q}} = e^{-i\delta Z t}$, with $\delta = -Jq$ for the star couplings.

For the trace inner product, we obtain fidelities for subspaces q as

$$\mathscr{F}_q := \mathrm{tr}\left(\tilde{U}_q(T)\tilde{U}_{\mathrm{goal,q}}^{\dagger}(T)\right) = 2\cos(JTq)\cos(JT\nu) + \frac{2q}{\nu}\sin(JTq)\sin(JT\nu)$$

$$\text{with } \nu = \sqrt{\frac{\pi}{4J^2T^2} + q^2}$$

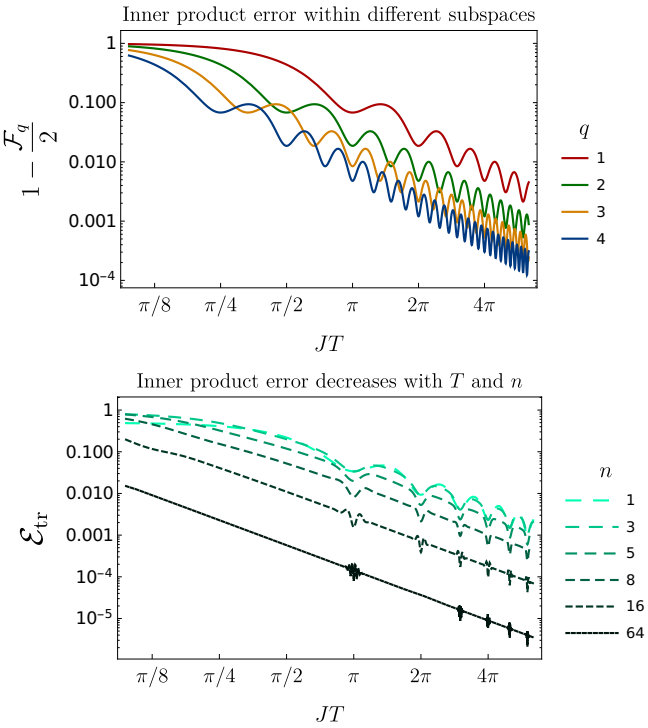

Figure 7.2: The inner product error as a function of gate time T, assuming the resonant subspace has weight $q_0 = 0$. Note that the vertical axes follow a logarithmic scale. Top: The error contribution for subspaces whose weights differ from q_0 by 1 up to 4. Bottom: The cumulative error $\mathscr{E}_{\mathrm{tr}}$, for various system sizes n.

In Fig. 7.2, we plot the dependence of $\mathscr{F}_q$ as a function of gate 'time' JT, as well as the average error $\mathscr{E}_{\mathrm{tr}}$ for varying n. We find that according to this metric, the gate fidelity actually *improves* with larger system sizes, which is explained as follows. For any n, there are n subspaces with weight $q = 1$ which are the least off-resonant, but an exponentially large number of subspaces with much larger off-resonance are added. Hence, the averaged error benefits more from the many off-resonant subsystems when n increases.

For the operator norm, we obtain

$$\begin{aligned}\tilde{U}_q(T) - \tilde{U}_{\mathrm{goal},q}(T) = \mathbb{1}\left(\cos(JTv) - \cos(JTq)\right) \\ + Z\left(\frac{iw}{v}\sin(JTv) - i\sin(JTq)\right) \\ + (\cos(\phi)X + \sin(\phi)Y)\left(\frac{-i\pi}{2JTv}\sin(JTv)\right),\end{aligned}$$

allowing us to efficiently calculate the exact operator norm error in each individual weight-q subspace. The results are shown in Fig. 7.3. It is clear that the most resonant subspace, $q = 1$, always contributes the largest error. Therefore, the max operation can be dropped in $\mathscr{E}_{\mathrm{norm}}$, and we find that operator norm error is actually *independent* of n.

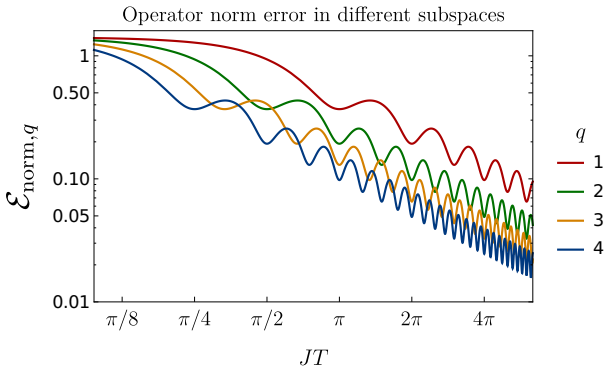

Figure 7.3: The operator norm error $\mathscr{E}_{\mathrm{norm},q}$ contributions due to subspaces with weights $q = 1,\ldots 4$, at various protocol times. The overall error $\mathscr{E}_{\mathrm{norm}}$ for the whole gate is always the maximum, hence is completely determined by $q = 1$.

The same derivation could be performed whenever a subspace different from $q_0 = 0$ is to be flipped. By choosing the driving frequency $\Delta = J(n-2q_0)$, one will approximately find the operation where ancilla is inverted if and only if the work qubits have weights $|\vec{x}|_H = q_0$. The values q in the above should then be replaced with $q - q_0$.

Lastly, we consider the effect of using single-quadrature driving instead of the two-quadrature driving fields we consider above. Hence, we assume that

$$\alpha(t) \propto \cos(\Delta_{\mathrm{res}} t) \propto \exp(i\Delta_{\mathrm{res}} t) + \exp(-i\Delta_{\mathrm{res}} t)$$

such that effectively *two* driving fields act on each two-dimensional subspace. The two resonant resonant energies differ by a sign namely Δ_{res} and $-\Delta_{\mathrm{res}}$. Assuming that H_{Ising} is the only Hamiltonian that acts on the qubits, then $\Delta_{\vec{x}=1\ldots1} = -\Delta_{\vec{x}=0\ldots0}$. This voids our argument that the subspace labeled $\vec{x} = 11\ldots1$ is the unique resonant subspace, because $\vec{x} = 00\ldots0$ is now also on resonance.

There are two straightforward solutions that prevent the transition $|0,0\ldots0\rangle \leftrightarrow |1,0\ldots0\rangle$ from taking place. We can do so by turning one work qubit into an ancilla that is initialized to the state $|1\rangle$, such that the $\vec{x} = 0\ldots0$ subspace is never populated. The other solution is to consider a local field of the form $H = BZ_0/2$ acting on the ancilla qubit, with some field strength B. The relevant energy gaps are then $B + \Delta_{\vec{x}=1\ldots1}$ and $B - \Delta_{\vec{x}=1\ldots1}$, which no longer differ by a sign. Most experimental quantum computers already feature some energy difference between the $|0\rangle$ and $|1\rangle$ state, making the second solution a very natural choice.

Moreover, note that under single-quadrature driving, our results are no longer exact. Still, the Rotating Wave Approximation (RWA) shows that our reasoning about resonant and off-resonant subspaces still holds as long as detunings are large compared to other energy scales.

7.4 Discussion of asymptotic scaling

In the above, we assumed that n qubits were strongly coupled to our ancilla, and that the *driving frequency* Δ_{res} has no bounds. Then, the protocol time and the errors are

roughly *constant* as a function of n. This is surprising, as this is a better asumptotic scaling than the $O(\log(n))$ time required by a gate-based quantum circuit. In particular, in our proposals in Chapters 5 and 6, the gate time increased *superpolynomially* with n.

Still, it is not immediately clear if our assumptions are realistic. Firstly, the oscillation frequency Δ_{res} for the resonant subspace $q_0 = n$ increases linearly with n in our protocol. This may not be realistic, and if one requires the frequency Δ_{res} to be bounded, then the Hamiltonian's energy scale needs to be scaled down with a factor $1/n$. This effectively causes all time scales to increase by a factor n, retrieving an $O(n)$ time protocol.

Secondly, coupling n qubits to a single ancilla would be challenging to realize in physical, 3-dimensional space, as each of these n qubits would need to be sufficiently close to the ancilla. Any realistic method to implement this would probably set a maximum for n.

7.5 Experimental implementations

We consider two experimental platforms on which our proposal could be implemented in near-term experiments. Firstly, ultracold atoms of the Rydberg type natively feature a strong Ising-type interaction [Saf16]. Various earlier proposals for multiqubit operations based on the Rydberg blockade interaction exist, such as Refs. [LFC+01; UF02; ISM11; Shi18], and some of these have been experimentally tested [EKW+15; ZSH+15]. The specific `Toffoli`-type gates have, to our best knowledge, never been implemented, but Ref. [GDM15] performs a detailed simulation of the $\texttt{Toffoli}_3$ proposed in Ref. [ISM11], finding that the multiqubit implementation may have advantages over a sequence of one- and two-qubit gates.

Secondly, trapped ions are very well suited to simulate the Ising model with all-to-all connectivity. These systems typically involve ionized atoms positioned on a line, and for each ion, two electronic states are chosen to form the qubit degree of freedom. By coupling the qubits to motional states of the ions using a two Raman lasers, an effective interaction between the qubits can be formed, which approximates the Ising model. The couplings strengths are then of the form $w_{jk} \propto 1/(j-k)^\alpha$ with $\alpha \in [0,3]$ [KCI+09; BR12; BSK+12; ISC+13]. The choice $\alpha = 0$ makes all interactions equal, leading to a highly symmetric system for which the energies $\bar{E}_{\vec{x}}$ are efficiently calculated.

We identify various challenges for a real-world implementation of our gate using trapped ions. Firstly, the amplitude of the Ising interaction J is determined by the off-resonance between the Raman lasers and a certain transition in which a phonon is created. Entanglement with phonons can be avoided by choosing a sufficiently large detuning, which in turn leads to a small interaction strength J. Because our resonant field on the ancilla must have an amplitude Ω that is much smaller than J, there are two mechanics at play that favor a very small value of Ω, leading to very long gate times for an accurate gate. Alternatively, choosing the Raman lasers closer to resonance with the relevant transition increases J, but causes the phonon number to oscillate with larger amplitude. Driving a transition between the states $|1,\vec{x}\rangle$ and $|0,\vec{x}\rangle$ when these are entangled to a different phonon number introduces unwanted errors in the final gate. Therefore, a competitive implementation of our proposal on trapped ions requires further optimization.

To illustrate, a closely related experiment was performed in Ref. [SSR+14]. Here, up to 18 ions are made to approximate some Ising interaction, while at the same time, a resonant driving field is applied to *all* ions simultaneously. The interaction strength is of the order of a few kHz, which is sufficiently strong to identify certain transitions for spectroscopic applications. However, we believe that the resulting evolution is too inaccurate to form a high-fidelity multiqubit gate at this point.

7.6 Conclusion

In conclusion, we studied resonant driving on an ancilla qubit coupled to n other qubits through Ising interactions, and find that a highly selective operation can be obtained, namely a a bitlip if and only if the work qubits have a certain Hamming weight. The Hamiltonian block-diagonalizes into invariant two-dimensional subspaces, and if the energies of each subspaces are known, then we can efficiently track the state's evolution within that space. This allows us to calculate exact values of the error compared to an ideal $\texttt{Toffoli}_n$ gate. The gate time, at constant error, is found to be a non-increasing function of the system size, under the assumption that interaction strengths remain constant and that the driving field can oscillate at arbitrary frequencies. For near-term quantum computers of moderate system size, this approach could lead to fast and high-precision multiqubit gates.

Part III

Adiabatic transport of quantum states

CHAPTER 8

STIRAP and CTAP on semi-bipartite graphs

8.1 Introduction

Recall from Section 3.2 that STImulated Raman Adiabatic Passage (STIRAP) is a state transfer protocol that acts on a three-state system. Labeling the states as $\{|j\rangle\}_{j=1}^{3}$, the protocol maps the state $|1\rangle$ to state $|3\rangle$ without requiring any direct interaction between $|1\rangle$ and $|3\rangle$. Rather, it couples these states to some intermediate state $|2\rangle$ by two tuned laser pulses [GRS+90]. A distinguishing feature is that state $|2\rangle$ is minimally populated, making the evolution largely insensitive to decoherence due to the intermediate state [VRS+17]. The protocol is now widely adopted in fields where accurate control of quantum states is vital, such as high precision measurement [Kas02; KBK+15], studies of atoms and molecules [KTS07; SPG+12; PRM15; MCM+17; CBC+17], and quantum information processing [PW02; THM03; PK04; TBJ+11; KCF13]. A recent review of results and applications can be found in Ref. [VRS+17].

A mathematically equivalent protocol can be used to spatially displace quantum amplitudes. In 2004, two independent works proposed state transfer of quantum particles over linear chains, by tuning the hopping strengths instead of laser fields: Ref. [ELC+04] considered neutral atoms in optical lattices, whilst Ref. [GCH+04] addressed electrons tunneling between quantum dots. The latter introduced the name Coherent Tunneling by Adiabatic Passage (CTAP), which we will also use to denote spatial transfer. Apart from particle tunneling, the same model applies to ferromagnetic spins under XX interaction [OEO+07], where a single spin excitation can be adiabatically transferred.

With the advent of quantum information processing, accurate control and high-fidelity qubit transport in increasingly large systems have become an important scientific challenge [DiV00; Pre18]. As we argue in Section 3.2.3, the majority of scientific attention focused on transfer over linear chains [VRS+17; MBA+16], whilst little is known about adiabatic transfer in more general systems. Already in the 90s, STIRAP was generalized to linear chains of odd length N, allowing transfer between the endpoints of the chain [MT97]. More recent work includes Refs. [BRG+12; Lon14], which consider square and triangular grids, and Ref. [GDH06], which addresses multiple parties dangling on a line, each of whom could send or receive the quantum state. Other works, such as Refs. [CFX+13; BJG15] describe a variation where the chain splits into multiple paths or branched endpoints. These protocols are shown to work by a clever mapping back to the original protocol on the chain.

We aim to find more general configurations that allow a similar transfer protocol, by describing a system's interactions in the language of graphs (Section 2.2.1): the vertices represent basis states and edges represent interactions. We look at bipartite graphs, where the basis states can be separated into two sets V_1 and V_2, such that each state interacts only with states outside its own set. If the two sets differ in size by one, then amplitude transfer between states in the bigger set may be possible. We can guarantee successful transfer when certain graph properties are satisfied, as made precise in Theorem 3.

Interestingly, our approach naturally provides a means to transfer amplitude to one out of multiple potential receivers, generalizing Ref. [GDH06]. We find that the final receiver need not yet be known when starting the protocol, which could be an advantage in quantum information processing.

These results advance the fields of STIRAP and spatial transfer in two ways. Firstly, they open the way to practical adiabatic passage in more general systems. Secondly, they shed light on possible perturbations in conventional STIRAP and their effect: we find that many perturbations, as long as they satisfy our assumptions, do not cause a qualitatively different effect on the state's evolution during the protocol.

Our treatment of bipartite graphs is reminiscent of the celebrated Morris-Shore (MS) transformation [MS83]. The transformation finds a unitary map A on the part V_1 and a unitary map B on part V_2, such that the system decomposes into a set of decoupled two-level systems, and a set of uncoupled states. Similar to the setting of MS, we focus on the uncoupled states, which are called dark states. Our contribution is distinct from work related to MS transformations, due to the focus on adiabatic transfer techniques, in which the MS transformation would continuously change in time. Therefore, it is not immediately clear how MS could guarantee that our adiabatic state remains nondegenerate, and we choose to resort to other techniques.

This chapter is organized as follows. In Section 8.2, we review the conventional STIRAP and CTAP protocol, after which we present our main result on more general graphs in Section 8.3. We then discuss the applicability in real-world systems in Section 8.4, and methods to obtain graphs that satisfy our assumptions in Section 8.5. We numerically test the scaling of the adiabatic gap in various graphs, and the fidelity of our protocol, in Section 8.6, and finish with a conclusion in Section 8.7.

8.2 Conventional STIRAP

The conventional STIRAP protocol (Fig. 8.1) deals with a three-dimensional quantum system, consisting of eigenstates $\{|j\rangle\}_{j=1}^{3}$ of some background Hamiltonian. To transfer amplitude from $|1\rangle$ to $|3\rangle$, a sequence of two laser pulses is applied: the Stokes pulse coupling $|2\rangle \leftrightarrow |3\rangle$, and the Pump pulse coupling $|1\rangle \leftrightarrow |2\rangle$. Throughout this section, we consider only the interaction picture and assume the rotating wave approximation to hold. The system's Hamiltonian then becomes

$$H = \begin{pmatrix} 0 & \Omega_P(t) & 0 \\ \Omega_P(t) & \varepsilon & \Omega_S(t) \\ 0 & \Omega_S(t) & 0 \end{pmatrix}. \tag{8.1}$$

Here, $\Omega_{S/P}$ denotes the Rabi frequency (amplitude) of the Stokes and Pump lasers, respectively, and ε absorbs the off-resonances, assuming both are equal in size. One can

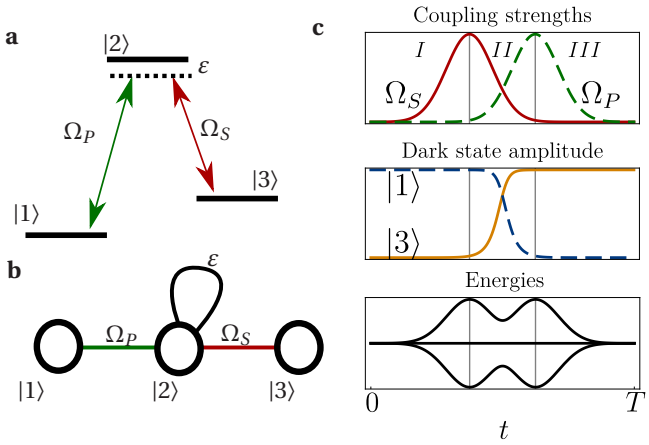

Figure 8.1: The conventional STIRAP/CTAP protocol on a three-site Λ system. **(a)** The energy diagram of the three states, coupled by the Stokes (S) and Pump (P) lasers, also represented as a graph in **(b)**. **(c)** Stacked plot showing the laser amplitudes, state amplitudes, and energies (eigenvalues λ) as a function of time, in arbitrary units. Stages I and III involve turning the couplings on/off, whereas stage II constitutes the relevant adiabatic driving part which transfers amplitude from state $|1\rangle$ to $|3\rangle$ as amplitudes Ω_S and Ω_P are slowly adjusted relative to each other.

check that one instantaneous eigenstate of H is the zero energy 'dark state' $|z\rangle$ given by

$$|z(t)\rangle = \frac{1}{\mathcal{N}} \begin{pmatrix} \Omega_P^{-1}(t) \\ 0 \\ -\Omega_S^{-1}(t) \end{pmatrix},$$

where $\mathcal{N}$ denotes the normalization. The dark state $|z\rangle$ has precisely the property that it transitions from $|1\rangle$ to $|3\rangle$ as Ω_S is gradually diminished while Ω_P is increased. Note the counter-intuitive order of the pulses, as indicated in Fig. 8.1. A key property of STIRAP is that the excited state $|2\rangle$ is never populated during this process, hence the protocol is independent of decoherence due to emission from this state. Thanks to this, and the inherent stability of adiabatic methods [CFP01], the protocol is relatively stable to experimental imperfections, and is broadly adopted in practice [VRS+17].

The setting where quantum particles can tunnel between three adjacent sites is mathematically equivalent to Eq. 8.1, where the parameters Ω now take the role of tunneling amplitudes. The same protocol can then be applied, leading to transfer of the particle wavefunction, as is the case in CTAP.

8.3 Generalizing STIRAP

We observe that a key property of STIRAP and CTAP is the existence of a unique zero-energy eigenstate at all times (guaranteeing adiabatic transfer), and that this state is localizable by lowering couplings incident to a particular site. This leads us to our main question: which other physical configurations pertain *precisely* one zero eigenvector, even when uncoupling a certain site?

We capture the more general configurations in the language of *weighted graphs* $G = (V, E, w)$. Here, the collection of vertices $V = \{v_j\}_{j=1}^{\dim(\mathcal{V})}$ corresponds to a set of basis states $\{|v_j\rangle\}_{j=1}^{\dim(\mathcal{V})}$ of Hilbert space $\mathcal{V}$. Two vertices $v, u \in V$ are connected by an edge $(u, v) \in E$ if and only if an interaction that couples states $|u\rangle$ and $|v\rangle$ can be applied. The weights $w : E \to \mathbb{C}$ assign a complex amplitude to each of the interactions. Weights evaluated on non-existent edges are zero: $w_{uv} = 0$ for all $(u, v) \notin E$. In the context of CTAP, the vertices should be interpreted as sites for the particle, and the edges indicate possible tunneling of the particle. In the context of STIRAP, vertices are energy levels, and edges are possible couplings by laser fields.

The *adjacency matrix* A_G of a graph is then defined as the matrix of weights, with matrix elements $(A_G)_{uv} = w_{uv}$. We impose hermiticity through $w_{uv} = w_{vu}^*$. For computational simplicity, we take the adjacency matrix to be constant (we consider it as a background), and define the *control Hamiltonian* H_G for a given graph G by

$$H_G(t) = \sum_{u,v \in V} f_{uv}(t) w_{uv} |u\rangle\langle v|, \qquad f_{uv}(t) = f_{vu}^*(t).$$

In this definition of the control Hamiltonian, we assume arbitrary time-dependent control over each allowed interaction, by tuning the *controls* $f_{uv}(t)$.

The graph G from which H_G is derived will be called the *interaction graph*, which restricts the allowed interactions in H_G. In the context of quickly oscillating laser fields, we obtain Hamiltonians H that are effectively time-independent except for the envelopes given by the functions $f_{uv}(t)$. The Hamiltonians we consider thus correspond to the interaction picture, in which quickly oscillating fields have either been absorbed into the on-site energies in the rotating frame, or where off-resonant fields are neglected by the rotating wave approximation.

Thanks to the mapping to graphs, we can use various notions from graph theory. We denote with $G - v$ the graph G in which the vertex v and all the edges incident to v are removed. A *bipartite graph* has a vertex set V which can be separated into two independent subsets V_1, V_2 such that each edge $(u, v) \in E$ must run *between* V_1 and V_2 (that is, $u \in V_1$ and $v \in V_2$ or vice-versa). In the following, we will encounter a certain variation on bipartite graphs:

Definition 1. A *semi-bipartite graph with parts* V_1 *and* V_2 [XWH+10; AK09] is a bipartite graph in which edges within V_2 are allowed (including self-loops), but edges within V_1 are still prohibited. For example, the graph in Fig. 8.1 is semi-bipartite with $V_1 = \{|1\rangle, |3\rangle\}$, but not bipartite unless the self-loop (the off-resonance of $|2\rangle$) is removed.

Note that for a connected bipartite graph, the decomposition $V = V_1 \sqcup V_2$ is determined uniquely (up to interchanging V_1 and V_2), while this is almost never the case for semi-bipartite graphs: any vertex in V_1 may be moved to V_2. Hence, the decomposition is an essential part of the data. However, for our results, we want to take $|V_1| = |V_2| + 1$, which means we cannot easily move points from V_1 to V_2.

We let $\mathcal{V}$ denote the vector space spanned by the states $|v\rangle$ corresponding to the vertices v in V. Likewise, we use $\mathcal{V}_1, \mathcal{V}_2$ to denote the subspaces corresponding to subsets V_1, V_2. We order the basis of $\mathcal{V}$ by first stating the elements of $\mathcal{V}_1$ and then the elements of $\mathcal{V}_2$. In this basis, the interaction graph has the form

$$A_G = \begin{pmatrix} 0 & B \\ B^T & C \end{pmatrix}, \tag{8.2}$$

where B is a matrix of size $|V_1| \times |V_2|$ and C has size $|V_2| \times |V_2|$. We will mostly use this form of A_G throughout this chapter.

Definition 2. We use *commensurate couplings* to denote the choice of couplings $f_{uv}(t)$ such that

$$\begin{aligned} f_{vu}(t) &= f_v(t) && \forall\, u \in V_2, v \in V_1\,; \\ f_{vu}(t) &= 1 && \forall\, u, v \in V_2\,. \end{aligned}$$

In other words, for each vertex $v \in V_1$, the incident couplings are changed proportionally, whereas all couplings within V_2 to be equal to one.

Note that the statement about commensurate couplings covers all couplings in a semi-bipartite graph. In such cases, with the interaction graph given in the form of Eq. 8.2, we may write

$$H_G(t) = F(t) A_G F^*(t)\,, \tag{8.3}$$

where $F(t) = \mathrm{diag}(f_1(t), \ldots, f_{|V_1|}(t), 1, \ldots 1)$.

We are now ready to state our main result. Consider a set of parties (vertices) $P \subseteq V_1$ located on a graph, who want to send a quantum state to each other. This turns out to be possible with a control Hamiltonian H_G, under certain graph restrictions, as made precise below.

Theorem 3. *Let $G = (V, E, w)$ be a connected, weighted, semi-bipartite graph with parts V_1 and V_2. Let $P = \{p_j\}_{j=1}^{k} \subseteq V_1$. We assume that*

1. *$|V_1| = |V_2| + 1$;*
2. *Either of the following:*
   - 2a. *For all p_j, $\det(A_{G-p_j}) \neq 0$;*
   - 2b. *A_G has a unique zero eigenvector, which has nonzero amplitude on each p_j.*

Then, for any $a, b \in P$, the following choice of commensurate couplings are such that $H_G(t)$ adiabatically transfers amplitude from a to b in total time T:

$$\begin{aligned} f_a(0) &= 0\,; \\ f_b(T) &= 0\,; \\ f_v(t) &\neq 0 \text{ for all } v \notin P\,; \\ &\text{No two } f_v(t) \text{ may be zero simultaneously.} \end{aligned} \tag{8.4}$$

Before we prove this theorem, we would like to analyse the statement first. The proof is given on Page 95, after Remark 5.

Firstly, note that $\det(A) \neq 0$ implies that A does not have a zero eigenvalue.

Moreover, the only couplings f_{uv} that actually *require* time-dependent control are those directly connected to sender and receiver; controlling any of the other couplings is optional. In fact, the control procedure can be performed locally and sequentially: it is possible to first only change the controls near a and then only those near b. An example is the choice

$$f_v(t) = \begin{cases} \min\{2t/T, 1\} & v = a\,; \\ \min\{1 - 2t/T, 1\} & v = b\,; \\ 1 & \text{else.} \end{cases}$$

In particular, the receiver, b, can be chosen after the process has been initialized.

The assumptions *2a* and *2b* are equivalent under the assumption of *1*. More precisely, the following proposition holds.

Proposition 4. *Let $G = (V, E, w)$ be a weighted, semi-bipartite graph with parts V_1 and V_2, such that $|V_1| = |V_2| + 1$, and let $p \in V_1$. Then the following are equivalent:*

a. $\det(A_{G-p}) \neq 0$*;*

b. A_G has a unique zero eigenvector, which has non-zero amplitude on p.

Proof. Let us first show that, thanks to $|V_1| = |V_2| + 1$, there must exist a zero-energy eigenvector $|z\rangle = (z_1, 0) \in \mathcal{V}_1$ whose nonzero amplitudes z_1 are only located on sites in V_1. This holds because in the eigenvalue equation, using the form of Eq. 8.2,

$$\begin{pmatrix} 0 & B \\ B^T & C \end{pmatrix} \begin{pmatrix} z_1 \\ 0 \end{pmatrix} = \begin{pmatrix} 0 \\ B^T z_1 \end{pmatrix} = 0\,,$$

the system of equations $B^T z_1 = 0$ has $|V_1|$ variables and $|V_2|$ constraints, hence it must always have at least one non-trivial solution.

We start with the implication from *a* to *b*. By the the previous argument, the rank of A_G can be at most $|V| - 1$. However, as $\det(A_{G-p}) \neq 0$, the submatrix A_{G-p} must be of maximal rank, which is also $|V| - 1$. As the rank of a submatrix gives a lower bound on the rank of a matrix, this shows that $\operatorname{rk} A_G \geq |V| - 1$. Therefore, there is a unique zero eigenvector.

Let this eigenvector be v, let its component at p be v_p, and its components away from p be $\tilde{v}$ (so $\tilde{v}$ is a vector with $|V| - 1$ components). We can write A_G as a block matrix

$$A_G = \begin{pmatrix} 0 & b_p \\ b_p^T & A_{G-p} \end{pmatrix},$$

where we wrote the component p as the first component for simplicity. As v is a zero eigenvector, we get

$$0 = A_G v = \begin{pmatrix} 0 & b_p \\ b_p^T & A_{G-p} \end{pmatrix} \begin{pmatrix} v_p \\ \tilde{v} \end{pmatrix} = \begin{pmatrix} b_p \tilde{v} \\ b_p^T v_p + A_{G-p} \tilde{v} \end{pmatrix}.$$

If now $v_p = 0$, then $\tilde{v} \neq 0$, as an eigenvector cannot be zero, but then $A_{G-p}\tilde{v} \neq 0$, as $\det(A_{G-p}) \neq 0$. This is a contradiction, so we must have $v_p \neq 0$.

Now we prove the implication from *b* to *a* by counterpositive. Hence we assume $\det(A_{G-p}) = 0$, and show that there exists a zero eigenvector of A_G whose p-component is zero. Again, for notational simplicity, we write the component p as the first component, so we have

$$A_G = \begin{pmatrix} 0 & B \\ B^T & C \end{pmatrix} = \begin{pmatrix} 0 & 0 & b_p \\ 0 & 0 & \tilde{B} \\ b_p^T & \tilde{B}^T & C \end{pmatrix}.$$

From this, we get

$$A_{G-p} = \begin{pmatrix} 0 & \tilde{B} \\ \tilde{B}^T & C \end{pmatrix},$$

where, crucially, the sizes of $\tilde{B}$ and C are equal by the assumption $|V_1| = |V_2| + 1$. Hence,

$$\det(A_{G-p}) = \pm \det(\tilde{B}\tilde{B}^T) = \pm \det(\tilde{B})^2\,.$$

Now, by assumption $\det(A_{G-p}) = 0$, so $\det(\tilde{B}^T) = 0$. Therefore, there exists a zero eigenvector u of $\tilde{B}^T$. If we define $v = (0, u, 0)$, then

$$A_G v = \begin{pmatrix} 0 & 0 & b_p \\ 0 & 0 & \tilde{B} \\ b_p^T & \tilde{B}^T & C \end{pmatrix} \begin{pmatrix} 0 \\ u \\ 0 \end{pmatrix} = \begin{pmatrix} 0 \\ 0 \\ \tilde{B}^T u \end{pmatrix} = 0,$$

so we have constructed a zero eigenvector of A_G with zero amplitude on p, giving a contradiction. □

Remark 5. In fact, the implication from *a* to *b* goes through even in the case G is not semi-bipartite; the proof does not use this assumption. However, for the other direction, it is essential.

Proof of Theorem 3. By the first part of the proof of Proposition 4, there exists a zero-energy eigenvector $|z\rangle$ for any choice of controls.

Clearly, the couplings $f_{uv}(t)$ in Eq. 8.4 are such that at times 0 and T, the respective states $|a\rangle$ and $|b\rangle$ are zero-energy eigenstates. We will argue that, using the given control scheme, the zero-energy subspace is one-dimensional at all times.

When all controls f_v are equal to one, then $H_G = A_H$ and the zero-energy eigenstate $|z\rangle$ is unique, by assumption *2.* When the couplings change commensurately, as long as they remain non-zero, the eigenstate $|z\rangle$ changes as

$$|z(t)\rangle \propto F(t)^{-1}|z\rangle, \tag{8.5}$$

as can be seen from Eq. 8.3. Because F is diagonal, $|z(t)\rangle$ is still located on V_1. It is unique, because given any zero eigenvector $|w\rangle$ of $H_G(t)$, $F(t)|w\rangle$ is an eigenvector of A_G, hence must be equal, up to scaling, to $|z\rangle$.

Special care has to be taken when reducing weights to zero. When reducing f_p ($p \in P$) towards zero, assumption *2a* guarantees that no zero eigenvectors occur on $G - p$, hence $|p\rangle$ must then be the unique zero eigenstate.

This shows that any controls f_v satisfying Eq. 8.4 indeed pertain a unique zero-energy eigenstate, and provide the correct initial and final state at times $t = 0$ and $t = T$. By the adiabatic theorem, a sufficiently high protocol time T allows state transfer at arbitrary accuracy. □

The unique zero-eigenstate $|z(t)\rangle$ has many favorable stability properties. Its eigenvalue is *exactly* 0 throughout the whole protocol, independent of changes to w_{uv}, as long as the graph remains semi-bipartite. The constant energy makes the state's dynamical phase easy to track. Moreover, it has exactly 0 amplitude on V_2, which makes it insensitive to any decoherence on sites in V_2. The state $|z\rangle$ generalizes the 'dark state' of conventional STIRAP and CTAP, inheriting important features that make these protocols attractive for practical purposes.

One might be concerned that, when reducing all controls $f_{p_j v}$ incident to a certain party p_j to zero, it is hard to maintain the commensurate ratios between the couplings. Luckily, it turns out that in such cases, commensurateness is not essential: the condition $\det(A_{G-p_j}) \neq 0$ guarantees that the zero eigenstate remains unique as long as all other sites remain commensurately coupled. This holds because the rank of A_G must be at least that of A_{G-p_j}, which shows that for *any* couplings between p_j and the rest of the graph, there can be at most one zero-energy state. This freedom gives the protocol a convenient stability to imperfect controls.

The time scale T required by the protocol is determined by the gap in the spectrum around the zero eigenvalue, as opposed to the well-studied gap between the lowest and second lowest energy [BH12]. To our best knowledge, little is known about the gap around zero, and characterizing its scaling is an interesting open problem. In Section 8.6 we numerically study the scaling for certain example graphs.

8.4 Applications

Our main result requires a physical system to obey our conventions of control Hamiltonian H_G for certain graphs G, with sufficiently flexible controls f_{uv}. Recall from Section 3.2.1 that this applies to the case of *single excitation hopping*, which describes the following example systems:

- Discrete energy levels coupled by (near-)resonant laser fields, like electronic levels in atoms or molecules, such as typically considered in STIRAP [VRS+17]. The lasers can also be off-resonant, as long as each state in V_2 has all of its incident couplings at the same off-resonance. Either way, a transformation to the interaction picture, and assumption of the Rotating Wave Approximation are required.
- Systems where a quantum particle 'hops' between coupled sites, such as electrons caught in quantum dots [GCH+04; HFJ+17], or atoms or atomic condensates trapped in optical potentials [ELC+04; GKW06; BDN12].
- An XX model of interacting spins, of the form

$$H_{\mathrm{XX}} = \frac{1}{2} \sum_{uv \in E} w_{uv} \left(X_u X_v + Y_u Y_v\right) + h \sum_{u \in V} Z_u,$$

  where $\{X_u, Y_u, Z_u\}$ are the Pauli matrices acting on the site u, in the sector with a single spin excitation [OEO+07].

The most interesting application might be in quantum information processing. As discussed in Section 3.2.1, quantum information can be transmitted whenever the states $|j\rangle$ represent the position of a quantum particle with internal degrees of freedom, as is the case with CTAP, or when a superposition between a shared vacuum and an excitation on a graph may be made. The latter applies to the XX model, where an initial state of the form

$$|\psi(0)\rangle = \alpha|0\rangle_a|0\ldots0\rangle + \beta|1\rangle_a|0\ldots0\rangle$$

can be initialized locally at site a.

In the context of information transfer, care has to be taken with the additional phase that is picked up throughout the protocol. As an example, in the XX model described above, the single-excitation subspace amplitude β picks up a relative phase $\beta \to e^{-ihT}\beta$ relative to the vacuum amplitude α. Moreover, the transfer protocol itself gives an additional phase to the transferred excitation, as previously observed by Ref. [GDH06]. This becomes relevant when dealing with the XX model, or when transporting entangled particles or states. Owing to Eq. 8.5, as long as the controls $f_{uv}(t)$ remain real-valued, the additional phase acquired by the state when transferring from site a to b is equal to $\arg(z_a/z_b)$, where z_a, z_b are elements of the zero-eigenvector $|z\rangle$ of A_G. Hence, for some applications, this vector may need to be explicitly calculated once.

As a potential realistic application, Ref. [VBC+17] observes that individual quantum processors based on quantum dots are limited in size, raising the need for communication between nearby processors. Our results readily generalize the CTAP protocol [GCH+04] to transfer electrons through a network of quantum dots, and the possibility to use more general graphs may be of great benefit for larger quantum computer architectures.

Another new application is in a delayed transfer scheme, which will be addressed in more detail in Chapter 9. In short, the sender a can initialize the system into the dark state $|z\rangle$ and leave it at that, such that any party in P can retrieve the quantum state, at any time they like. This opens the possibility to share unclonable quantum information among many parties without yet knowing which party is required to obtain the information.

8.5 Examples of viable graphs

The main assumptions of Theorem 3, especially requirement *2*, may not be very intuitive, but can be guaranteed in certain cases. In this section, we present two results in this direction. First, we discuss a procedure to generate viable graphs, by iteratively adding or removing dangling vertices. Next, we show that for any graph that allows, for each p_j, a perfect matching when a party p_j is removed, our assumptions are satisfied with probability 1 when the weights w_{uv} are chosen at random.

8.5.1 Adding and removing vertex pairs where one is dangling preserves the nullity

Consider a setting where one knows a graph G and a set of parties P that satisfy the assumptions of Theorem 3. One may now extend the graph by connecting first a vertex u in an arbitrary way, and then connecting a vertex v only to u. It turns out that, for any choice of non-zero weights, the number of zero eigenvectors does not change in this process.

We make this precise as follows. For an $(n \times n)$-matrix A, let $\eta(A) = n - \mathrm{rk}(A)$ denote the nullity of the matrix.

Lemma 6. *Let G be a graph with a vertex v of degree 1, whose unique neighbor is u ($u \neq v$). Then*

$$\eta(A_G) = \eta\left(A_{G-\{v,u\}}\right).$$

Proof. Let $\tilde{G}$ denote the graph $G - \{v, u\}$. Assuming for convenience that v and u are the first and second column of the adjacency matrix A_G respectively, we can write

$$A_G = \begin{pmatrix} 0 & w_{uv} & 0 \\ w_{vu} & w_{uu} & b \\ 0 & b^T & A_{\tilde{G}} \end{pmatrix}.$$

We can write any vector $|z\rangle$ as $(z_v, z_u, \tilde{z})$. Now $w_{uv} \neq 0$ and

$$0 = A_G|z\rangle = \begin{pmatrix} 0 & w_{uv} & 0 \\ w_{vu} & w_{uu} & b \\ 0 & b^T & A_{\tilde{G}} \end{pmatrix} \begin{pmatrix} z_v \\ z_u \\ \tilde{z} \end{pmatrix} = \begin{pmatrix} w_{uv} z_u \\ w_{vu} z_v + w_{uu} z_u + b \cdot \tilde{z} \\ b^T z_u + A_{\tilde{G}} \tilde{z} \end{pmatrix},$$

implying that $z_u = 0$, and hence also $z_v = -\frac{1}{w_{vu}} b \cdot \tilde{z}$, and $A_{\tilde{G}} \tilde{z} = 0$. Hence, we get a linear isomorphism $\ker A_G \to \ker A_{\tilde{G}}$: $(z_v, z_u, \tilde{z}) \mapsto \tilde{z}$ with inverse $\tilde{z} \mapsto (-\frac{1}{w_{vu}} b \cdot \tilde{z}, 0, \tilde{z})$. As the nullity is the dimension of the kernel, this shows $\eta(A_G) = \eta(A_{\tilde{G}})$. □

Note that in Lemma 6, we did not require the assumption of semi-bipartiteness, although the latter is still required for our adiabatic protocol. We obtain the following corollary.

Corollary 7. *Suppose G is a semi-bipartite graph with parts V_1 and V_2 such that $|V_1| = |V_2| + 1$. Fix a set of parties $P \subseteq V_1$. Suppose v is a dangling vertex, $v \notin P$, whose unique neighbor is u. Then condition 2 of Theorem 3 holds for G if and only if it holds for $G - \{u, v\}$.*

Proof. Recall that one of the two equivalent statements of condition *2* is that $\det(A_{G-p_j}) \neq 0$, for all $p_j \in P$. Let us first assume that G satisfies this condition. Because $\det(A_{G-p_j}) \neq 0$, the nullity of A_{G-p_j} is non-zero. By Lemma 6, the nullity of $A_{G-\{u,v\})-p_j}$ is also non-zero, hence it has a non-zero determinant and thus satisfies condition *2a* as well. The same reasoning also proves the other direction. □

Corollary 7 shows that new viable graphs can be generated by adding or removing vertices from existing graphs that are already known satisfy the assumptions of Theorem 3. When adding vertices, one may first connect a vertex u in *any* way, as long as the semi-bipartiteness is not violated, and then attach a vertex v only to u. When removing vertices, one must find a dangling vertex v and remove it together with its neighbor u, as long as the connectedness is preserved. On graphs generated this way, the requirements of Theorem 3 can be guaranteed.

When adding new vertices to a graph this way, it may also be possible to add the new vertices to the set of parties P, under the following conditions. It is never possible to add a vertex $u \in V_1$ to the set P when u is adjacent to a dangling vertex. For a new dangling vertex $v \in V_1$ that is to be added to the set P, assumption *2b* requires that the zero eigenvector of the new adjacency matrix has nonzero amplitude on v. By the relation $z_v = -\frac{1}{w_{vu}} b \cdot \tilde{z}$ found in Lemma 6, we require $b \cdot \tilde{z}$ to be non-zero.

Below, we give two example of new families of graphs that allow adiabatic transfer. Various examples of viable graphs are also depicted in Fig. 8.2.

Example 8 (Subdivided trees)**.** Let $T = (V_T, E_T)$ be any tree. We define the subdivided tree $\widetilde{T} = (V_{\widetilde{T}}, E_{\widetilde{T}})$ by adding a vertex right in the middle of every edge. To be precise, the new vertex set $V_{\widetilde{T}} = V_T \sqcup E_T$ is given by the vertices and edges of T, and the edge set $E_{\widetilde{T}} = \{\{v, e\} : v \in V_T, e \in E_T, v \in e\}$ consists of edges that connect each vertex $v \in V_T$ to its incident edges $e \in E_T$. An example of such a subdivided tree is shown in Fig. 8.3. The decomposition $V_{\widetilde{T}} = V_T \sqcup E_T$ guarantees that $\widetilde{T}$ is a bipartite graph, and since T is a tree, $|V_T| = |E_T| + 1$, hence the relation between the sizes of both parts is automatically satisfied. Moreover, we can iteratively remove leaves from the tree to reduce to a single vertex or single edge, showing that any $\widetilde{T}$ constructed this way satisfies the conditions of Theorem 3.

Example 9 (Hexagonal grids)**.** Hexagonal grids can be constructed from two-vertex unit cells that are all oriented in the same direction. To be precise, if one considers the hexagonal grid to be infinite, then our hexagonal grid graphs are finite subgraphs of the hexagonal grid, which must be connected. These graphs are bipartite, with each unit

cell containing one vertex from V_1 and one from V_2. If we start with a single vertex, and keep attaching unit cells in a hexagonal grid pattern such that one of the newly attached vertices is dangling, then each of the grids constructed this way satisfies the conditions of Theorem 3. Note that this generates only a subset of all possible subgraphs of hexagonal grids.

8.5.2 Graphs with certain matchings make the protocol work almost surely

A *perfect matching* in a graph G is a set of disjoint edges that covers all the vertices. In this section, we show that on semi-bipartite graphs G where $G - \{p_i\}$ has a perfect matching for all i, taking arbitary weights from a continuous distribution results in an interaction graph that satisfies the conditions of Theorem 3 with probability one. This gives another way to generate a large class of graphs on which the adiabatic transfer protocol works.

Theorem 10. *Let $G = (V, E, w)$ be a weighted semi-bipartite graph with parts V_1 and V_2 where $|V_1| = |V_2| + 1$. Let $P = \{p_j\}_{j=1}^k \subseteq V_1$. Suppose that for all i there exists a perfect matching in $G - p_i$. Then, if weights w_{uv} are chosen randomly from a contiuous distibution (meaning that no value has positive probability) for all $uv \in E$, we find* $\det(A_{G-p_j}) \neq 0$ *for all p_j with probability* 1.

Note that the theorem exactly gives us condition *2a* required by the protocol.

Proof. It suffices to prove that $\det(A_{G-p_i}) \neq 0$ with probability 1 for a fixed $i \in \{1, \ldots, k\}$; the claim of the theorem then follows since a countable intersection of events with probability 1 still has probability 1.

Let $p = p_i$ be given. We will first permute the rows and columns of the matrix A_{G-p} to bring it in a convenient form; such a permutation only affects the determinant of the matrix by a sign, which is irrelevant to us.

By assumption, there is a perfect matching on the graph $G - p$. Since $|V_1 \setminus \{p\}| = |V_2|$ and there are no edges within V_1, any perfect matching must use only edges between V_1 and V_2. Let $u_1v_1, \ldots, u_kv_k \in E \cap (V_1 \times V_2)$ denote the edges given in a perfect matching on $G - p$. Permute the rows and columns such that the rows are in the order $u_1, v_1, u_2, v_2, \ldots$ and the columns are in the order $v_1, u_1, v_2, u_2, \ldots$. We show with an inductive argument that for all $\ell \in \{1, \ldots, k\}$, the matrix A_ℓ on the first 2ℓ rows and columns has non-zero determinant with probability 1. This proves the claim.

For $\ell = 1$, we consider

$$\det \begin{pmatrix} w_{u_1v_1} & 0 \\ w_{v_1v_1} & w_{u_1v_1} \end{pmatrix} = w_{u_1v_1}^2,$$

since $w_{u_1u_1} = 0$ as $u_1 \in V_1$. As $w_{v_1v_1}$ is sampled uniformly at random from $[0, 1]$, this is non-zero with probability 1. Now suppose we have shown the statement up to some ℓ. We find

$$\det \begin{pmatrix} A_\ell & b_1 & b_2 \\ d_1 & w_{u_{\ell+1}v_{\ell+1}} & 0 \\ d_2 & w_{v_{\ell+1}v_{\ell+1}} & w_{u_{\ell+1}v_{\ell+1}} \end{pmatrix} = \det(A_\ell) w_{u_{\ell+1}v_{\ell+1}}^2 + b w_{u_{\ell+1}v_{\ell+1}} + c$$

for some b and c which do not depend on $w_{u_{\ell+1}v_{\ell+1}}$, and where we may assume that $\det(A_\ell) \neq 0$. Since the other entries do not depend on $w_{u_{\ell+1}v_{\ell+1}}$ and this gets sampled independently of the other entries, we may view $\det(A_\ell)$, b and c as constants.

Since there are at most two possible values in $[0,1]$ which make a quadratic polynomial ax^2+bx+c equal to zero (if $a \neq 0$), with probability 1 the expression will be non-zero. Continuing until $\ell+1=k$, we conclude $\det(A_{G-p}) \neq 0$ with probability 1 as desired. □

Remark 11. From the proof, it follows that the assumptions in Theorem 10 can be relaxed: the requirement that the weights are chosen from a continuous distribution is only necessary for the edges involved in the matching.

In fact, it is possible to show that the adjacency matrix of G is equivalent to a matrix with non-zero entries on the diagonal if and only if there is a perfect matching. Limited generalisation is also possible to non-bipartite graphs.

The proof of Theorem 10 also suggests a (weak) lower bound on the determinant $\det(A_{G-p_i})$ with some probability, and hence on the eigenvalue gap of A_G. For details, we refer to Ref. [GGK19].

8.6 Numerics

Our results state merely that adiabatic transfer is possible at *some* timescale, to which we remained agnostic. Especially the randomly-weighted graphs with perfect matchings in Section 8.5.2 potentially give rise to a configurations with a very small energy gap, giving rise to long transfer times T. An in-depth study of the gap between the zero eigenvalue and the next on semi-bipartite graphs is left as an open problem, but to give *some* indication of the quantitative behavour of our protocol, we resort to numerics. First, we calculate the scaling of the energy gap for various graphs. After that, we consider fidelity of transfer in subdivided trees of various depths.

Gap scaling Fig. 8.2 depicts the scaling of the energy gap around the zero energy state, as a function of the number of vertices $|V|$. We do this for various types of graphs, which are generated as follows:

- *Star graphs* have k 'arms', linear chains of length m, connected to a single center vertex. Interestingly, the eigenvalue gaps do not change as the number of arms increases. We fix the number of arms to three and vary the chain lengths to make larger graphs.
- *Hexagonal grids* consist of unit cells of size 2. We take k^2 copies of these unit cells and place them on a $k \times k$ square grid, which is connected as indicated in Fig. 8.2. To enforce an odd number of sites, we remove a single site in the top-right corner, leading to $2k^2-1$ sites in total. Interestingly, the hexagonal grids are the only graph configuration we considered whose gap decays superpolynomially (yet slower than an exponential). Randomly perturbing weights does not change this behavior.
- *Square grids* are chosen to have k by k vertices, where k is an odd number.
- Our *bipartite graphs* consist of two parts of size $m+1$ and m, respectively. Each potential edge which can be laid to connect the two parts is added with probability $p = 0.81$. Because these graphs are also random, for each datapoint, we also averaged the gap size over 50 random instantiations of the edge set. The thickness of the line indicates the standard deviation.

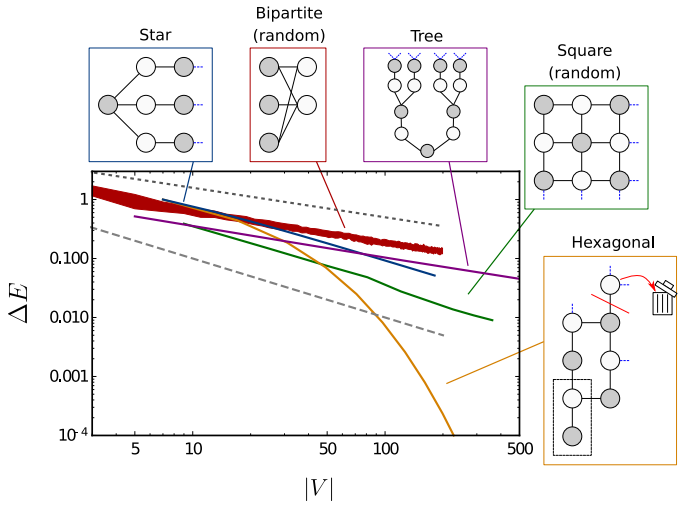

Figure 8.2: Scaling of the eigenvalue gap ΔE between the unique zero eigenvalue and the closest other eigenvalue, on a log-log scale. These are calculated for various bipartite graphs of various sizes $|V|$. The annotation (random) indicates that the weights were randomly chosen in the interval [0,2] to guarantee a unique zero eigenvector. The lower dashed line indicates $\Delta E = 1/|V|$, and the upper dashed line follows $\Delta E = 10/\sqrt{|V|}$. Interestingly, for most of the graphs we study, the gaps decay scales proportional to $1/|V|$ or slower. Hexagonal grids are an exception, as these are found to decay superpolynomially.

- Subdivided binary *trees* are generated as in Example 8: starting from a complete binary tree of certain depth, we create an additional vertex on each edge, which makes sure that $|V_1| = |V_2| + 1$.

For most graphs, we consider the unweighted versions, setting $w_{uv} = 1$ whenever the corresponding edge is present. Some graphs have the annotation 'random', which means that the graphs typically do not have a unique zero eigenvalue when all weights equal one; we then ensure a unique zero eigenvector by multiplying each weight w_{uv} with a random number chosen independently and uniformly chosen between 0 and 2. We took the average energy gap over 50 such perturbations.

These results show that the energy gap often decays roughly as $\Delta E \propto |V|^{-1}$ or slower, similarly to conventional STIRAP over a linear chain, with hexagonal grids being an exception.

Transfer fidelities To assess the actual accuracy of our protocol, we numerically simulate the time evolution of a transfered state. As graphs, we choose subdivided binary trees of depth k, as these allow transfer between a large number of parties. For example, each leave (endpoint) of the tree is a potential party, allowing $|P| = 2^k$ different parties to participate. In our simulations, we choose to transfer a state between parties a and b which are at maximum distance from each other. This setup is depicted in Fig. 8.3.

We define the transfer error as $\mathscr{E} = 1 - |\langle b|U_T|a\rangle|$, where U_T denotes the unitary time-evolution operator as found by numerically solving Schrödinger's Equation, and

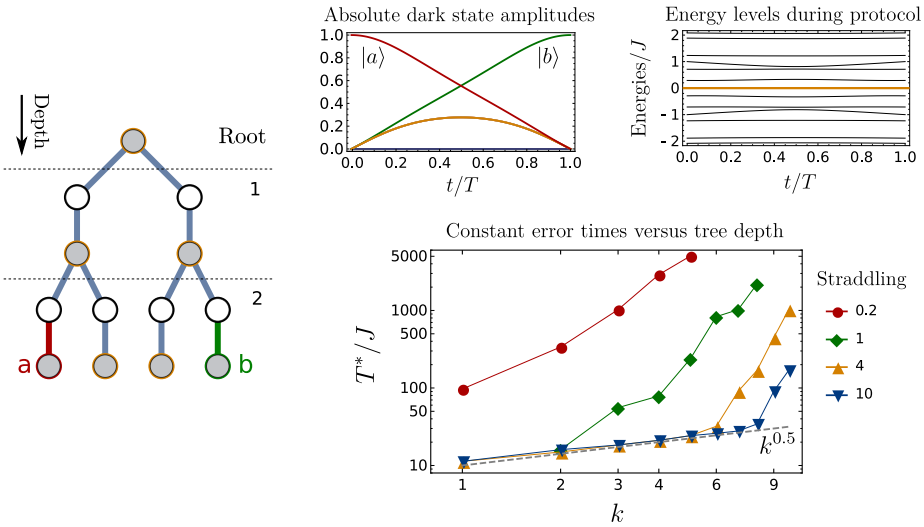

Figure 8.3: Simulation results on tree graphs are presented. A tree of depth $k = 2$ is shown on the left, with receivers a and b maximally separated. The top charts show the ideal state evolution over time, and the energy levels during the protocol. The bottom chart shows how the times T^* required for constant fidelity increase steeply with k, except when sufficiently strong straddling is applied, leading to $T^* \propto k^{0.5}$ (dashed line). Note that the size of the graph is *exponential* in k.

T is the total protocol's time. We choose simple time-dependent couplings $f_a = Jt/T$ and $f_b = J(1 - t/T)$, while all other controls remain $f_v = 1$. Moreover, we define T^* as the lowest time for which $\mathscr{E} < 0.05$, setting a bar for transfer with 95% fidelity.

Owing to the exponentially large size $|V|$ of the graphs, the time required rapidly increases with k (Fig. 8.3). Interestingly, we find that the technique of straddling [MT97; GCH+04], in which all controls f_v except for f_a and f_b are multiplied by a factor s, flattens the scaling down to roughly $T^* \approx 10\sqrt{k}$, up to a certain k where the steep increase is observed again. Ref. [GCH+05] already predicted a favorable scaling $T^* \propto \sqrt{n}$ for linear chains of length n in the strong straddling limit. It is surprising that here, we find a similar scaling in k rather than n, even though the number of vertices increases exponentially in k.

There are various reasons to believe that the strong straddling scaling cannot remain valid for increasingly large systems, for example due to Lieb-Robinson bounds [LR72]. Still, with a modest straddling factor $s = 10$, transfer at favorable scaling $T^* \propto \sqrt{\log(|P|)}$ is observed for graphs of up to 1000 sites, showing that near-term experiments can benefit from this effect.

8.7 Conclusion

To summarize, we extend the set of graphs in which STIRAP-like protocols are known to work. The sufficient requirements are made precise in assumptions *1* and *2* of Theorem 3, which can be guaranteed using the techniques in Section 8.5. We inherit the most important properties of the conventional protocols: the adiabatic controls do not

require precise amplitudes or timings, the system's energy is *exactly* zero at all times, and the fidelity is largely insensitive to decay on sites in V_2. Various extensions, such as straddling and multi-party transfer, can be readily incorporated. In the studied example of tree-shaped graphs, we find that with mild straddling the fidelities are much better than naively expected.

As our requirements are sufficient but not necessary, we would be interested to see further work explore other graphs with unique zero eigenstates, and give guarantees on spectral gaps around the zero eigenvalue for specific graphs. Moreover, we look forward to seeing state-of-the-art experiments test our results in practice.

CHAPTER 9

State transfer in bipartite anti-ferromagnetic spin networks

9.1 Introduction

In Section 3.2, we argued that reliable transport of quantum states is essential for future quantum information technologies [DiV00]. If the quantum information is carried by a spin degree of freedom, then it is a natural choice to transport the states over a network of spinful particles [Bos07; NJ14].

In this chapter, which is based on Ref. [Gro19], we consider such a system of spinful particles, where the spins are coupled through anti-ferromagnetic (AFM) isotropic Heisenberg interactions. We show that, if Alice and Bob can adiabatically change the strengths of the couplings surrounding a small subsystem of a suitable network, then they can send each other quantum information and establish entanglement.

The protocols, as illustrated in Fig. 9.1, are then straightforward: to transfer a spin state, Alice starts uncoupled from the rest of the system and initializes her site in a state ψ. The rest of the system must be in a ground state with total spin $s = 0$. She then adiabatically ramps up some coupling to connect to the system, after which Bob ramps down the couplings connecting his site, finding ψ at his now isolated site. Likewise, Alice and Bob can establish maximally entangled states between their sites by starting with the full network, including their sites, in a global $s = 0$ ground state. They then adiabatically uncouple their sites from the system, ending up with the unique $s = 0$ state shared between their sites. Such protocols are abundant in existing literature (see Section 3.2), but this literature focused mainly on linear chains.

This contribution strengthens previous results by proving that protocols on a chain do indeed always work in the adiabatic limit, whilst extending the applicability to much more general network graphs, under the assumptions given below. In particular, we allow different spins per site, we allow more general adiabatic paths, and sender/receiver are not limited to sit at the ends of the system. Moreover, we extend the state transfer protocol such that a state is not immediately transferred, but rather encoded in the ground state of the whole system. After any amount of time, one out of various parties can then decide to localize the state at their site, using only local controls, without requiring any action from the other parties.

The intuition that inspired this work is that the Heisenberg coupling preserves the total spin $\hat{S}^2$, and its z component $\hat{S}^z$, of the whole system. If the final state has one part which is in a total spin 0 ground state, then the rest of the system must have copied

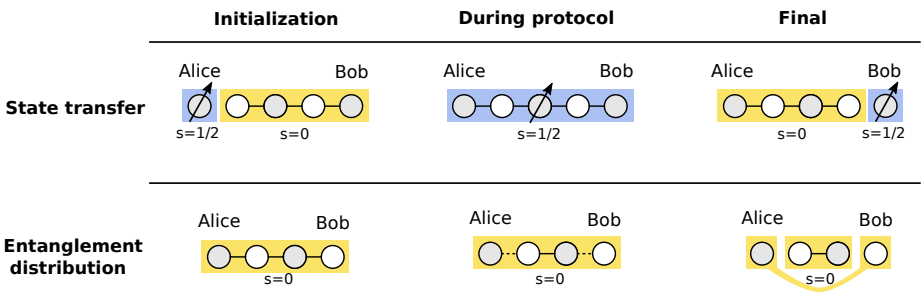

Figure 9.1: A sketch of the intuition behind our results. In the state transfer protocol, Alice initializes a spinful state while the rest of the system has zero total spin. The whole system then exhibits the same spin properties as the initialized state. After an appropriate adiabatic trajectory, Bob becomes disconnected. If the remainder of the system has a spin-zero ground state, then Bob's site must contain all spin information. Similarly, in entanglement distribution, Alice and Bob start with a state with zero total spin. After they disconnect, if the remainder of the system has total spin zero, then they must also share a total spin zero state.

whatever the initial spin properties were. The adiabatic theorem guarantees that, as long as couplings are changed sufficiently slowly with respect to a nonzero energy gap, the precise details of the procedure are unimportant. This reasoning is depicted in Fig. 9.1.

Our results require the following assumptions. Recall the definition of g in Eq. 2.30, which is the difference between the maximum total spin of both parts. To transfer a spin-s state, all parties must have $g = s$, and the system without either of the parties must consist of connected components, each of which must have $g = 0$. For entanglement distribution, both parties must hold a subsystem with a g of opposite sign, and the global system must start connected and have $g = 0$. When the two parties are disconnected, the leftover system must again consist of components with $g = 0$ each. For either protocol, the precise details of the adiabatic path are unimportant, as long as the whole system satisfies a criterion we call *spin-s compatible* at all times, which guarantees the uniqueness of the ground state. We do not prove that these requirements are optimal, hence further generalizations may be possible.

9.1.1 Chapter structure

The remainder of this chapter is laid out as follows. Section 9.2 contains the main technical part of our work, as we make our intuition on the conservation of total spin more concrete, and we prove that given our graph restrictions, there is a unique ground state. Section 9.3 provides more details on our adiabatic protocols, Section 9.4 discusses errors in real-world implementations, and Section 9.6 addresses possible near-term experimental implementations. We finish with a discussion and outlook in Section 9.7.

9.2 Ground states of symmetry-protected subspaces

9.2.1 Preliminaries

We give a quick recap of our graph-theoretic conventions introduced in Section 2.2.1 and the theory of spin particles and the Heisenberg model in Section 2.5.

Consider a network of spins, described by a graph $G = (V, E, w)$, with on each vertex (or site) $j \in V$ a spin particle with total spin s_j, described by the spin operator $\vec{S}_j = (\hat{S}_j^x, \hat{S}_j^y, \hat{S}_j^z)^T$. Note that we allow a different value of spin s_j per site. Spins which share an edge $(j,k) \in E$ interact with isotropic, anti-ferromagnetic Heisenberg interaction of strength w_{jk}, and we assume full control over each of these interaction strengths. Such a system is described by the Hamiltonian

$$H = \sum_{(j,k)\in E} w_{jk}\, \vec{S}_j \cdot \vec{S}_k, \qquad (w_{jk} > 0). \tag{9.1}$$

As before, to avoid confusion between operators and their eigenvalues, we denote spin operators in upper case with a hat, and scalars as lower-case symbols without hat. We define the spin operators $\vec{S}_{\text{tot}} = \sum_{j\in V} \vec{S}_j$, such that $\hat{S}^2_{\text{tot}}$ has eigenvalues $s(s+1)$, and total spin z-component $\hat{S}^z_{\text{tot}} = \sum_{j\in V} \hat{S}^z_j$ which has eigenvalues m, taking on values ranging from $-s$ up to s in integer steps. Likewise, for a subsystem $I \subset V$ we denote the total spin operator on sites within that subsystem as $\vec{S}_I = \sum_{j\in I} \vec{S}_j$ with corresponding spin values s_I and z-magnetization m_I. We use the term singlet to denote a state with $s = 0$.

Because H, $\hat{S}_{\text{tot}}$ and $\hat{S}^z_{\text{tot}}$ mutually commute, s and m can be used to index eigenstates of H. We let $\mathscr{H}_{s,m}$ denote the subspace with fixed values s and m. For systems with at least three sites, $\mathscr{H}_{s,m}$ may consist of more than one state, hence we require a third quantum number to establish a complete basis. We denote the eigenbasis of H as $|s,r,m\rangle$, where the label $r \in \{0,1,2,\ldots\}$ orders the states within $\mathscr{H}_{s,m}$ by *increasing* energy[1]. Fig. 9.2 graphically depicts this decomposition of the total Hilbert space.

We denote the $2s+1$-dimensional spin-s representation of SU(2) as (s). It is known from representation theory that the space of n spin particles $s_1, s_2, \ldots, s_j, \ldots, s_n$ decomposes as

$$\bigotimes_{j=1}^{n} (s_j) = \bigoplus_s N^s_{s_1,s_2,\ldots s_n} (s) \tag{9.2}$$

where the multiplicities $N^s_{s_1,s_2,\ldots s_n}$ of spin representation (s) can be found by consecutive application of Eq. 2.28.

We say that the network graph G is bipartite if for all edges $(j,k) \in E$, we have $j \in V_1$ and $k \in V_2$ or vice versa. Two sites j and k are connected if there exists a sequence $(J_{j,a_1}, J_{a_1,a_2}, \ldots J_{a_n,k})$ of nonzero elements. A graph or subsystem is connected if all pairs of vertices within that graph or subsystem are connected. If a system is not connected, then we use connected components to mean the largest possible subsystems in which all vertices are connected. The spin imbalance g of a spin system on a bipartite graph is defined as:

$$g = \sum_{j\in V_1} s_j - \sum_{j\in V_2} s_j = \max s_{V_1} - \max s_{V_2}. \tag{9.3}$$

[1] The label r is ill-defined whenever states have degenerate energies. This should cause no ambiguities in this work, as we consider only the ground state, which is assumed to be non-degenerate within the appropriate subspace.

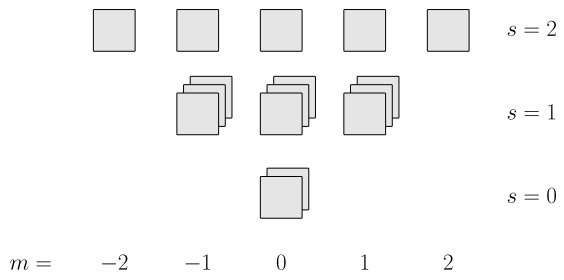

Figure 9.2: The decomposition of our Hilbert space using quantum numbers s, m and r, here depicted for the case of four spin-$\frac{1}{2}$ particles. For each total spin $s = 0, 1$ or 2 (vertical), the $2s+1$ possible z-magnetizations m are laid out horizontally. The multiplicities of the spin spaces $N^{\{0,1,2\}}_{\frac{1}{2},\frac{1}{2},\frac{1}{2},\frac{1}{2}}$ are 2, 3 and 1, respectively, and states that differ by multiplicity-label r are depicted in the depth-dimension. This way, each square corresponds to single state. The Hamiltonian H must preserve labels s and m, hence perturbing w_{jk} can only excite states that differ in label r.

Note that spin imbalances can be simply added when combining spin systems: if subsystems have spin imbalances $g_1, g_2, \ldots$, then the combined system has a spin imbalance $g = \sum g_j$. The Lieb-Mattis theorem [LM62] (see Section 2.5) states that each connected component with spin imbalance g_j has a unique spin-s_j subspace as ground subspace, whose the total spin $s_j = |g_j|$.

Our protocols critically rely on the adiabatic theorem [BF28] (see Section 3.1.3), and throughout this work, we will assume that the changes to the Hamiltonian are sufficiently slow compared to the relevant energy gap. In our case, this gap typically refers to the energy difference between the ground state and the first excited state, within a symmetry-protected sector (typically $\mathscr{H}_{s,m}$). Often, the gap may vanish in the thermodynamic limit, but we restrict ourselves to finite-sized systems. Still, for finite systems it is possible that the ground state becomes degenerate, in which case the gap closes and the adiabatic theorem can not be applied.

9.2.2 Preservation of the ground state of $\mathscr{H}_{s,m}$

For our adiabatic protocols, we aim to show that information can be encoded in a protected subspace, in such a way that amplitude can not leak out of the subspace, and such that the subspace has a gap at all times. For the state transfer protocol, we aim to encode a quantum state $|\psi\rangle \in \mathbb{C}^{2s+1}$ as $|\psi\rangle = \sum_{m=-s}^{+s} \psi_m |s, 0, m\rangle$, hence out of all the possible spin-s subspaces (s) we require that one is the unique lowest energy subspace. Note that, for fixed s and r but varying m, all states have the exact same energy under H, guaranteeing that no relative phases occur within this subspace. Likewise, for entanglement distribution, we want to work within the unique global ground state which must have total spin $s = 0$.

In this section, we show the following:

1. The subspace $\mathscr{H}_{s,m}$ is conserved under H at all times.

2. On a connected and bipartite graph with $|g| \leq s$, the subspace $\mathscr{H}_{s,m}$ has a unique ground state.

3. If a bipartite system is not connected, but consists of connected components with spin imbalances $g_1, g_2, \dots g_l$, then the subspace $\mathscr{H}_{s,m}$ has a unique ground state if $N^s_{|g_1|,|g_2|,\dots,|g_l|} = 1$.

4. If one connected component has a spin imbalance $g = g_0 \neq 0$ while all other components have $g = 0$, then the full information encoded in the lowest-energy spin-g_0 subspace is accessible at the component with spin imbalance g_0.

We will argue why these observations hold in the remainder of this section, leaving in-depth discussion of our protocols for the next section. We stress that the requirements presented here are merely *sufficient* requirements and by no means the most general *necessary* conditions possible. By separating these conditions from the protocols, future generalizations can be straightforwardly applied to the protocols.

1. The subspace $\mathscr{H}_{s,m}$ is conserved under H at all times. This property follows because each individual term $(\hat{S}_j \cdot \hat{S}_k)$ of H commutes with $\hat{S}_{\text{tot}}$ and $\hat{S}^z_{\text{tot}}$, hence H can not change the quantum numbers s and m, not even if the w_{jk} are time-dependent.

2. For $s \geq |g|$, $\mathscr{H}_{s,m}$ has a unique ground state. The proof of this claim follows from the results by Lieb and Mattis in Ref. [LM62], as restated in Section 2.5. We crucially need two of their findings:

> Assume the system is connected and bipartite, with spin imbalance g. Then the following holds:
>
> 1. Within a subspace of fixed $\hat{S}^z_{\text{tot}} = m_0$, there is a unique ground state.
> 2. If $m_0 \geq |g|$, then this unique ground state has $s = m_0$.

From these observations, it follows that if $m_0 \geq |g|$, the subspace $\mathscr{H}_{s=m_0,m=m_0}$ has a unique ground state. What about the other spaces? Recall that for fixed s, all values of m have the same energy. Hence if $\mathscr{H}_{m_0,m_0}$ has a unique ground state, then all $\mathscr{H}_{m_0,m}$ have the same energies and in particular also a unique ground state. We conclude that any $\mathscr{H}_{s,m}$ with $s \geq |g|$ has a unique ground state, while we can not make general statements about total spins smaller than $|g|$.

Let us take a step back here. With the previous two points, we have shown that in all connected and bipartite systems with $s \geq |g|$, one may adiabatically tune w_{jk} without exciting the ground state $|s, 0, m\rangle$ of $\mathscr{H}_{s,m}$: The quantum numbers s and m can never be changed by H, and the adiabatic theorem says that quantum number $r = 0$ is approximately conserved. However, when the system becomes disconnected, these results no longer hold. We therefore carefully analyze what happens upon disconnecting parts of the system, and we give sufficient conditions that guarantee a unique ground state.

3. On disconnected subsystems. First, let us define precisely what we mean with connecting and disconnecting[2]. We consider a system consisting of two subsystems L

[2] Note the difference between '(dis)connecting' (the procedure described here) and '(dis)connected' (a property of a graph), although our definitions are such that no ambiguities should occur for any English conjugation of these words.

and R. Let the Hamiltonian on the combined system be of the form

$$H' = H_L + H_R + \sum_i \epsilon_i \hat{S}_{l_i} \cdot \hat{S}_{r_i}, \tag{9.4}$$

where H_L and H_R act only on subsystems L and R respectively, whilst l_i are sites in L and r_i are sites in R. With connecting, we mean that the all parameters ϵ_i initially start at 0, and at least one of the ϵ_i is adiabatically increased to some positive nonzero value, such that the combined system becomes connected. Likewise, if at least one ϵ_i is nonzero, we may disconnect L from R by adiabatically lowering all ϵ_i down to zero.

For disconnected systems, the uniqueness of the ground state of $\mathscr{H}_{s,m}$ does not necessarily hold any more. One might naively think that upon sending all $\epsilon_i \to 0$, the adiabatic process is saved because of two effects: If some $\epsilon_i \neq 0$ then there must be a unique ground state, and if all $\epsilon_i = 0$ the two subsystems are completely disconnected, hence we may as well look only at the ground states in each subsystem individually. However, if the gap closes *asymptotically* as $\epsilon_i \to 0$, then our adiabatic trajectory potentially traverses a region with *infinitesimally* small gap, hence the adiabatic time scale blows up.

To avoid such divergences, we require that both the connected (some $\epsilon_i > 0$) and the disconnected (all $\epsilon_i = 0$) configurations have a unique ground state. Then, because the eigenvalues of H' are continuous functions of ϵ_i, asymptotic vanishing of the gap is ruled out.

We propose the following sufficient requirement that guarantees a unique ground state of $\mathscr{H}_{s,m}$: all connected components, labeled by $1, 2, \ldots l$, must have spin imbalances $g_1, g_2, \ldots, g_l$ such that $N^s_{|g_1|,|g_2|,\ldots|g_l|} = 1$. We will henceforth call this requirement *spin-s compatible*. We prove its validity as follows: each component j has a unique spin-s_j ground subspace with total spin $s_j = |g_j|$. The degeneracy of these subspaces allows the combined system to configure itself in various possible total spin configuration, according to Eq. 9.2. However, if $N^s_{|g_1|,|g_2|,\ldots|g_l|} = 1$, then there is just a single way in which the global ground subspace can configure itself that is compatible with total spin s, hence the ground state of $\mathscr{H}_{s,m}$ must be unique. In particular, this means that we may adiabatically connect and disconnect without disturbing the ground state of $\mathscr{H}_{s,m}$, as long as a system is spin-s compatible both before and after the (dis)connection.

4. If only a single component has nonzero spin imbalance, then all ground subspace information is accessible there. Let $\{g_0, 0, 0, \ldots\}$ be the spin imbalances of the connected components of some system, such that the spin imbalance of the combined system is g_0. In general, it holds that $N^{|g_0|}_{|g_0|,0,0,\ldots} = 1$, which means that $\mathscr{H}_{|g_0|,m}$ has a unique ground state. We know precisely what this ground state looks like: all $g = 0$ components are in their unique singlet ground state, while the component with $g = g_0$ is in the state $||g_0|, 0, m\rangle$. These states, with m ranging from $-|g_0| \leq m \leq |g_0|$, span the ground subspace of the global system, and are completely determined by the component with nonzero spin imbalance. Any operations performed on the subsystem with $g = g_0$ are in one-to-one correspondence with changes in the global ground subspace, and vice-versa.

In summary, throughout this section we showed that if the system remains spin-s compatible, then the couplings w_{jk} of H can be changed adiabatically without affecting a quantum state's amplitude on the ground state of $\mathscr{H}_{s,m}$. Moreover, by changing

the couplings w_{jk} of a system with total spin s in such a way that all components have $g = 0$ except for a single component which has $g = s$, then the amplitudes of $\mathscr{H}_{s,m}$ for all m are locally available at the latter component.

9.3 Applications

We discuss two applications in the context of quantum information, which are based on the results from the previous section: sharing a quantum state among multiple parties, and establishing entanglement between two parties. Fig. 9.3 shows these protocols on example graphs. The protocols assume a network graph that is bipartite and connected, but couplings w_{jk} could be brought down to zero to break the connectedness. In order to check the correctness of the protocols, one should check two aspects. Firstly, a system initialized with total spin s should always have a unique ground state in $\mathscr{H}_{s,m}$, which we enforce by requiring that the system is spin-s compatible at all times. Secondly, the initial and final states should be well understood such that they provide the utility that we claim. We illustrate situations in which our requirements are not fulfilled in Fig. 9.4.

9.3.1 Sharing a quantum state between multiple parties, such that any party can access the state

Consider a setup where ℓ cooperating parties $p_1, p_2, \ldots, p_\ell$ hold subsystems of a graph G. In case one party p_i experiences an emergency, it needs access to the state $|\psi\rangle = \sum_{m=-s}^{s} \psi_m |m\rangle \in \mathbb{C}^{2s+1}$, preferably without requiring any activity of the other parties. Because cloning $|\psi\rangle$ is generally impossible, the best option is to find a way to share the state between the parties. A protocol that offers a solution is as follows:

- Initialization: Without loss of generality, assume initially p_1 holds $|\psi\rangle$ locally. The system must be configured such that p_1 is disconnected from the rest of the system, and p_1 fully determines the ground state of the full system. p_1 can now initialize its subsystem in the state $|\psi'\rangle = \sum_{m=-s}^{s} \psi_m |s, 0, m\rangle$.

- Forming a resource state: p_1 connects to the system, and any other connections must be made such that all parties are on the same connected component. The state $|\psi'\rangle$ is now encoded in the spin-s ground subspace of this component.

- Finalization: To access the information, any party p_i can adiabatically disconnect, in such a way that it localizes the ground subspace information at its subsystem.

This protocol generalizes the transfer of a quantum state between two parties located at the ends of a chain, such as considered in Refs. [OSF+13; AHH+17].

Let us discuss the requirements for graphs that allow such protocols. Firstly, to localize the ground state information at a single subsystem, the most general requirement we found is that any disconnected party p_i should have $|g_i| = s$ while all other connected components have $g = 0$. Then from this, we derive that all parties p_i must have the same spin imbalance g_i (with the same sign), which follows because $G/\{p_i\}$ should have $g = 0$ for any party p_i. The same holds for the resource state, where the

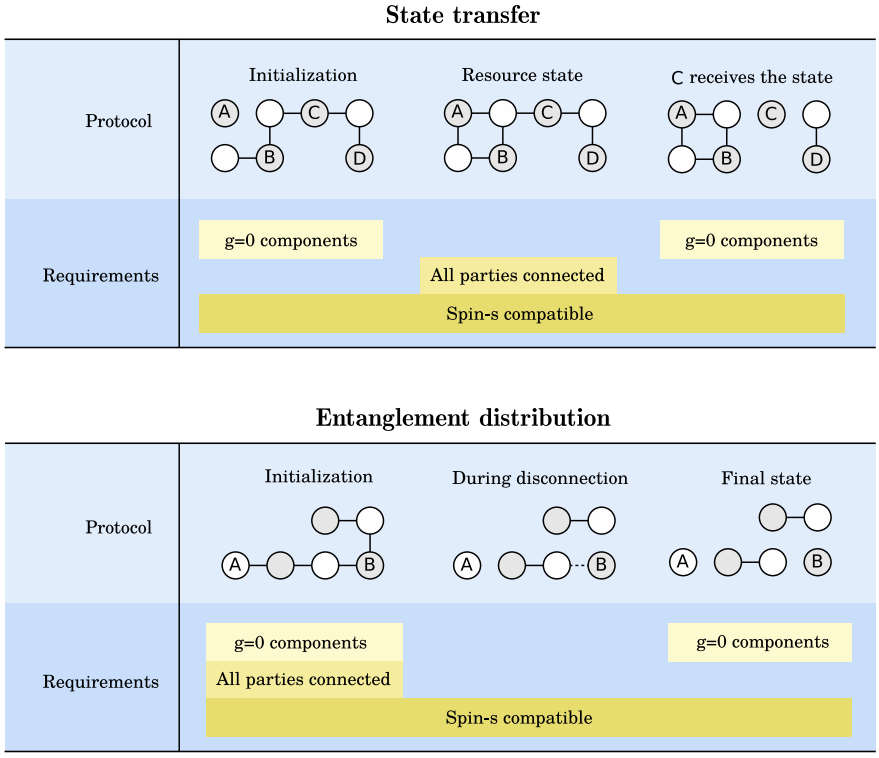

Figure 9.3: Example of a state transfer and an entanglement distribution protocol, where we assume each site holds a particle with the same spin s. For readability, we label parties p_i with capital letters. In the top panel, A initializes the system into a resource state encoding its original spin state, which is later obtained at C. Note that all indicated parties can be valid receivers. In the bottom panel, the system is initialized in a global singlet, after which A and B disconnect to obtain singlet entanglement between their sites. At various stages in these protocols, the network must obey requirements such as (from top to bottom) all connected components except for the disconnected parties have $g = 0$, all parties must be connected, and throughout the whole protocol, the graph must remain spin-s compatible.

component containing the parties must have spin imbalance equal to g_i while the rest of the components have $g = 0$.

In between the initialization, the resource state configuration, and the finalization, the only constraint is that spin-s compatibility is preserved, which is a less stringent requirement. For example, there could be more than a single connected component with $g \neq 0$ as long as $N^s_{|g_1|,|g_2|,\ldots} = 1$.

An interesting situation occurs when one of the parties holds a subsystem which is not connected. In that case, transfer is still possible as long as $N^s_{|g_1|,|g_2|,\ldots} = 1$ for a party whose connected components have spin imbalances $g_1, g_2, \ldots$. If there are two connected components, this generally holds for any $|g_1 - g_2| \leq s \leq g_1 + g_2$. For three or more connected components, this condition can only be met when $\sum_i |g_i| = s$. Moreover, the combined spin imbalance must match the imbalance of the other parties, hence $|\sum_i g_i| = s$. We conclude that for more than two components, parties may have disconnected subsystems as long as all connected components have spin imbalances with the same sign (plus any number of $g = 0$ components), which properly add up to s.

9.3.2 Distributing maximally entangled singlet states

In this protocol, two parties p_1 and p_2 both hold subsystems on a graph G. The ground subspaces of both parties are brought into the maximally entangled singlet state.

1. Initialization: The system must be in the unique ground state which has $s = 0$.

2. Finalization: Both parties are disconnected from the system, in such a way that the final state is a singlet on $G/\{p_1, p_2\}$, in tensor product with a singlet on $\{p_1, p_2\}$.

Again, we turn to analyzing the requirements for allowed graphs. Firstly, to form a singlet state together, the parties p_1 and p_2 must have $|g_1| = |g_2|$. Because also $G/\{p_1, p_2\}$ should have $g = 0$ and G must have $g = 0$, if follows that $g_1 = -g_2$.

In principle, the initial state allows any configuration with a unique spin-0 ground state. However, if p_1 and p_2 are restricted to controlling only the couplings directly surrounding their own subsystem, then the system must start such that the two parties are connected. For the final state, in order to be sure that the parties are not entangled with the rest of the system, the most general constraint we are aware of is that $G/\{p_1, p_2\}$ must consist only of components with $g = 0$.

The precise trajectory of the coupling w_{jk} is irrelevant as long as the system remains spin-0 compatible. Also, after the protocol is finished, individual connected components that remain can again be used as a starting stage for the same protocol. Notice that distributing entanglement between more than two parties in a single step is generally more complicated, because for multiple parties the spin-0 compatibility is easily broken.

A closely related idea for entanglement generation was presented earlier in [CDR06], where spins p_1 and p_2 sit at ends of a linear spin-$\frac{1}{2}$ chain, but p_1, p_2 are coupled more weakly to their neighbors than the spins in the bulk of the chain. By making this coupling ratio more extreme, the ground state was found to exhibit increasingly strong long-distance entanglement between the outermost spins. A later follow-up paper, Ref. [CDR07], investigated the usefulness of these outermost qubits

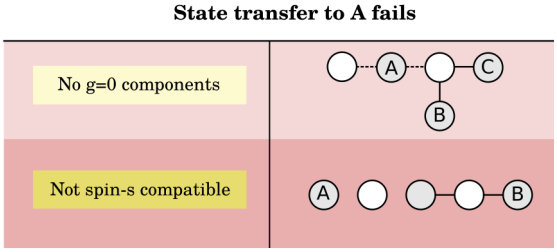

Figure 9.4: Example issues that occur when graph requirements are not fulfilled. In the top row, party A cannot be disconnected in such a way that all other components have $g = 0$, eventually breaking spin-s compatibility when the dotted couplings are set to 0. In the bottom row, the networks are such that A and B could in principle complete both protocols successfully, but during each protocol, disconnections are made such that spin-s compatibility is broken. In each of these cases, the ground state of the relevant $\mathscr{H}_{s,m}$ could become degenerate.

in low-temperature chains for the teleportation protocol. Our results extend these earlier findings of long-distance entanglement to more general spin networks, and place them in a quantum control perspective.

9.4 Errors and scaling

So far, we dealt with the uniqueness of the ground state to prove that an adiabatic protocol is viable at *some* time scale, to which we remained agnostic. Moreover, we assumed perfectly sterile conditions: zero temperature and no interactions beyond those of Eq. 9.1. For real-world implementations, the actual scaling of protocol time and error susceptibility as a function of the number of sites N would be of great importance, yet unfortunately, we are unable to give an in-depth and fully general characterization. Rather, this section collects known results related to this context, and numerically analyses the timing and errors in small systems.

Adiabatic processes are typically analyzed from the perspective of the energy gap Δ, where the duration of the protocol T is taken to scale as $T \propto \Delta^{-2}$ [CFP01]. The Haldane conjecture states that linear Heisenberg chains consisting of particles with half-integer spin exhibit a $\Delta \propto 1/N$ gap, whereas integer spin particles feature a unique ground state with a constant gap [AL86]. However, care has to be taken that these results assume periodic boundary conditions which are not readily compatible with our protocols. For spin-1 particles, open boundary conditions give rise to four low-lying states separated from the rest of the spectrum by a constant gap. These lower states live in different spaces $\mathscr{H}_{s,m}$, and their energies grow exponentially close in the thermodynamic limit [Ken90].

The nature of the errors that arise during the protocol then depend on whether the system is truly $SU(2)$-symmetric: if it is, then only the gaps within the relevant $\mathscr{H}_{s,m}$ are of any importance, and a system will not leave this subspace. However, to our best knowledge, all realistic systems described by Eq. 9.1 consist of spin particles whose magnetic moment interacts with magnetic fields $\vec{B}$, leading to interactions of the form $H = \sum_j \vec{B}_j \cdot \hat{S}_j$. Such fields break the $SU(2)$ symmetry, such that $\mathscr{H}_{s,m}$ may no longer be conserved. However, if $\vec{B}_j$ is a constant function of j, then the protocols could still

work, as we discuss in section 9.6.

Nonetheless, many results indicate that just the gap by itself does not necessarily reflect the viability of adiabatic protocols [PG08; LGC17]. Therefore, explicit numerical simulations of the full protocol appear to be the most informative. Such simulations have been performed for linear chains of spin-1/2 particles [OSF+13; AHH+17], and for entanglement distribution on a spin-1/2 chain with the purpose of teleportation [CDR07]. The latter work also calculates the gap in their system for lengths of up to one hundred. In Refs. [ERS07; FBM+15], closely related protocols are simulated.

Another important issue arises due to the fragility of Lieb and Mattis' statement that the ground state has definite total spin $s = |\max s_{V_1} - \max s_{V_2}|$, which is a fundamental building block of our protocols. Inhomogeneous magnetic fields of the form $B(\hat{S}^z_{V_1} - \hat{S}^z_{V_2})$ with amplitude $B = O(1/N)$ can cause the ground state to have significant amplitude spread out over various spin sectors [KP89; Wez07]. Moreover, frustrated interactions such as $\hat{S}\cdot\hat{S}$ coupling between next-nearest neighbors may break the result of Lieb and Mattis.

We conclude that many threats can be identified, yet a general understanding of how these affect an adiabatic protocol is lacking. To give at least some insight in the practical performance of our protocols, we resort to numerical simulation. We select a concrete system that showcases our main contributions by allowing multi-party transfer and non-linear graph layout, namely qubits on a star-shaped graph.

9.5 Numerics on star graphs

We consider systems consisting of qubits ($s_j = \frac{1}{2}$) arranged in the shape of a star, where a center qubit is connected to M arms each consisting of a linear chain of K qubits, as depicted in Fig. 9.5. The total number of qubits is $KM+1$. Note that such graphs reduce to a linear chain for $M = 1, 2$.

In the case of state transfer, the arm length K must be even, allowing the center qubit to qualify as sender or receiver, as well as all qubits that are an even number of sites away from the center. We locate our sender p_1 at the center, and place receiver p_2 at the very end of the first arm. All couplings w_{jk} are set to uniform strength J, except for the couplings connected to p_1 or p_2, which we give time-dependent amplitudes $f(t)$ and $g(t)$ respectively. We choose

$$f(t) = J\sin\left(\frac{\pi t}{2T}\right), \quad g(t) = J\cos\left(\frac{\pi t}{2T}\right) \tag{9.5}$$

where T is the total duration of the protocol.

Having defined our time-dependent Hamiltonian, we numerically solve Schrödinger's equation to find the unitary time-propagation U_T. As initial state we choose $|\psi(t=0)\rangle = |\psi_0\rangle_{p_1} \otimes |0,0,0\rangle_{V/p_1}$, where $|0,0,0\rangle$ is the global ground state with properties $s = 0, m = 0$. The state $|\psi_0\rangle_{p_1}$ is the state initialized by sender p_1, the choice of which does not influence the protocol's fidelity at this point, thanks to global $SU(2)$ symmetry. We then define the transfer error as

$$\mathscr{E} = 1 - \langle\psi_0| \quad \mathrm{tr}_{V/p_2}\Big(|\psi(T)\rangle\langle\psi(T)|\Big) \quad |\psi_0\rangle$$
$$\text{where } |\psi(T)\rangle = U_T|\psi(0)\rangle.$$

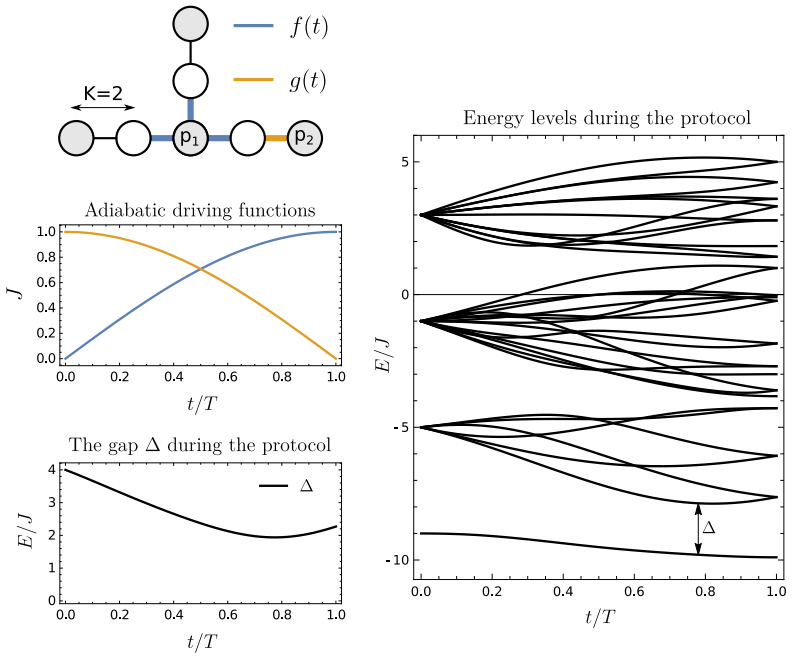

Figure 9.5: For the adiabatic transfer protocol in a system of size $M = 3$ and $K = 2$, we display a sketch of the star-shaped system, the driving functions f and g, and the size of the energy gap Δ as a function of time. On the right, all energy levels as a function of time are displayed. All units are normalized with respect to the protocol time T and the coupling strength J.

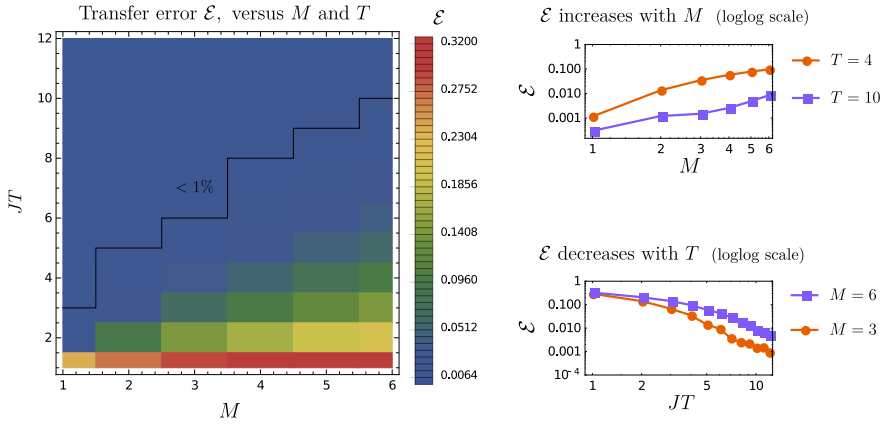

Figure 9.6: Transfer error $\mathscr{E}$, for various choices of T and M, for systems with arm length $K = 2$. For the small systems that we study, the fidelity seems to quickly converge to errors of less than 1%, indicated by the black zig-zag line, for protocol times just slightly larger than the intrinsic time scale $1/J$ of the system. On the right, cutouts of the main plot are displayed for fixed times (top) and fixed number of arms (bottom) on a log-log scale.

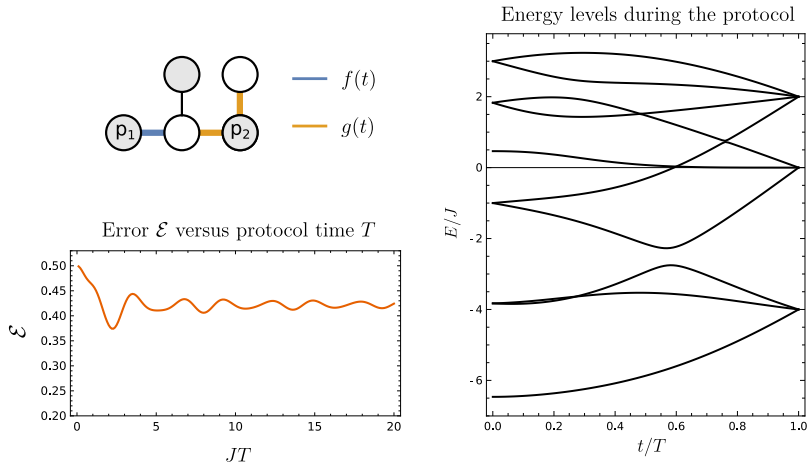

Figure 9.7: An example of a transfer protocol in which our requirements are violated. The left panel displays the graph layout and the time-dependence of the couplings connected to p_1 and p_2. Because p_2 is unable to disconnect while preserving spin-s compatibility, there is a possibility that the relevant energy gap closes, which we indeed find here. As a result, the transfer error does not asymptotically decay to 0 as a function of T.

Here, $\mathrm{tr}_{V/p_2}(\cdot)$ denotes the partial trace of the whole system except for site p_2. Fig. 9.5 depicts the driving functions f and g, and the movement of the energy levels and the gap during the protocol.

Fig. 9.6 shows our results for the transfer fidelity for various protocol times T and number of arms M, with arm length fixed to $K = 2$. For these small system sizes, very low error rates of less than 1% are readily obtained without further optimization of the protocol. Still, scaling up the system size by increasing M clearly requires longer protocol times to achieve the same low errors. We leave the precise scaling of transfer fidelity for larger systems, possibly using optimizations beyond the adiabatic approximation, as an open question.

9.5.1 A numerical example where assumptions are violated

A minimal example of a transfer protocol that does not match our requirements is displayed in Fig. 9.7. The bottom-left panel shows a graph in which p_1 can disconnect while leaving all other components in $g = 0$, but p_2 cannot. Choosing spin-1/2 particles ($s_j = s = 1/2$) and the same time-dependent functions f and g for the couplings incident to p_1 and p_2 as before (Eq. 9.5), we calculate the energy levels over time, and the protocol error as a function of total protocol time T. Because the spin-s compatibility is broken at the point $t = T$, there is no longer a guaranteed energy gap within $\mathscr{H}_{s,m}$, and we indeed find that relevant gap closes precisely at time T. This has a devastating effect on the transfer error, which barely drops below 0.5, the latter corresponding to uniformly random outcomes at p_2. Importantly, the transfer error does not asymptotically decay to 0 as a function of T, a generic indicator that adiabatic transport fails.

9.6 Experimental implementations

The Heisenberg coupling of Eq. 9.1 can be approximated by systems forming a Fermi-Hubbard model in a regime of half-filling and strong on-site repulsion. Experimental platforms which have been proposed for quantum information processing in such regimes include ultracold atoms trapped in optical potentials [MDZ+15; MCJ+17] and electrons trapped in quantum dots [LD98; HKP+07]. Selectively varying the coupling between ultracold atoms requires delicate control over the trapping potential. In quantum dots, individual coupling strengths w_{jk} are directly controlled using electronic gate voltages [HFJ+17], making them a promising candidate for experimental implementation of our protocols.

Typical experiments will deal with a global magnetic field, adding a term of the form $\vec{B}\cdot\sum_{j\in V}\hat{S}_j$ to the Hamiltonian. A field $\vec{B}$ oriented perfectly along the z-axis commutes with total spin operators $\hat{S}_{\text{tot}}$ and $\hat{S}^z_{\text{tot}}$, hence it does not change our conclusions on conservation of $\mathscr{H}_{s,m}$ and the uniqueness of the ground state within these spaces. However, a relative dynamical phase between subspaces that differ in m has to be accounted for. Moreover, it is no longer guaranteed that the global ground state is in spin sector $s = |g|$. More problematic could be magnetic noise which breaks the SU(2) symmetry. Minimizing the influence of such fields would be a major experimental challenge, and would form an interesting topic of further theoretical research.

9.7 Discussion and outlook

Given a physical system described by Eq. 9.1, there would be multiple ways to transfer quantum information, primarily through a quench [Bos07], by a sequence of swapping operations, or by using the adiabatic steps that we propose. Our adiabatic approach has the disadvantage of having stringent cooling requirements and inherently slow dynamics. Moreover, it is unclear how the protocol time and error scale for large systems. On the other hand, adiabatic protocols have an advantage when it comes to control requirements, being relatively robust to decoherence and control errors [FBM+15; CFP01], and requiring only a small number of couplings w_{jk} to be adjustable as a function of time. The lower complexity of control makes such protocols worthwhile candidates for experiments on near-term quantum devices. We also note that our protocol could form a building block for an atomic swap operation that is repeated many times, allowing a trade-off between control complexity and time complexity, as the time of swap operations scales linearly with transfer distance.

Throughout this work, we remained agnostic with regards to the initialization of the ground state. Preparation can in principle be done by cooling, but having a system capable of adiabatically changing its couplings, it could be preferable to start from a simple initial state which has an adiabatic connection to the required ground state. Such a protocol was addressed in Ref. [FBM+15] for a spin-1 chain: start with a chain of sites with only the *odd* couplings active, such that the ground state is formed by two-site singlets. One can then adiabatically ramp up the even couplings to obtain the ground state of the fully coupled chain. Such initial states are either easier to cool, because their gap does not scale with the system size, or they may be prepared from a computational basis state using a quantum circuit of constant depth. Using our results, this initialization protocol readily extends to more general spin networks and any total

spin s, with as only restriction that the system must remain spin-s compatible during the process.

From a practical perspective, we note that many optimizations can be made to our protocol, most notably by circumventing diabatic errors through so-called shortcuts to adiabaticity [CK19]. For example, Ref. [AHH+17] studies such improvements for precisely our protocol on a linear chain. We would be very interested to see future work generalize similar results to different graph structures.

On the theoretical side, we note that we have by no means exploited all the symmetries of Heisenberg systems yet. For example, we showed that *each* $\mathscr{H}_{s,m}$ has a unique ground state, yet our protocols must stick to the global ground state due to our connection/disconnection procedure. Moreover, we proved that our requirements for a unique ground state are sufficient, but not that they are necessary; we expect that further generalizations are possible here, extending the applicability of adiabatic protocols. In a similar spirit, one might exploit ferromagnetic variations of the Lieb-Mattis theorem [NS05] if one circumvents problems arising from addition of spin quantum numbers. We believe that further examination of these open ends could lead to a better theoretical understanding of spin chains, and novel applications.

Part IV

The Closing Matters

Bibliography

[ABB14] B. Alkurtass, L. Banchi, and S. Bose. *Optimal Quench for Distance-Independent Entanglement and Maximal Block Entropy*. Physical Review A **90**, 4 (2014), p. 042304. DOI: 10.1103/PhysRevA.90.042304.

[AC13] A. Ajoy and P. Cappellaro. *Quantum Simulation via Filtered Hamiltonian Engineering: Application to Perfect Quantum Transport in Spin Networks*. Physical Review Letters **110**, 22 (2013), p. 220503. DOI: 10.1103/PhysRevLett.110.220503.

[ACD+04] C. Albanese, M. Christandl, N. Datta, and A. Ekert. *Mirror Inversion of Quantum States in Linear Registers*. Physical Review Letters **93**, 23 (2004), p. 230502. DOI: 10.1103/PhysRevLett.93.230502.

[AHH+17] R. R. Agundez, C. D. Hill, L. C. L. Hollenberg, S. Rogge, and M. Blaauboer. *Superadiabatic Quantum State Transfer in Spin Chains*. Physical Review A **95**, 1 (2017), p. 012317. DOI: 10.1103/PhysRevA.95.012317.

[AK09] O. Al-Kofahi and A. Kamal. *Network Coding-Based Protection of Many-to-One Wireless Flows*. Selected Areas in Communications, IEEE Journal on **27** (2009), pp. 797–813. DOI: 10.1109/JSAC.2009.090619.

[AL86] I. Affleck and E. H. Lieb. *A Proof of Part of Haldane's Conjecture on Spin Chains*. Letters in Mathematical Physics **12**, 1 (1986), pp. 57–69. DOI: 10.1007/BF00400304.

[ÁMD+10] G. A. Álvarez, M. Mishkovsky, E. P. Danieli, et al. *Perfect State Transfers by Selective Quantum Interferences within Complex Spin Networks*. Physical Review A **81**, 6 (2010), p. 060302. DOI: 10.1103/PhysRevA.81.060302.

[Aro19] J. Aron. *IBM Unveils Its First Commercial Quantum Computer*. New Scientist (2019).

[AS10] A. Altland and B. D. Simons. *Condensed Matter Field Theory*. 2nd edition. New York: Cambridge University Press, 2010. ISBN: 978-0-521-76975-4.

[BB84] C. H. Bennett and G. Brassard. *Quantum Cryptography: Public Key Distribution and Coin Tossing*. Proceedings of the IEEE International Conference on Computers, Systems and Signal Processing. Bangalore, India, 1984, pp. 175–179.

[BBP+96a] C. H. Bennett, H. J. Bernstein, S. Popescu, and B. Schumacher. *Concentrating Partial Entanglement by Local Operations*. Physical Review A **53**, 4 (1996), pp. 2046–2052. DOI: 10.1103/PhysRevA.53.2046.

[BBP+96b] C. H. Bennett, G. Brassard, S. Popescu, et al. *Purification of Noisy Entanglement and Faithful Teleportation via Noisy Channels*. Physical Review Letters **76**, 5 (1996), pp. 722–725. DOI: 10.1103/PhysRevLett.76.722.

[BBR+18] O. Bechler, A. Borne, S. Rosenblum, et al. *A Passive Photon–Atom Qubit Swap Operation*. Nature Physics **14**, 10 (2018), p. 996. DOI: 10.1038/s41567-018-0241-6.

[BCG+17] L. Banchi, G. Coutinho, C. Godsil, and S. Severini. *Pretty Good State Transfer in Qubit Chains—The Heisenberg Hamiltonian*. Journal of Mathematical Physics **58**, 3 (2017), p. 032202. DOI: 10.1063/1.4978327.

[BDN12] I. Bloch, J. Dalibard, and S. Nascimbène. *Quantum Simulations with Ultracold Quantum Gases*. Nature Physics **8**, 4 (2012), pp. 267–276. DOI: 10.1038/nphys2259.

[BF28] M. Born and V. Fock. *Beweis des Adiabatensatzes*. Zeitschrift für Physik **51**, 3 (1928), pp. 165–180. DOI: 10.1007/BF01343193.

[BFF+11] R. Bachman, E. Fredette, J. Fuller, et al. *Perfect State Transfer on Quotient Graphs* (2011). arXiv: 1108.0339.

[BGS08] A. Bernasconi, C. Godsil, and S. Severini. *Quantum Networks on Cubelike Graphs*. Physical Review A **78**, 5 (2008), p. 052320. DOI: 10.1103/PhysRevA.78.052320.

[BH12] A. E. Brouwer and W. H. Haemers. *Spectra of Graphs*. Universitext. New York: Springer-Verlag, 2012. ISBN: 978-1-4614-1938-9.

[BJG15] C. Batey, J. Jeske, and A. D. Greentree. *Dark State Adiabatic Passage with Branched Networks and High-Spin Systems: Spin Separation and Entanglement*. Frontiers in ICT **2** (2015). DOI: 10.3389/fict.2015.00019.

[BKM+14] R. Barends, J. Kelly, A. Megrant, et al. *Superconducting Quantum Circuits at the Surface Code Threshold for Fault Tolerance*. Nature **508**, 7497 (2014), pp. 500–503. DOI: 10.1038/nature13171.

[BKM16] K. R. Brown, J. Kim, and C. Monroe. *Co-Designing a Scalable Quantum Computer with Trapped Atomic Ions*. npj Quantum Information **2** (2016), p. 16034. DOI: 10.1038/npjqi.2016.34.

[BKR+08] J. Benhelm, G. Kirchmair, C. F. Roos, and R. Blatt. *Towards Fault-Tolerant Quantum Computing with Trapped Ions*. Nature Physics **4**, 6 (2008), pp. 463–466. DOI: 10.1038/nphys961.

[BL18] J. Bardin and E. Lucero. *On the Path to Cryogenic Control of Quantum Processors*. Aug. 2018. URL: https://ai.googleblog.com/2019/02/on-path-to-cryogenic-control-of-quantum.html (visited on 08/12/2019).

[BMM+10] D. Burgarth, K. Maruyama, M. Murphy, et al. *Scalable Quantum Computation via Local Control of Only Two Qubits*. Physical Review A **81**, 4 (2010), p. 040303. DOI: 10.1103/PhysRevA.81.040303.

[Bos03] S. Bose. *Quantum Communication through an Unmodulated Spin Chain*. Physical Review Letters **91**, 20 (2003), p. 207901. DOI: 10.1103/PhysRevLett.91.207901.

[Bos07] S. Bose. *Quantum Communication through Spin Chain Dynamics: An Introductory Overview*. Contemporary Physics **48**, 1 (2007), pp. 13–30. DOI: 10.1080/00107510701342313.

[BP09] M. Bašić and M. D. Petković. *Some Classes of Integral Circulant Graphs Either Allowing or Not Allowing Perfect State Transfer*. Applied Mathematics Letters **22**, 10 (2009), pp. 1609–1615. DOI: 10.1016/j.aml.2009.04.007.

[BR12] R. Blatt and C. F. Roos. *Quantum Simulations with Trapped Ions*. Nature Physics **8**, 4 (2012), pp. 277–284. DOI: 10.1038/nphys2252.

[BRG+12] C. J. Bradly, M. Rab, A. D. Greentree, and A. M. Martin. *Coherent Tunneling via Adiabatic Passage in a Three-Well Bose-Hubbard System*. Physical Review A **85**, 5 (2012), p. 053609. DOI: 10.1103/PhysRevA.85.053609.

[BSK+12] J. W. Britton, B. C. Sawyer, A. C. Keith, et al. *Engineered Two-Dimensional Ising Interactions in a Trapped-Ion Quantum Simulator with Hundreds of Spins*. Nature **484**, 7395 (2012), pp. 489–492. DOI: 10.1038/nature10981.

[BSK+17] H. Bernien, S. Schwartz, A. Keesling, et al. *Probing Many-Body Dynamics on a 51-Atom Quantum Simulator*. Nature **551**, 7682 (2017), pp. 579–584. DOI: 10.1038/nature24622.

[BWP+17] J. Biamonte, P. Wittek, N. Pancotti, et al. *Quantum Machine Learning*. Nature **549**, 7671 (2017), pp. 195–202. DOI: 10.1038/nature23474.

[CAJ05] S. R. Clark, C. M. Alves, and D. Jaksch. *Efficient Generation of Graph States for Quantum Computation*. New Journal of Physics **7** (2005), pp. 124–124. DOI: 10.1088/1367-2630/7/1/124.

[Cal69a] F. Calogero. *Ground State of a One-Dimensional N-Body System*. Journal of Mathematical Physics **10**, 12 (1969), pp. 2197–2200. DOI: 10.1063/1.1664821.

[Cal69b] F. Calogero. *Solution of a Three-Body Problem in One Dimension*. Journal of Mathematical Physics **10**, 12 (1969), pp. 2191–2196. DOI: 10.1063/1.1664820.

[Cal71] F. Calogero. *Solution of the One-Dimensional N-Body Problems with Quadratic and/or Inversely Quadratic Pair Potentials*. Journal of Mathematical Physics **12**, 3 (1971), pp. 419–436. DOI: 10.1063/1.1665604.

[CBC+17] A. Ciamei, A. Bayerle, C.-C. Chen, B. Pasquiou, and F. Schreck. *Efficient production of long-lived ultracold* Sr_2 *molecules*. Physical Review A **96**, 1 (2017), p. 013406. DOI: 10.1103/PhysRevA.96.013406.

[CDE+04] M. Christandl, N. Datta, A. Ekert, and A. J. Landahl. *Perfect State Transfer in Quantum Spin Networks*. Physical Review Letters **92**, 18 (2004), p. 187902. DOI: 10.1103/PhysRevLett.92.187902.

[CDR06] L. Campos Venuti, C. Degli Esposti Boschi, and M. Roncaglia. *Long-Distance Entanglement in Spin Systems*. Physical Review Letters **96**, 24 (2006), p. 247206. DOI: 10.1103/PhysRevLett.96.247206.

[CDR07] L. Campos Venuti, C. Degli Esposti Boschi, and M. Roncaglia. *Qubit Teleportation and Transfer across Antiferromagnetic Spin Chains*. Physical Review Letters **99**, 6 (2007), p. 060401. DOI: 10.1103/PhysRevLett.99.060401.

[CFH97] D. G. Cory, A. F. Fahmy, and T. F. Havel. *Ensemble Quantum Computing by NMR Spectroscopy*. Proceedings of the National Academy of Sciences **94**, 5 (1997), pp. 1634–1639. DOI: 10.1073/pnas.94.5.1634.

[CFM17] F. T. Chong, D. Franklin, and M. Martonosi. *Programming Languages and Compiler Design for Realistic Quantum Hardware*. Nature **549**, 7671 (2017), pp. 180–187. DOI: 10.1038/nature23459.

[CFP01] A. M. Childs, E. Farhi, and J. Preskill. *Robustness of Adiabatic Quantum Computation*. Physical Review A **65**, 1 (2001), p. 012322. DOI: 10.1103/PhysRevA.65.012322.

[CFX+13] B. Chen, W. Fan, Y. Xu, Y.-D. Peng, and H.-Y. Zhang. *Multipath Adiabatic Quantum State Transfer*. Physical Review A **88**, 2 (2013), p. 022323. DOI: 10.1103/PhysRevA.88.022323.

[CG11] W.-C. Cheung and C. Godsil. *Perfect State Transfer in Cubelike Graphs*. Linear Algebra and its Applications. Special Issue in Honor of Dragos Cvetkovic **435**, 10 (2011), pp. 2468–2474. DOI: 10.1016/j.laa.2011.04.022.

[CH12] N. Chancellor and S. Haas. *Using the J1–J2 Quantum Spin Chain as an Adiabatic Quantum Data Bus*. New Journal of Physics **14**, 9 (2012), p. 095025. DOI: 10.1088/1367-2630/14/9/095025.

[Cit16] R. Citro. *Ultracold Atoms: A Topological Charge Pump*. Nature Physics **12**, 4 (2016), pp. 288–289. DOI: 10.1038/nphys3649.

[CK19] A. del Campo and K. Kim. *Focus on Shortcuts to Adiabaticity*. New Journal of Physics **21**, 5 (2019), p. 050201. DOI: 10.1088/1367-2630/ab1437.

[CSF+12] B. Chen, Q. Shen, W. Fan, and Y. Xu. *Long-Range Adiabatic Quantum State Transfer through a Linear Array of Quantum Dots*. Science China Physics, Mechanics and Astronomy **55**, 9 (2012), pp. 1635–1640. DOI: 10.1007/s11433-012-4841-3.

[CSH+16] R. J. Chapman, M. Santandrea, Z. Huang, et al. *Experimental Perfect State Transfer of an Entangled Photonic Qubit*. Nature Communications **7** (2016), p. 11339. DOI: 10.1038/ncomms11339.

[DBE95] D. Deutsch, A. Barenco, and A. Ekert. *Universality in Quantum Computation*. Proceedings of the Royal Society of London. Series A: Mathematical and Physical Sciences (1995). DOI: 10.1098/rspa.1995.0065.

[DiV00] D. P. DiVincenzo. *The Physical Implementation of Quantum Computation*. Fortschritte der Physik **48**, 9-11 (2000), pp. 771–783. DOI: 10.1002/1521-3978(200009)48:9/11<771::AID-PROP771>3.0.CO;2-E.

[DMH+18] E. F. Dumitrescu, A. J. McCaskey, G. Hagen, et al. *Cloud Quantum Computing of an Atomic Nucleus*. Physical Review Letters **120**, 21 (2018), p. 210501. DOI: 10.1103/PhysRevLett.120.210501.

[DP10] D. Dong and I. R. Petersen. *Quantum Control Theory and Applications: A Survey*. IET Control Theory Applications **4**, 12 (2010), pp. 2651–2671. DOI: 10.1049/iet-cta.2009.0508.

[DTM+18] A. Dréau, A. Tchebotareva, A. E. Mahdaoui, C. Bonato, and R. Hanson. *Quantum Frequency Conversion of Single Photons from a Nitrogen-Vacancy Center in Diamond to Telecommunication Wavelengths*. Physical Review Applied **9**, 6 (2018), p. 064031. DOI: 10.1103/PhysRevApplied.9.064031.

[DWa18] D-Wave Press Releases. *D-Wave Announces D-Wave 2000Q Quantum Computer and First System Order*. Jan. 2018. URL: https://www.dwavesys.com/press-releases/d-wave%C2%A0announces%C2%A0d-wave-2000q-quantum-computer-and-first-system-order (visited on 08/12/2019).

[ECP10] J. Eisert, M. Cramer, and M. B. Plenio. *Colloquium: Area Laws for the Entanglement Entropy*. Reviews of Modern Physics **82**, 1 (2010), pp. 277–306. DOI: 10.1103/RevModPhys.82.277.

[EKW+15] M. Ebert, M. Kwon, T. G. Walker, and M. Saffman. *Coherence and Rydberg Blockade of Atomic Ensemble Qubits*. Physical Review Letters **115**, 9 (2015), p. 093601. DOI: 10.1103/PhysRevLett.115.093601.

[ELC+04] K. Eckert, M. Lewenstein, R. Corbalán, et al. *Three-Level Atom Optics via the Tunneling Interaction*. Physical Review A **70**, 2 (2004), p. 023606. DOI: 10.1103/PhysRevA.70.023606.

[ERS07] K. Eckert, O. Romero-Isart, and A. Sanpera. *Efficient Quantum State Transfer in Spin Chains via Adiabatic Passage*. New Journal of Physics **9**, 5 (2007), pp. 155–155. DOI: 10.1088/1367-2630/9/5/155.

[FBM+15] U. Farooq, A. Bayat, S. Mancini, and S. Bose. *Adiabatic Many-Body State Preparation and Information Transfer in Quantum Dot Arrays*. Physical Review B **91**, 13 (2015), p. 134303. DOI: 10.1103/PhysRevB.91.134303.

[FML+17] C. Figgatt, D. Maslov, K. A. Landsman, et al. *Complete 3-Qubit Grover Search on a Programmable Quantum Computer*. Nature Communications **8**, 1 (2017), p. 1918. DOI: 10.1038/s41467-017-01904-7.

[Fra93] H. Frahm. *Spectrum of a Spin Chain with Inverse Square Exchange*. Journal of Physics A: Mathematical and General **26**, 10 (1993), pp. L473–L479. DOI: 10.1088/0305-4470/26/10/002.

[FSB+12] A. Fedorov, L. Steffen, M. Baur, M. P. da Silva, and A. Wallraff. *Implementation of a Toffoli Gate with Superconducting Circuits*. Nature **481**, 7380 (2012), pp. 170–172. DOI: 10.1038/nature10713.

[GCH+04] A. D. Greentree, J. H. Cole, A. R. Hamilton, and L. C. L. Hollenberg. *Coherent Electronic Transfer in Quantum Dot Systems Using Adiabatic Passage*. Physical Review B **70**, 23 (2004), p. 235317. DOI: 10.1103/PhysRevB.70.235317.

[GCH+05] A. D. Greentree, J. H. Cole, A. R. Hamilton, and L. C. L. Hollenberg. *Scaling of Coherent Tunneling Adiabatic Passage in Solid-State Coherent Quantum Systems*. Smart Materials, Nano-, and Micro-Smart Systems. Ed. by J.-C. Chiao, D. N. Jamieson, L. Faraone, and A. S. Dzurak. Sydney, Australia, 2005, p. 72. DOI: 10.1117/12.583193.

[GCS17] J. M. Gambetta, J. M. Chow, and M. Steffen. *Building Logical Qubits in a Superconducting Quantum Computing System*. npj Quantum Information **3**, 1 (2017), p. 2. DOI: 10.1038/s41534-016-0004-0.

[GDH06] A. D. Greentree, S. J. Devitt, and L. C. L. Hollenberg. *Quantum-Information Transport to Multiple Receivers*. Physical Review A **73**, 3 (2006), p. 032319. DOI: 10.1103/PhysRevA.73.032319.

[GDM15] J. Gulliksen, D. B. R. Dasari, and K. Mølmer. *Characterization of How Dissipation and Dephasing Errors Accumulate in Quantum Computers*. EPJ Quantum Technology **2**, 1 (2015), pp. 1–10. DOI: 10.1140/epjqt17.

[GGK19] K. Groenland, C. Groenland, and R. Kramer. *Adiabatic Transfer of Amplitude Using STIRAP-like Protocols Generalizes to Many Bipartite Graphs* (2019). arXiv: 1904.09915.

[GK14] A. D. Greentree and B. Koiller. *Dark-State Adiabatic Passage with Spin-One Particles*. Physical Review A **90**, 1 (2014), p. 012319. DOI: 10.1103/PhysRevA.90.012319.

[GKS+12] C. Godsil, S. Kirkland, S. Severini, and J. Smith. *Number-Theoretic Nature of Communication in Quantum Spin Systems*. Physical Review Letters **109**, 5 (2012), p. 050502. DOI: 10.1103/PhysRevLett.109.050502.

[GKW06] E. M. Graefe, H. J. Korsch, and D. Witthaut. *Mean-Field Dynamics of a Bose-Einstein Condensate in a Time-Dependent Triple-Well Trap: Nonlinear Eigenstates, Landau-Zener Models, and Stimulated Raman Adiabatic Passage*. Physical Review A **73**, 1 (2006), p. 013617. DOI: 10.1103/PhysRevA.73.013617.

[Gla81] A. Glaser. *History of Binary and Other Nondecimal Numeration*. Revised. Los Angeles, CA: Tomash, 1981. ISBN: 978-0-938228-00-4.

[GNL18] A. Gratsea, G. M. Nikolopoulos, and P. Lambropoulos. *Photon-Assisted Quantum State Transfer and Entanglement Generation in Spin Chains*. Physical Review A **98**, 1 (2018), p. 012304. DOI: 10.1103/PhysRevA.98.012304.

[God12] C. Godsil. *State Transfer on Graphs*. Discrete Mathematics. Algebraic Graph Theory — A Volume Dedicated to Gert Sabidussi on the Occasion of His 80th Birthday **312**, 1 (2012), pp. 129–147. DOI: 10.1016/j.disc.2011.06.032.

[GP19] M. J. Gullans and J. R. Petta. *Protocol for a Resonantly Driven Three-Qubit Toffoli Gate with Silicon Spin Qubits*. Physical Review B **100**, 8 (2019), p. 085419. DOI: 10.1103/PhysRevB.100.085419.

[Gri05] D. Griffiths. *Introduction to Quantum Mechanics*. Pearson International Edition. Pearson Prentice Hall, 2005. ISBN: 978-0-13-111892-8.

[Gro19] K. Groenland. *Adiabatic State Distribution Using Anti-Ferromagnetic Spin Systems*. SciPost Physics **6**, 1 (2019), p. 011. DOI: 10.21468/SciPostPhys.6.1.011.

[Gro96] L. K. Grover. *A Fast Quantum Mechanical Algorithm for Database Search*. Proceedings of the Twenty-Eighth Annual ACM Symposium on Theory of Computing. STOC '96. New York, NY, USA: ACM, 1996, pp. 212–219. ISBN: 978-0-89791-785-8. DOI: 10.1145/237814.237866.

[GRS+90] U. Gaubatz, P. Rudecki, S. Schiemann, and K. Bergmann. *Population Transfer between Molecular Vibrational Levels by Stimulated Raman Scattering with Partially Overlapping Laser Fields. A New Concept and Experimental Results*. The Journal of Chemical Physics **92**, 9 (1990), pp. 5363–5376. DOI: 10.1063/1.458514.

[GS18] K. Groenland and K. Schoutens. *Many-Body Strategies for Multiqubit Gates: Quantum Control through Krawtchouk-Chain Dynamics*. Physical Review A **97**, 4 (2018), p. 042321. DOI: 10.1103/PhysRevA.97.042321.

[GS19] K. Groenland and K. Schoutens. *Quantum Gates by Resonantly Driving Many-Body Eigenstates, with a Focus on Polychronakos' Model*. Journal of Statistical Mechanics: Theory and Experiment **2019**, 7 (2019), p. 073103. DOI: 10.1088/1742-5468/ab25e2.

[GZC03] J. J. Garcia-Ripoll, P. Zoller, and J. I. Cirac. *Fast and Robust Two-Qubit Gates for Scalable Ion Trap Quantum Computing*. Physical Review Letters **91**, 15 (2003), p. 157901. DOI: 10.1103/PhysRevLett.91.157901.

[Hac19] R. Hackett. *Google Claims 'Quantum Supremacy,' Marking a Major Milestone in Computing*. Sept. 2019. URL: https://fortune.com/2019/09/20/google-claims-quantum-supremacy/ (visited on 09/27/2019).

[Hal88] F. D. M. Haldane. *Exact Jastrow-Gutzwiller resonating-valence-bond ground state of the spin-1/2 antiferromagnetic Heisenberg chain with* $1/r^2$ *exchange*. Physical Review Letters **60**, 7 (1988), pp. 635–638. DOI: 10.1103/PhysRevLett.60.635.

[HFJ+17] T. Hensgens, T. Fujita, L. Janssen, et al. *Quantum Simulation of a Fermi–Hubbard Model Using a Semiconductor Quantum Dot Array*. Nature **548**, 7665 (2017), pp. 70–73. DOI: 10.1038/nature23022.

[HHT+92] F. D. M. Haldane, Z. N. C. Ha, J. C. Talstra, D. Bernard, and V. Pasquier. *Yangian Symmetry of Integrable Quantum Chains with Long-Range Interactions and a New Description of States in Conformal Field Theory*. Physical Review Letters **69**, 14 (1992), pp. 2021–2025. DOI: 10.1103/PhysRevLett.69.2021.

[HKP+07] R. Hanson, L. P. Kouwenhoven, J. R. Petta, S. Tarucha, and L. M. K. Vandersypen. *Spins in Few-Electron Quantum Dots*. Reviews of Modern Physics **79**, 4 (2007), pp. 1217–1265. DOI: 10.1103/RevModPhys.79.1217.

[HYC+19] W. Huang, C. H. Yang, K. W. Chan, et al. *Fidelity Benchmarks for Two-Qubit Gates in Silicon*. Nature **569**, 7757 (2019), p. 532. DOI: 10.1038/s41586-019-1197-0.

[IBM] IBM Q webpage. URL: https://www.research.ibm.com/ibm-q/ (visited on 08/12/2019).

[IGM+05] E. K. Irish, J. Gea-Banacloche, I. Martin, and K. C. Schwab. *Dynamics of a Two-Level System Strongly Coupled to a High-Frequency Quantum Oscillator*. Physical Review B **72**, 19 (2005), p. 195410. DOI: 10.1103/PhysRevB.72.195410.

[Int18] Intel Newsroom. *2018 CES: Intel Advances Quantum and Neuromorphic Computing Research*. Jan. 2018. URL: https://newsroom.intel.com/news/intel-advances-quantum-neuromorphic-computing-research/ (visited on 08/12/2019).

[Ion18] IonQ Press Releases. *IonQ harnesses single-atom qubits to build the world's most powerful quantum computer*. Dec. 2018. URL: https://ionq.com/news/december-11-2018 (visited on 08/14/2019).

[ISC+13] R. Islam, C. Senko, W. C. Campbell, et al. *Emergence and Frustration of Magnetism with Variable-Range Interactions in a Quantum Simulator*. Science **340**, 6132 (2013), pp. 583–587. DOI: 10.1126/science.1232296.

[ISM11] L. Isenhower, M. Saffman, and K. Mølmer. *Multibit CkNOT Quantum Gates via Rydberg Blockade*. Quantum Information Processing **10**, 6 (2011), p. 755. DOI: 10.1007/s11128-011-0292-4.

[Ist00] S. Istrail. *Statistical Mechanics, Three-Dimensionality and NP-Completeness: I. Universality of Intracatability for the Partition Function of the Ising Model Across Non-Planar Surfaces (Extended Abstract)*. Proceedings of the Thirty-Second Annual ACM Symposium on Theory of Computing. STOC '00. New York, NY, USA: ACM, 2000, pp. 87–96. ISBN: 978-1-58113-184-0. DOI: 10.1145/335305.335316.

[Jor18] S. Jordan. *Quantum Algorithm Zoo*. Aug. 2018. URL: http://quantumalgorithmzoo.org/ (visited on 08/12/2019).

[JW28] P. Jordan and E. Wigner. *Über das Paulische Äquivalenzverbot*. Zeitschrift für Physik **47**, 9 (1928), pp. 631–651. DOI: 10.1007/BF01331938.

[Kas02] M. A. Kasevich. *Coherence with Atoms*. Science **298**, 5597 (2002), pp. 1363–1368. DOI: 10.1126/science.1079430.

[Kat11] M. O. Katanaev. *Adiabatic Theorem for Finite Dimensional Quantum Mechanical Systems*. Russian Physics Journal **54**, 3 (2011), pp. 342–353. DOI: 10.1007/s11182-011-9620-5.

[Kay10] A. Kay. *Perfect, Efficient, State Transfer and Its Application as a Constructive Tool*. International Journal of Quantum Information **08**, 04 (2010), pp. 641–676. DOI: 10.1142/S0219749910006514.

[KBK+15] K. Kotru, D. L. Butts, J. M. Kinast, and R. E. Stoner. *Large-Area Atom Interferometry with Frequency-Swept Raman Adiabatic Passage*. Physical Review Letters **115**, 10 (2015), p. 103001. DOI: 10.1103/PhysRevLett.115.103001.

[KCF13] T. S. Koh, S. N. Coppersmith, and M. Friesen. *High-Fidelity Gates in Quantum Dot Spin Qubits*. Proceedings of the National Academy of Sciences **110**, 49 (2013), pp. 19695–19700. DOI: 10.1073/pnas.1319875110.

[KCI+09] K. Kim, M.-S. Chang, R. Islam, et al. *Entanglement and Tunable Spin-Spin Couplings between Trapped Ions Using Multiple Transverse Modes*. Physical Review Letters **103**, 12 (2009), p. 120502. DOI: 10.1103/PhysRevLett.103.120502.

[KE05] A. Kay and M. Ericsson. *Geometric Effects and Computation in Spin Networks*. New Journal of Physics **7** (2005), pp. 143–143. DOI: 10.1088/1367-2630/7/1/143.

[Ken90] T. Kennedy. *Exact Diagonalisations of Open Spin-1 Chains*. Journal of Physics: Condensed Matter **2**, 26 (1990), pp. 5737–5745. DOI: 10.1088/0953-8984/2/26/010.

[KP10] A. Kay and P. J. Pemberton-Ross. *Computation on Spin Chains with Limited Access*. Physical Review A **81**, 1 (2010), p. 010301. DOI: 10.1103/PhysRevA.81.010301.

[KP89] C. Kaiser and I. Peschel. *Ground State Properties of a Quantum Antiferromagnet with Infinite-Range Interactions*. Journal of Physics A: Mathematical and General **22**, 19 (1989), pp. 4257–4261. DOI: 10.1088/0305-4470/22/19/018.

[KRH+17] N. Kalb, A. A. Reiserer, P. C. Humphreys, et al. *Entanglement Distillation between Solid-State Quantum Network Nodes*. Science **356**, 6341 (2017), pp. 928–932. DOI: 10.1126/science.aan0070.

[KTS07] P. Král, I. Thanopulos, and M. Shapiro. *Colloquium: Coherently Controlled Adiabatic Passage*. Reviews of Modern Physics **79**, 1 (2007), pp. 53–77. DOI: 10.1103/RevModPhys.79.53.

[LD98] D. Loss and D. P. DiVincenzo. *Quantum Computation with Quantum Dots*. Physical Review A **57**, 1 (1998), pp. 120–126. DOI: 10.1103/PhysRevA.57.120.

[LFC+01] M. D. Lukin, M. Fleischhauer, R. Cote, et al. *Dipole Blockade and Quantum Information Processing in Mesoscopic Atomic Ensembles*. Physical Review Letters **87**, 3 (2001), p. 037901. DOI: 10.1103/PhysRevLett.87.037901.

[LFS+19] K. A. Landsman, C. Figgatt, T. Schuster, et al. *Verified Quantum Information Scrambling*. Nature **567**, 7746 (2019), p. 61. DOI: 10.1038/s41586-019-0952-6.

[LGC17] O. Lychkovskiy, O. Gamayun, and V. Cheianov. *Time Scale for Adiabaticity Breakdown in Driven Many-Body Systems and Orthogonality Catastrophe*. Physical Review Letters **119**, 20 (2017), p. 200401. DOI: 10.1103/PhysRevLett.119.200401.

[Llo96] S. Lloyd. *Universal Quantum Simulators*. Science **273**, 5278 (1996), pp. 1073–1078. DOI: 10.1126/science.273.5278.1073.

[LM62] E. Lieb and D. Mattis. *Ordering Energy Levels of Interacting Spin Systems*. Journal of Mathematical Physics **3**, 4 (1962), pp. 749–751. DOI: 10.1063/1.1724276.

[LMH+18] X. Li, Y. Ma, J. Han, et al. *Perfect Quantum State Transfer in a Superconducting Qubit Chain with Parametrically Tunable Couplings*. Physical Review Applied **10**, 5 (2018), p. 054009. DOI: 10.1103/PhysRevApplied.10.054009.

[Lon14] S. Longhi. *Coherent Transfer by Adiabatic Passage in Two-Dimensional Lattices*. Annals of Physics **348** (2014), pp. 161–175. DOI: 10.1016/j.aop.2014.05.020.

[LR72] E. H. Lieb and D. W. Robinson. *The Finite Group Velocity of Quantum Spin Systems*. Communications in Mathematical Physics **28**, 3 (1972), pp. 251–257. DOI: 10.1007/BF01645779.

[LSM61] E. Lieb, T. Schultz, and D. Mattis. *Two Soluble Models of an Antiferromagnetic Chain*. Annals of Physics **16**, 3 (1961), pp. 407–466. DOI: 10.1016/0003-4916(61)90115-4.

[MB11] O. Mülken and A. Blumen. *Continuous-Time Quantum Walks: Models for Coherent Transport on Complex Networks*. Physics Reports **502**, 2 (2011), pp. 37–87. DOI: 10.1016/j.physrep.2011.01.002.

[MBA+16] R. Menchon-Enrich, A. Benseny, V. Ahufinger, et al. *Spatial Adiabatic Passage: A Review of Recent Progress*. Reports on Progress in Physics **79**, 7 (2016), p. 074401. DOI: 10.1088/0034-4885/79/7/074401.

[MCJ+17] A. Mazurenko, C. S. Chiu, G. Ji, et al. *A Cold-Atom Fermi–Hubbard Antiferromagnet*. Nature **545**, 7655 (2017), pp. 462–466. DOI: 10.1038/nature22362.

[MCM+17] S. A. Moses, J. P. Covey, M. T. Miecnikowski, D. S. Jin, and J. Ye. *New Frontiers for Quantum Gases of Polar Molecules*. Nature Physics **13**, 1 (2017), pp. 13–20. DOI: 10.1038/nphys3985.

[MDZ+15] S. Murmann, F. Deuretzbacher, G. Zürn, et al. *Antiferromagnetic Heisenberg Spin Chain of a Few Cold Atoms in a One-Dimensional Trap*. Physical Review Letters **115**, 21 (2015). DOI: 10.1103/PhysRevLett.115.215301.

[MM12] B. M. McCoy and J.-M. Maillard. *The Importance of the Ising Model*. Progress of Theoretical Physics **127**, 5 (2012), pp. 791–817. DOI: 10.1143/PTP.127.791.

[Mon16] A. Montanaro. *Quantum Algorithms: An Overview*. npj Quantum Information **2** (2016), p. 15023. DOI: 10.1038/npjqi.2015.23.

[Mos75] J. Moser. *Dynamical Systems, Theory and Applications*. Vol. 38. Lecture Notes in Physics. Seattle, WA: Springer-Verlag, 1975. ISBN: 978-3-540-37505-0.

[MRR+14] C. Monroe, R. Raussendorf, A. Ruthven, et al. *Large-Scale Modular Quantum-Computer Architecture with Atomic Memory and Photonic Interconnects*. Physical Review A **89**, 2 (2014), p. 022317. DOI: 10.1103/PhysRevA.89.022317.

[MS83] J. R. Morris and B. W. Shore. *Reduction of Degenerate Two-Level Excitation to Independent Two-State Systems*. Physical Review A **27**, 2 (1983), pp. 906–912. DOI: 10.1103/PhysRevA.27.906.

[MT97] V. S. Malinovsky and D. J. Tannor. *Simple and Robust Extension of the Stimulated Raman Adiabatic Passage Technique to N -Level Systems*. Physical Review A **56**, 6 (1997), pp. 4929–4937. DOI: 10.1103/PhysRevA.56.4929.

[NC10] M. A. Nielsen and I. L. Chuang. *Quantum Computation and Quantum Information*. Cambridge University Press, 2010. ISBN: 978-1-107-00217-3. DOI: 10.1017/CBO9780511976667.

[NJ14] G. M. Nikolopoulos and I. Jex, eds. *Quantum State Transfer and Network Engineering*. Quantum Science and Technology. Berlin Heidelberg: Springer-Verlag, 2014. ISBN: 978-3-642-39936-7.

[NPL04] G. M. Nikolopoulos, D. Petrosyan, and P. Lambropoulos. *Electron Wavepacket Propagation in a Chain of Coupled Quantum Dots*. Journal of Physics: Condensed Matter **16**, 28 (2004), pp. 4991–5002. DOI: 10.1088/0953-8984/16/28/019.

[NS05] B. Nachtergaele and S. Starr. *Ferromagnetic Lieb-Mattis Theorem*. Physical Review Letters **94**, 5 (2005), p. 057206. DOI: 10.1103/PhysRevLett.94.057206.

[OEO+07] T. Ohshima, A. Ekert, D. K. L. Oi, D. Kaslizowski, and L. C. Kwek. *Robust State Transfer and Rotation through a Spin Chain via Dark Passage* (2007). arXiv: quant-ph/0702019.

[OMA+17] J. S. Otterbach, R. Manenti, N. Alidoust, et al. *Unsupervised Machine Learning on a Hybrid Quantum Computer* (2017). arXiv: 1712.05771.

[OSF+13] S. Oh, Y.-P. Shim, J. Fei, M. Friesen, and X. Hu. *Resonant Adiabatic Passage with Three Qubits*. Physical Review A **87**, 2 (2013), p. 022332. DOI: 10.1103/PhysRevA.87.022332.

[PG08] A. Polkovnikov and V. Gritsev. *Breakdown of the Adiabatic Limit in Low-Dimensional Gapless Systems*. Nature Physics **4**, 6 (2008), pp. 477–481. DOI: 10.1038/nphys963.

[PK04] E. Paspalakis and N. J. Kylstra. *Coherent Manipulation of Superconducting Quantum Interference Devices with Adiabatic Passage*. Journal of Modern Optics **51**, 11 (2004), pp. 1679–1689. DOI: 10.1080/09500340408232482.

[PKK+13] A. Perez-Leija, R. Keil, A. Kay, et al. *Coherent Quantum Transport in Photonic Lattices*. Physical Review A **87**, 1 (2013), p. 012309. DOI: 10.1103/PhysRevA.87.012309.

[Pol93] A. P. Polychronakos. *Lattice Integrable Systems of Haldane-Shastry Type*. Physical Review Letters **70**, 15 (1993), pp. 2329–2331. DOI: 10.1103/PhysRevLett.70.2329.

[Pre13] J. Preskill. *Sufficient Condition on Noise Correlations for Scalable Quantum Computing*. Quantum Information and Computation **13** (2013), pp. 3–4. DOI: https://doi.org/10.26421/QIC13.3-4.

[Pre18] J. Preskill. *Quantum Computing in the NISQ Era and Beyond*. Quantum **2** (2018), p. 79. DOI: 10.22331/q-2018-08-06-79.

[PRM15] D. Petrosyan, D. D. B. Rao, and K. Mølmer. *Filtering Single Atoms from Rydberg-Blockaded Mesoscopic Ensembles*. Physical Review A **91**, 4 (2015), p. 043402. DOI: 10.1103/PhysRevA.91.043402.

[PW02] J. Pachos and H. Walther. *Quantum Computation with Trapped Ions in an Optical Cavity*. Physical Review Letters **89**, 18 (2002), p. 187903. DOI: 10.1103/PhysRevLett.89.187903.

[RGG+19] S. E. Rasmussen, K. Groenland, R. Gerritsma, K. Schoutens, and N. T. Zinner. *Single-step implementation of high fidelity n-bit Toffoli gate* (2019). arXiv: 1910.07548.

[Rig18] C. Rigetti. *The Rigetti 128-Qubit Chip and What It Means for Quantum*. Aug. 2018. URL: https://medium.com/rigetti/the-rigetti-128-qubit-chip-and-what-it-means-for-quantum-df757d1b71ea (visited on 08/12/2019).

[RL18] P. Rebentrost and S. Lloyd. *Quantum Computational Finance: Quantum Algorithm for Portfolio Optimization* (2018). arXiv: 1811.03975.

[RNT+17] P. Roushan, C. Neill, J. Tangpanitanon, et al. *Spectroscopic Signatures of Localization with Interacting Photons in Superconducting Qubits*. Science **358**, 6367 (2017), pp. 1175–1179. DOI: 10.1126/science.aao1401.

[RRG07] T. C. Ralph, K. J. Resch, and A. Gilchrist. *Efficient Toffoli Gates Using Qudits*. Physical Review A **75**, 2 (2007), p. 022313. DOI: 10.1103/PhysRevA.75.022313.

[RRS18] G. Ramírez, J. Rodríguez-Laguna, and G. Sierra. *Breaking the Area Law: The Rainbow State* (2018). arXiv: 1812.11495.

[Saf16] M. Saffman. *Quantum Computing with Atomic Qubits and Rydberg Interactions: Progress and Challenges*. Journal of Physics B: Atomic, Molecular and Optical Physics **49**, 20 (2016), p. 202001. DOI: 10.1088/0953-4075/49/20/202001.

[Sha88] B. S. Shastry. *Exact Solution of an S=1/2 Heisenberg Antiferromagnetic Chain with Long-Ranged Interactions*. Physical Review Letters **60**, 7 (1988), pp. 639–642. DOI: 10.1103/PhysRevLett.60.639.

[Shi18] X.-F. Shi. *Deutsch, Toffoli, and Cnot Gates via Rydberg Blockade of Neutral Atoms*. Physical Review Applied **9**, 5 (2018), p. 051001. DOI: 10.1103/PhysRevApplied.9.051001.

[Sho94] P. W. Shor. *Algorithms for Quantum Computation: Discrete Logarithms and Factoring*. Proceedings 35th Annual Symposium on Foundations of Computer Science. 1994, pp. 124–134. DOI: 10.1109/SFCS.1994.365700.

[SM09] V. V. Shende and I. L. Markov. *On the CNOT-Cost of TOFFOLI Gates*. Quantum Information and Computation **9**, 5&6 (2009), pp. 0463–0486. DOI: https://doi.org/10.26421/QIC9.5-6.

[SPG+12] S. Stellmer, B. Pasquiou, R. Grimm, and F. Schreck. *Creation of Ultracold Sr_2 Molecules in the Electronic Ground State*. Physical Review Letters **109**, 11 (2012), p. 115302. DOI: 10.1103/PhysRevLett.109.115302.

[SS03] N. Schuch and J. Siewert. *Natural Two-Qubit Gate for Quantum Computation Using the XY Interaction*. Physical Review A **67**, 3 (2003), p. 032301. DOI: 10.1103/PhysRevA.67.032301.

[SSR+14] C. Senko, J. Smith, P. Richerme, et al. *Coherent Imaging Spectroscopy of a Quantum Many-Body Spin System*. Science **345**, 6195 (2014), pp. 430–433. DOI: 10.1126/science.1251422.

[Sut71] B. Sutherland. *Exact Results for a Quantum Many-Body Problem in One Dimension*. Physical Review A **4**, 5 (1971), pp. 2019–2021. DOI: 10.1103/PhysRevA.4.2019.

[Sut72] B. Sutherland. *Exact Results for a Quantum Many-Body Problem in One Dimension. II.* Physical Review A **5**, 3 (1972), pp. 1372–1376. DOI: 10.1103/PhysRevA.5.1372.

[Sut75] B. Sutherland. *Exact Ground-State Wave Function for a One-Dimensional Plasma.* Physical Review Letters **34**, 17 (1975), pp. 1083–1085. DOI: 10.1103/PhysRevLett.34.1083.

[SZR+17] M. Soltani, M. Zhang, C. Ryan, et al. *Efficient Quantum Microwave-to-Optical Conversion Using Electro-Optic Nanophotonic Coupled Resonators.* Physical Review A **96**, 4 (2017), p. 043808. DOI: 10.1103/PhysRevA.96.043808.

[TBJ+11] N. Timoney, I. Baumgart, M. Johanning, et al. *Quantum Gates and Memory Using Microwave-Dressed States.* Nature **476**, 7359 (2011), pp. 185–188. DOI: 10.1038/nature10319.

[THM03] F. Troiani, U. Hohenester, and E. Molinari. *High-Finesse Optical Quantum Gates for Electron Spins in Artificial Molecules.* Physical Review Letters **90**, 20 (2003), p. 206802. DOI: 10.1103/PhysRevLett.90.206802.

[Tho83] D. J. Thouless. *Quantization of Particle Transport.* Physical Review B **27**, 10 (1983), pp. 6083–6087. DOI: 10.1103/PhysRevB.27.6083.

[TSS+19] D. Tiarks, S. Schmidt-Eberle, T. Stolz, G. Rempe, and S. Dürr. *A Photon–Photon Quantum Gate Based on Rydberg Interactions.* Nature Physics **15**, 2 (2019), p. 124. DOI: 10.1038/s41567-018-0313-7.

[UF02] R. G. Unanyan and M. Fleischhauer. *Efficient and Robust Entanglement Generation in a Many-Particle System with Resonant Dipole-Dipole Interactions.* Physical Review A **66**, 3 (2002), p. 032109. DOI: 10.1103/PhysRevA.66.032109.

[VBC+17] L. M. K. Vandersypen, H. Bluhm, J. S. Clarke, et al. *Interfacing Spin Qubits in Quantum Dots and Donors—Hot, Dense, and Coherent.* npj Quantum Information **3**, 1 (2017), p. 34. DOI: 10.1038/s41534-017-0038-y.

[VRL10] G. Vitagliano, A. Riera, and J. I. Latorre. *Volume-Law Scaling for the Entanglement Entropy in Spin-1/2 Chains.* New Journal of Physics **12**, 11 (2010), p. 113049. DOI: 10.1088/1367-2630/12/11/113049.

[VRS+17] N. V. Vitanov, A. A. Rangelov, B. W. Shore, and K. Bergmann. *Stimulated Raman Adiabatic Passage in Physics, Chemistry, and Beyond.* Reviews of Modern Physics **89**, 1 (2017), p. 015006. DOI: 10.1103/RevModPhys.89.015006.

[VS19] B. A. van Voorden and K. Schoutens. *Topological Quantum Pump of Strongly Interacting Fermions in Coupled Chains.* New Journal of Physics **21**, 1 (2019), p. 013026. DOI: 10.1088/1367-2630/aaf748.

[VVN+17] B. Vogell, B. Vermersch, T. E. Northup, B. P. Lanyon, and C. A. Muschik. *Deterministic Quantum State Transfer between Remote Qubits in Cavities.* Quantum Science and Technology **2**, 4 (2017), p. 045003. DOI: 10.1088/2058-9565/aa868b.

[VZ12] L. Vinet and A. Zhedanov. *Almost Perfect State Transfer in Quantum Spin Chains.* Physical Review A **86**, 5 (2012), p. 052319. DOI: 10.1103/PhysRevA.86.052319.

[WBB16] M. Wollenhaupt, T. Bayer, and T. Baumert. *Control of Ultrafast Electron Dynamics with Shaped Femtosecond Laser Pulses: From Atoms to Solids. Ultrafast Dynamics Driven by Intense Light Pulses: From Atoms to Solids, from Lasers to Intense X-Rays*. Ed. by M. Kitzler and S. Gräfe. Springer Series on Atomic, Optical, and Plasma Physics. Cham: Springer International Publishing, 2016, pp. 63–122. ISBN: 978-3-319-20173-3_4. DOI: 10.1007/978-3-319-20173-3_4.

[WE19] S. Woerner and D. J. Egger. *Quantum Risk Analysis*. npj Quantum Information **5**, 1 (2019), pp. 1–8. DOI: 10.1038/s41534-019-0130-6.

[WEH18] S. Wehner, D. Elkouss, and R. Hanson. *Quantum Internet: A Vision for the Road Ahead*. Science **362**, 6412 (2018). DOI: 10.1126/science.aam9288.

[Wez07] J. van Wezel. *Quantum Mechanics and the Big World: Order, Broken Symmetry and Coherence in Quantum Many-Body Systems*. PhD Dissertation. Leiden University, 2007.

[Wie17] K. Wiesner. *The Careless Use of Language in Quantum Information* (2017). arXiv: 1705.06768.

[Wol19] R. de Wolf. *Quantum Computing: Lecture Notes*. 2019. arXiv: 1907.09415.

[Woo18] J. R. Wootton. *Benchmarking of Quantum Processors with Random Circuits* (2018). arXiv: 1806.02736.

[XWH+10] K. Xu, R. Williams, S.-H. Hong, Q. Liu, and J. Zhang. *Semi-Bipartite Graph Visualization for Gene Ontology Networks*. Graph Drawing. Ed. by D. Eppstein and E. R. Gansner. Lecture Notes in Computer Science. Springer Berlin Heidelberg, 2010, pp. 244–255. ISBN: 978-3-642-11805-0.

[YDY13] N. Yu, R. Duan, and M. Ying. *Five Two-Qubit Gates Are Necessary for Implementing the Toffoli Gate*. Physical Review A **88**, 1 (2013), p. 010304. DOI: 10.1103/PhysRevA.88.010304.

[ZLZ+05] J. Zhang, G. L. Long, W. Zhang, et al. *Simulation of Heisenberg XY interactions and realization of a perfect state transfer in spin chains using liquid nuclear magnetic resonance*. Physical Review A **72**, 1 (2005), p. 012331. DOI: 10.1103/PhysRevA.72.012331.

[ZPH+17] J. Zhang, G. Pagano, P. W. Hess, et al. *Observation of a Many-Body Dynamical Phase Transition with a 53-Qubit Quantum Simulator*. Nature **551**, 7682 (2017), pp. 601–604. DOI: 10.1038/nature24654.

[ZSH+15] J. Zeiher, P. Schauß, S. Hild, et al. *Microscopic Characterization of Scalable Coherent Rydberg Superatoms*. Physical Review X **5**, 3 (2015), p. 031015. DOI: 10.1103/PhysRevX.5.031015.

[ZSR+18] D. M. Zajac, A. J. Sigillito, M. Russ, et al. *Resonantly Driven CNOT Gate for Electron Spins*. Science **359**, 6374 (2018), pp. 439–442. DOI: 10.1126/science.aao5965.

List of symbols and notation

General symbols

$\mathscr{H}$	Hilbert space (Section 2.2)
$\|s\rangle_H$	quantum state ket, with label s, stated in the (eigen)basis labeled by H
$\mathbb{1}_n$	identity matrix (of dimension n)
$..^*$	complex conjugate
$..^\dagger$	Hermitian conjugate (i.e. conjugate and transpose) of an operator
$+$h.c.	add the Hermitian conjugate of previous term
$\|..\|$	absolute value, or (Euclidean) length of a vector, or determinant of a matrix
$\|..\|_H$	Hamming weight (number of ones) of a bit string
$\|\|..\|\|$	the operator norm of an operator or matrix

Roman

E	edge set of a graph
$f_j,\ f_j^\dagger$	local fermionic annihilation and creation operators at site j (Section 2.4)
$g_{(j)}$	spin imbalance (of the jth connected component) (Section 2.5)
G	graph
$h_j,\ h_{jk}$	specific Hamiltonian terms
H	Hamiltonian (Section 2.2, Section 3.1)
i	imaginary unit, $i^2 = -1$
m	total z-magnetization, i.e. eigenvalue of $\hat{S}^z_{\text{tot}}$ (Section 2.5)
n, N	system size, depending on context
$N^s_{s_1,\ldots,s_n}$	multiplicity of subspace with total spin s (Section 2.5)
$O(f(x))$	big O notation, indicating that scaling is similar to $f(x)$ in some limit
t	time
s	total spin, as in the eigenvalue $s(s+1)$ of $\vec{S}^2_{\text{tot}}$ (Section 2.5)
$\hat{S}$	spin operators in various forms, see Section 2.5
T	stopping time of a protocol
U_t	unitary time evolution operator, after time t
V	vertex set of a graph
w	weights of a graph, or coupling strengths in a Hamiltonian (Eq. 2.9)
X, Y, Z	Pauli matrices (Eq. 2.2).

Greek

β^{pq}_{jk}	parameter for 2-local Hamiltonians (Eq. 2.8)
δ	off-resonance (Section 3.1.2)
δ_{jk}	Kronecker delta (0 if $j \neq k$, and 1 if $j = k$)
Δ	energy gap, difference between two eigenvalues
$\vec{\sigma}^{[\alpha]}_{(j)}$	Pauli matrices $\{X, Y, Z\}$ [the αth element] (acting on qubit j) (Eq. 2.2)
$\sigma^+,\ \sigma^-$	raising and lowering operators (Eq. 2.4)
$\|\Psi\rangle$	general quantum state
$\|\psi_j\rangle$	eigenstate with label j
ω_{drive}	driving frequency (parameter in a Hamiltonian)
ω_{rf}	angular velocity of rotating frame (Section 3.1.2)
Ω	Rabi frequency (Sections 3.1.1 and 3.1.2)

Nederlandse samenvatting

Protocollen voor kleine quantumcomputers

De belangrijkste resultaten van dit proefschrift verdelen we in twee categorieën. In Deel II behandelen we protocollen die leiden tot logische poorten (*gates*) op meeredere qubits door middel van resonante aansturing (*driving*), en in Deel III richten we ons op het adiabatisch verplaatsen van quantumtoestanden. De voorgaande hoofdstukken in Deel I bevatten een introductie tot deze onderwerpen.

In **Deel II** construeren we multiqubit gates, zoals de $\texttt{Toffoli}_N$. Deze zijn essentieel in veel quantumalgoritmes, maar blijken lastig uit te voeren op experimentele quantumcomputers. In tegenstelling tot de gebruikelijke aanpak waarbij grote operaties worden gecompileerd to een reeks schakelingen op weinig qubits, gebruiken wij een Hamiltoniaan de leidt tot een continue evolutie in een sterk gekoppeld quantumsysteem. De selectiviteit van resonant driving maakt het mogelijk om slechts 2 van de 2^N eigentoestanden van een achtergrondveld te verwisselen, wat leidt tot een operatie die we $\texttt{iSWAP}$ noemen. Om deze operatie nuttig te maken voor quantumcomputers, introduceren we *eigengates* die deze eigentoestanden terugzetten naar de computationele basis.

We bouwen en simuleren dergelijke gates in drie verschillende systemen. De eerste is de Krawtchoukketen, een voorbeeld van een XX keten met enkel koppelingen tussen naastgelegen qubits ($H = \sum_j J_j \left(X_j X_{j+1} + Y_j Y_{j+1}\right)$). Het systeem heeft bijzondere eigenschappen, zoals een lineaire dispersie, een tijdsevolutie die elke toestand doet spiegelen, en bovendien een overzichtelijke eigengate. We vinden dat lokale driving kan leiden tot unieke overgangen tussen de toestanden $|1^{\frac{N}{2}}\ 0^{\frac{N}{2}}\rangle$ en $|0^{\frac{N}{2}}\ 1^{\frac{N}{2}}\rangle$, en we analyseren numeriek de fouten die optreden bij ketens van lengte $N = 4$ en $N = 6$.

Ten tweede beschouwen we een voorbeeld van een XXX keten met koppelingen over lange afstanden ($H = \sum_{j<k} J_{j,k} \left(\vec{\sigma}_j \cdot \vec{\sigma}_k\right)$), welke door Polychronakos is geïntroduceerd als een variant op het Haldane-Shastry model. Een quench met deze Hamiltoniaan blijkt zelf een eigengate te zijn, en wel voor een keten van de vorm $H = \sum_{j<k} J_{jk} \left(X_j Y_k - Y_j X_k\right)$. Weer simuleren we de fouten die optreden bij resonant driving voor lengtes $N = 4$ en $N = 6$.

De vorige twee systemen hebben helaas kleine matrixelementen tussen de eigentoestanden die we willen verwisselen, waardoor de gates lang duren. Daarom bekijken we een derde model die dit probleem niet heeft, namelijk een Ising model ($H = \sum_{jk} J_{jk} Z_j Z_k$) waarbij een speciale qubit een positieve koppeling heeft met elk ander qubit. De speciale qubit maakt onder resonant driving enkel een overgang wanneer de andere qubits de toestand $|1\rangle$ aannemen, precies zoals bij de $\texttt{Toffoli}$-gate. We vinden dat de benodigde tijd voor onze gate dit keer constant blijft onder toenemende N, wat een verbetering is over gebruikelijke compileertechnieken. Echter, onze aannames over het koppelen van het speciale qubit met N anderen, en de driving frequentie die steeds groter wordt, zijn mogelijk niet realistisch voor grote N. Toch kan dit protocol nuttig zijn voor middelgrote quantumcomputers.

In **Deel III** bestuderen we protocollen waarbij een quantumtoestand wordt verplaatst door een natuurkundig model gedefinieerd op een graaf. Dergelijke protocollen

worden veelvuldig toegepast bij huidige natuur- en scheikunde-experimenten, en worden mogelijk belangrijk voor toekomstige quantumcomputers. We beschouwen twee verschillende modellen.

In ons eerste model kan een enkel kwantumdeeltje tunnelen tussen de knopen van een graaf. Twee bestaande protocollen, met de namen STImulated Raman Adiabatic Passage (STIRAP) and Coherent Tunnelling by Adiabatic Passage (CTAP), staan toe zulke deeltjes te verplaatsen tussen de eindpunten van een keten, waarbij het systeem telkens precies nul energie heeft. Ons resultaat is dat deze protocollen op veel meer grafen werken, namelijk (semi-)bipartite grafen met een volmaakte knopenkoppeling wanneer de zender wordt weggelaten, en wanneer de ontvanger wordt weggelaten. Veel van de belangrijke voordelen van STIRAP en CTAP, zoals bescherming tegen bepaalde vormen van decoherentie, blijven gelden. We testen het protocol op een boomstructuur, waarbij de zender en ontvanger zich op een blad bevinden. Het protocol blijkt verrassend accuraat, vooral wanneer de verzender en ontvanger een zwakkere interactie hebben dan de overige knopen.

Het tweede model is een anti-ferromagnetisch XXX spinsysteem, waarbij de interacties tussen spindeeltjes worden vastgelegd door een graaf. We vinden weer dat eerdere protocollen op lineaire ketens ook toepasbaar zijn op algemenere grafen, namelijk bipartite grafen met een bepaalde balans tussen de maximale spin op de partities. Onder vergelijkbare voorwaarden kan verstrengeling tussen verweggelegen knopen worden gevormd. We analyseren de nauwkeurigheid van de protocollen op een kleine stervormige graaf, en bespreken een mogelijke experimentele test.

Acknowledgements

First and foremost, I would like to thank my advisors Harry and Kareljan. As a starting PhD student, I came out of a previous project in artificial intelligence and felt like I had very limited background knowledge about the field of quantum computing, neither about the condensed matter theory required to understand small quantum computers, nor the advanced mathematics needed to understand the computer science aspects and algorithms. Nevertheless, Harry and Kareljan remained resolutely positive and enthusiastic about my work, even when our first results were not received as well as we had hoped. Please keep doing this for all your future students, especially to those that had some setbacks, as I believe that a student that feels that he/she is doing well can be much more motivated.

Especially to Kareljan, I greatly enjoyed our collaboration on the papers on multiqubit gates, which resulted in Part II of this thesis. I learned a lot about condensed matter techniques, writing good papers, and dealing with the politics that pop up when dealing with journals or other scientists. Apart from the papers we wrote together, you were also a great help with my other results on state transfer. I ended up appealing to you for various technical questions, for advise about presentation of the result, about potential journals, and for proof-reading the manuscripts. In the end, you suggested that you did not need to be part of the list of authors - a very generous gesture that endowed me the scientific honor of a single-author paper. Many thanks for all of the above!

Having made my first steps into the world of state transfer, I appealed to Carla and Reinier to help me deal with a question about eigenvalues of graphs. Initially, I was hoping that the answer to this question was already known for decades in the mathematics community, providing me some lemma's that I could readily turn into a physics paper. Of course, nothing comes as easy as that, and we ended up solving this problem by ourselves. I greatly enjoyed this collaboration, blending our different expertises, which I think yielded a great result.

I am also grateful for much help that I got on the contents on this thesis from Jasper and Rene. The state transfer ideas all incubated thanks to Jasper's lectures I was allowed to visit, and found a more concrete form thanks to many later discussions. Rene's expertise on trapped ions proved invaluable to develop the ideas on the Ising star model in an experimental context.

To the reading committee of this thesis: many thanks for taking your time to evaluate my dissertation, and to take part in the opposition during the defense.

To all the fellow junior researchers at and around QuSoft, including Freek, Joris, Tom, Joran, Álvaro, Farrokh, Arjan, Yfke, Florian, Jan, Jana, Lars, Srini, Teresa, Simon, Jonas, Sebastian, Bas, Harold, Chris Majenz, Chris Cade, Mathys, Ralph, András, Sander, Isabella, Ruben, Ido, Alex, Yinan, Subha: thanks for the wonderful time at CWI. I will surely remember all the blackboard discussions, the intense fußball matches, the lunches, the conferences, and the occasional cakes. To Freek and Joris, many thanks for all the aid with more involved mathematics, especially the representation theory of spins. Especially to Tom, it was great to start our PhD programmes (pretty much) at the same time and to grow to become increasingly experienced scientists together. I am also indebted to you for all the computer help you gave me, including simple stuff such as how to exit VIM, but also running computations on parallel machines and hacking the screen resolution of old displays.

De afgelopen vier jaar waren natuurlijk ook buiten werk om een leuke tijd, vooral dankzij alle mensen die ik heb ontmoet of beter heb leren kennen in deze periode.

Bedankt aan mijn huisgenoten, voor gezellige etentjes, de borrels en feestjes, en alle discussies over het leven, de maatschappij, of natuurkunde (of het tolereren ervan).

Aan mijn vrienden in de schaduwhark, dankzij jullie ben ik dusdanig enthousiast geworden over natuurkunde dat ik er zelfs mijn werk van heb gemaakt. Bedankt voor alle jarenlange gezelligheid, de festivals, de reisjes voor wintersport of surfen, en natuurlijk de legendarische pannenkoeken-avonden.

Voor alle natuur- en wiskunden bij NSA, bedankt dat jullie zorgen dat de UvA niet alleen een geweldige plek is om dingen te leren, maar ook een uitstekende bron van gezelligheid en een locatie voor de gekste evenementen.

Aan de volleyballers van UvO en daarbuiten, bedankt voor alle geweldige momenten in de sportzaal, op het zand, op het gras, of in de kroeg.

Bart, Pelle, Nikè, Alexander en Manon, geweldig dat we elkaar nogsteeds regelmatig zien; ik geniet altijd erg van onze spelletjesmiddagen, etentjes, en natuurlijk de decenniale reis naar Rome.

Aan mijn paranimfen Etienne en Leonie: bedankt dat jullie me willen versterken bij de organisatie van alles wat bij de promotie komt kijken.

Etienne, over de afgelopen tien jaar heb ik gigantisch veel van je geleerd, over uiteenlopende onderwerpen zoals lifehacks, wetenschap, sport (van triathlons tot Cleveland Browns en Ajax) en heel veel muziek.

Lieve Leonie, het was geweldig om elkaar deze jaren steeds beter te leren kennen. Ik ben dol op ons leven vol reizen, sporten, festivals en andere activiteiten, en ik hoop dat we na onze PhDs hier ook nog vele jaren mee doorgaan.

Aan mijn ouders Jos en Annelies, en zusje Carla, ontzettend bedankt dat jullie er altijd voor me zijn, voor de goede zorgen, voor al het belangrijke levensadvies, en dat ik bij jullie altijd een veilige plek heb waar ik terug kan keren.

Titles in the ILLC Dissertation Series:

ILLC DS-2009-01: **Jakub Szymanik**
Quantifiers in TIME and SPACE. Computational Complexity of Generalized Quantifiers in Natural Language

ILLC DS-2009-02: **Hartmut Fitz**
Neural Syntax

ILLC DS-2009-03: **Brian Thomas Semmes**
A Game for the Borel Functions

ILLC DS-2009-04: **Sara L. Uckelman**
Modalities in Medieval Logic

ILLC DS-2009-05: **Andreas Witzel**
Knowledge and Games: Theory and Implementation

ILLC DS-2009-06: **Chantal Bax**
Subjectivity after Wittgenstein. Wittgenstein's embodied and embedded subject and the debate about the death of man.

ILLC DS-2009-07: **Kata Balogh**
Theme with Variations. A Context-based Analysis of Focus

ILLC DS-2009-08: **Tomohiro Hoshi**
Epistemic Dynamics and Protocol Information

ILLC DS-2009-09: **Olivia Ladinig**
Temporal expectations and their violations

ILLC DS-2009-10: **Tikitu de Jager**
"Now that you mention it, I wonder...": Awareness, Attention, Assumption

ILLC DS-2009-11: **Michael Franke**
Signal to Act: Game Theory in Pragmatics

ILLC DS-2009-12: **Joel Uckelman**
More Than the Sum of Its Parts: Compact Preference Representation Over Combinatorial Domains

ILLC DS-2009-13: **Stefan Bold**
Cardinals as Ultrapowers. A Canonical Measure Analysis under the Axiom of Determinacy.

ILLC DS-2010-01: **Reut Tsarfaty**
Relational-Realizational Parsing

ILLC DS-2010-02: **Jonathan Zvesper**
Playing with Information

ILLC DS-2010-03: **Cédric Dégremont**
The Temporal Mind. Observations on the logic of belief change in interactive systems

ILLC DS-2010-04: **Daisuke Ikegami**
Games in Set Theory and Logic

ILLC DS-2010-05: **Jarmo Kontinen**
Coherence and Complexity in Fragments of Dependence Logic

ILLC DS-2010-06: **Yanjing Wang**
Epistemic Modelling and Protocol Dynamics

ILLC DS-2010-07: **Marc Staudacher**
Use theories of meaning between conventions and social norms

ILLC DS-2010-08: **Amélie Gheerbrant**
Fixed-Point Logics on Trees

ILLC DS-2010-09: **Gaëlle Fontaine**
Modal Fixpoint Logic: Some Model Theoretic Questions

ILLC DS-2010-10: **Jacob Vosmaer**
Logic, Algebra and Topology. Investigations into canonical extensions, duality theory and point-free topology.

ILLC DS-2010-11: **Nina Gierasimczuk**
Knowing One's Limits. Logical Analysis of Inductive Inference

ILLC DS-2010-12: **Martin Mose Bentzen**
Stit, Iit, and Deontic Logic for Action Types

ILLC DS-2011-01: **Wouter M. Koolen**
Combining Strategies Efficiently: High-Quality Decisions from Conflicting Advice

ILLC DS-2011-02: **Fernando Raymundo Velazquez-Quesada**
Small steps in dynamics of information

ILLC DS-2011-03: **Marijn Koolen**
The Meaning of Structure: the Value of Link Evidence for Information Retrieval

ILLC DS-2011-04: **Junte Zhang**
System Evaluation of Archival Description and Access

ILLC DS-2011-05: **Lauri Keskinen**
Characterizing All Models in Infinite Cardinalities

ILLC DS-2011-06: **Rianne Kaptein**
Effective Focused Retrieval by Exploiting Query Context and Document Structure

ILLC DS-2011-07: **Jop Briët**
Grothendieck Inequalities, Nonlocal Games and Optimization

ILLC DS-2011-08: **Stefan Minica**
Dynamic Logic of Questions

ILLC DS-2011-09: **Raul Andres Leal**
Modalities Through the Looking Glass: A study on coalgebraic modal logic and their applications

ILLC DS-2011-10: **Lena Kurzen**
Complexity in Interaction

ILLC DS-2011-11: **Gideon Borensztajn**
The neural basis of structure in language

ILLC DS-2012-01: **Federico Sangati**
Decomposing and Regenerating Syntactic Trees

ILLC DS-2012-02: **Markos Mylonakis**
Learning the Latent Structure of Translation

ILLC DS-2012-03: **Edgar José Andrade Lotero**
Models of Language: Towards a practice-based account of information in natural language

ILLC DS-2012-04: **Yurii Khomskii**
Regularity Properties and Definability in the Real Number Continuum: idealized forcing, polarized partitions, Hausdorff gaps and mad families in the projective hierarchy.

ILLC DS-2012-05: **David García Soriano**
Query-Efficient Computation in Property Testing and Learning Theory

ILLC DS-2012-06: **Dimitris Gakis**
Contextual Metaphilosophy - The Case of Wittgenstein

ILLC DS-2012-07: **Pietro Galliani**
The Dynamics of Imperfect Information

ILLC DS-2012-08: **Umberto Grandi**
Binary Aggregation with Integrity Constraints

ILLC DS-2012-09: **Wesley Halcrow Holliday**
Knowing What Follows: Epistemic Closure and Epistemic Logic

ILLC DS-2012-10: **Jeremy Meyers**
Locations, Bodies, and Sets: A model theoretic investigation into nominalistic mereologies

ILLC DS-2012-11: **Floor Sietsma**
Logics of Communication and Knowledge

ILLC DS-2012-12: **Joris Dormans**
Engineering emergence: applied theory for game design

ILLC DS-2013-01: **Simon Pauw**
Size Matters: Grounding Quantifiers in Spatial Perception

ILLC DS-2013-02: **Virginie Fiutek**
Playing with Knowledge and Belief

ILLC DS-2013-03: **Giannicola Scarpa**
Quantum entanglement in non-local games, graph parameters and zero-error information theory

ILLC DS-2014-01: **Machiel Keestra**
Sculpting the Space of Actions. Explaining Human Action by Integrating Intentions and Mechanisms

ILLC DS-2014-02: **Thomas Icard**
The Algorithmic Mind: A Study of Inference in Action

ILLC DS-2014-03: **Harald A. Bastiaanse**
Very, Many, Small, Penguins

ILLC DS-2014-04: **Ben Rodenhäuser**
A Matter of Trust: Dynamic Attitudes in Epistemic Logic

ILLC DS-2015-01: **María Inés Crespo**
Affecting Meaning. Subjectivity and evaluativity in gradable adjectives.

ILLC DS-2015-02: **Mathias Winther Madsen**
The Kid, the Clerk, and the Gambler - Critical Studies in Statistics and Cognitive Science

ILLC DS-2015-03: **Shengyang Zhong**
Orthogonality and Quantum Geometry: Towards a Relational Reconstruction of Quantum Theory

ILLC DS-2015-04: **Sumit Sourabh**
Correspondence and Canonicity in Non-Classical Logic

ILLC DS-2015-05: **Facundo Carreiro**
Fragments of Fixpoint Logics: Automata and Expressiveness

ILLC DS-2016-01: **Ivano A. Ciardelli**
Questions in Logic

ILLC DS-2016-02: **Zoé Christoff**
Dynamic Logics of Networks: Information Flow and the Spread of Opinion

ILLC DS-2016-03: **Fleur Leonie Bouwer**
What do we need to hear a beat? The influence of attention, musical abilities, and accents on the perception of metrical rhythm

ILLC DS-2016-04: **Johannes Marti**
Interpreting Linguistic Behavior with Possible World Models

ILLC DS-2016-05: **Phong Lê**
Learning Vector Representations for Sentences - The Recursive Deep Learning Approach

ILLC DS-2016-06: **Gideon Maillette de Buy Wenniger**
Aligning the Foundations of Hierarchical Statistical Machine Translation

ILLC DS-2016-07: **Andreas van Cranenburgh**
Rich Statistical Parsing and Literary Language

ILLC DS-2016-08: **Florian Speelman**
Position-based Quantum Cryptography and Catalytic Computation

ILLC DS-2016-09: **Teresa Piovesan**
Quantum entanglement: insights via graph parameters and conic optimization

ILLC DS-2016-10: **Paula Henk**
Nonstandard Provability for Peano Arithmetic. A Modal Perspective

ILLC DS-2017-01: **Paolo Galeazzi**
Play Without Regret

ILLC DS-2017-02: **Riccardo Pinosio**
The Logic of Kant's Temporal Continuum

ILLC DS-2017-03: **Matthijs Westera**
Exhaustivity and intonation: a unified theory

ILLC DS-2017-04: **Giovanni Cinà**
Categories for the working modal logician

ILLC DS-2017-05: **Shane Noah Steinert-Threlkeld**
Communication and Computation: New Questions About Compositionality

ILLC DS-2017-06: **Peter Hawke**
The Problem of Epistemic Relevance

ILLC DS-2017-07: **Aybüke Özgün**
Evidence in Epistemic Logic: A Topological Perspective

ILLC DS-2017-08: **Raquel Garrido Alhama**
Computational Modelling of Artificial Language Learning: Retention, Recognition & Recurrence

ILLC DS-2017-09: **Miloš Stanojević**
Permutation Forests for Modeling Word Order in Machine Translation

ILLC DS-2018-01: **Berit Janssen**
Retained or Lost in Transmission? Analyzing and Predicting Stability in Dutch Folk Songs

ILLC DS-2018-02: **Hugo Huurdeman**
Supporting the Complex Dynamics of the Information Seeking Process

ILLC DS-2018-03: **Corina Koolen**
Reading beyond the female: The relationship between perception of author gender and literary quality

ILLC DS-2018-04: **Jelle Bruineberg**
Anticipating Affordances: Intentionality in self-organizing brain-body-environment systems

ILLC DS-2018-05: **Joachim Daiber**
Typologically Robust Statistical Machine Translation: Understanding and Exploiting Differences and Similarities Between Languages in Machine Translation

ILLC DS-2018-06: **Thomas Brochhagen**
Signaling under Uncertainty

ILLC DS-2018-07: **Julian Schlöder**
Assertion and Rejection

ILLC DS-2018-08: **Srinivasan Arunachalam**
Quantum Algorithms and Learning Theory

ILLC DS-2018-09: **Hugo de Holanda Cunha Nobrega**
Games for functions: Baire classes, Weihrauch degrees, transfinite computations, and ranks

ILLC DS-2018-10: **Chenwei Shi**
Reason to Believe

ILLC DS-2018-11: **Malvin Gattinger**
New Directions in Model Checking Dynamic Epistemic Logic

ILLC DS-2018-12: **Julia Ilin**
Filtration Revisited: Lattices of Stable Non-Classical Logics

ILLC DS-2018-13: **Jeroen Zuiddam**
Algebraic complexity, asymptotic spectra and entanglement polytopes

ILLC DS-2019-01: **Carlos Vaquero**
What Makes A Performer Unique? Idiosyncrasies and commonalities in expressive music performance

ILLC DS-2019-02: **Jort Bergfeld**
Quantum logics for expressing and proving the correctness of quantum programs

ILLC DS-2019-03: **András Gilyén**
Quantum Singular Value Transformation & Its Algorithmic Applications

ILLC DS-2019-04: **Lorenzo Galeotti**
The theory of the generalised real numbers and other topics in logic

ILLC DS-2019-05: **Nadine Theiler**
Taking a unified perspective: Resolutions and highlighting in the semantics of attitudes and particles

ILLC DS-2019-06: **Peter T.S. van der Gulik**
Considerations in Evolutionary Biochemistry

ILLC DS-2019-07: **Frederik Möllerström Lauridsen**
Cuts and Completions: Algebraic aspects of structural proof theory

ILLC DS-2020-01: **Mostafa Dehghani**
Learning with Imperfect Supervision for Language Understanding

ILLC DS-2020-02: **Koen Groenland**
Quantum protocols for few-qubit devices